

Density based Kinetic Monte Carlo Methods

vorgelegt von
Diplom-Physiker
Lorenzo Mandreoli
Berlin

Fakultät II-Mathematik und Naturwissenschaften
der Technischen Universität Berlin
zur Erlangung des akademischen Grades
Dr.rer.nat.

genehmigte Dissertation

Promotionausschuss:

Vorsitzender: Prof. Dr. Wolfgang Richter
Berichter: Prof. Dr. Eckehard Schöll
Berichter: Prof. Dr. Jörg Neugebauer

Tag der wissenschaftlichen Aussprache: 17.12.2004

Berlin 2005

D 83

Contents

1	Introduction	5
1.1	Semiconductor Technology	5
1.2	Epitaxial Growth	7
1.3	Structure of the Work	12
2	Methods for crystal growth simulations	13
2.1	Microscopic methods for crystal growth	16
2.1.1	Ab initio calculation	16
2.1.2	Transition state theory	18
2.2	Mesoscopic methods for crystal growth	20
2.2.1	Rate Equations	22
2.2.2	Scaling Laws	24
2.2.3	Continuum methods	28
2.2.4	Kinetic Monte Carlo	29
2.2.5	Hybrid methods: The Level Set Method	34
3	An adatom density approach to nucleation and diffusion	37
3.1	A Probability interpretation of Adatom Diffusion	39
3.1.1	Diffusion coefficient	39
3.1.2	Master equation for diffusion processes	40
3.1.3	Adatom Probability KMC for diffusion processes	41
3.1.4	Hyper Jump KMC	43
3.1.5	2D diffusion	47
3.2	Nucleation	50
3.2.1	Hartree approximation	53
3.2.2	Hartree-Fock approximation	54
3.2.3	Hartree approximation with a nucleation term	55
3.2.4	Nucleation with Hyper Jump KMC	59
3.3	Conclusions	61
4	Density Based KMC methods (AP-KMC): Fundamentals and Definitions	62
4.1	Master equation for crystal Growth	62

4.2	Kinetic Monte Carlo	66
4.3	Description of AP-KMC	70
4.3.1	Model Structure	71
4.3.2	Non-Interacting adatoms	71
4.3.3	Interacting adatoms	78
4.4	Longer time steps and higher density terms	80
4.5	Implementation of AP-KMC	81
4.6	AD-KMC	81
4.7	Conclusion	84
5	Statistical Tests for the Submonolayer growth	85
5.1	Island nucleation density	85
5.2	Island size distribution	86
5.3	Island shapes	89
5.4	Capture zones	89
	Conclusions and Outlooks	93
	A Markov Processes and derivation of the Master equation	95
	B Distributions	97
	C Numerical solution of the Rate Equation with Mathematica	100
	D Analytical Solution of the Diffusion Equation	102
	E Numerical Solution of the Diffusion Equation	104
E.0.1	Explicit Method	104
E.0.2	Implicit Method	105
E.0.3	Crank-Nicholson	105

Chapter 1

Introduction

1.1 Semiconductor Technology

How important is the semiconductor industry for our society today? To give a quantitative answer to this question it is useful to have a look at some economical data for the sector. In 2002 the sales of the semiconductor industry reached 70 billions \$ in the US and 141 billions \$ worldwide.¹ Just to have an idea this corresponds to the gross domestic product (GDP) of a nation like Finland.² The transistor production has been increasing exponentially over the last decades (see Fig. 1.1). This has been possible thanks to strong investments for research. In 2002 in the US 18% of the sales have been invested for research, this means 10 billions \$. More information about the actual stand of research and new prospective of the semiconductor industry is given by the International Technology Roadmap for Semiconductors.³ Semiconductors are used in many different industrial sectors from the computer industry to the car and communication industry (see Fig. 1.1).

Semiconductor devices can be very complicated structures. This is the case for example for optoelectronics devices such as light-emitting diodes (LED's) or laser diodes. These devices consist of vertically stacked thin films that differ by the material, alloy composition, or doping as shown in Fig. 1.2, for the example of a vertical cavity semiconducting laser (VCSL), which is a specialized laser diode widely used for fiber optics communications. To employ quantum effects some of these structures are only a few atomic layers thick. For the performance/efficiency of such devices the quality of the interfaces between the different layers is crucial. Epitaxial growth is a key technique in fabricating these devices, which requires a control at the atomic layer. In the next section the main characteristics of epitaxial growth will be discussed.

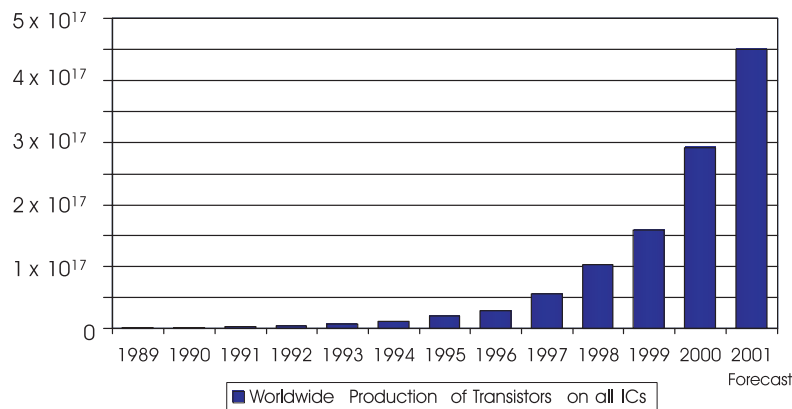
¹Source: www.semichips.org

²Finland's GDP: 130.8 billions (2002), source:www.worldbank.org

³<http://public.itrs.net>

a)

450,000,000,000,000,000 Transistors Produced in 2001



Source: SIA



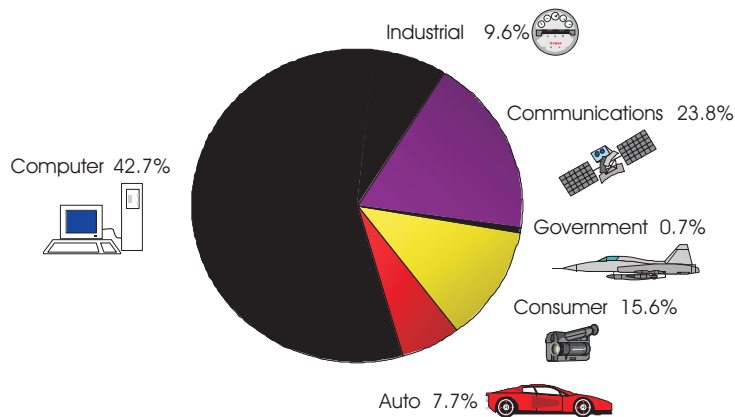
4/10/2003

SIA Master Presentation

96

b)

Semiconductors are Pervasive



2001 World Market = \$139 Billion



4/10/2003

SIA Master Presentation

109

Figure 1.1: a) Transistor production worldwide between 1989 and 2001 b) Sectors where transistors are used.

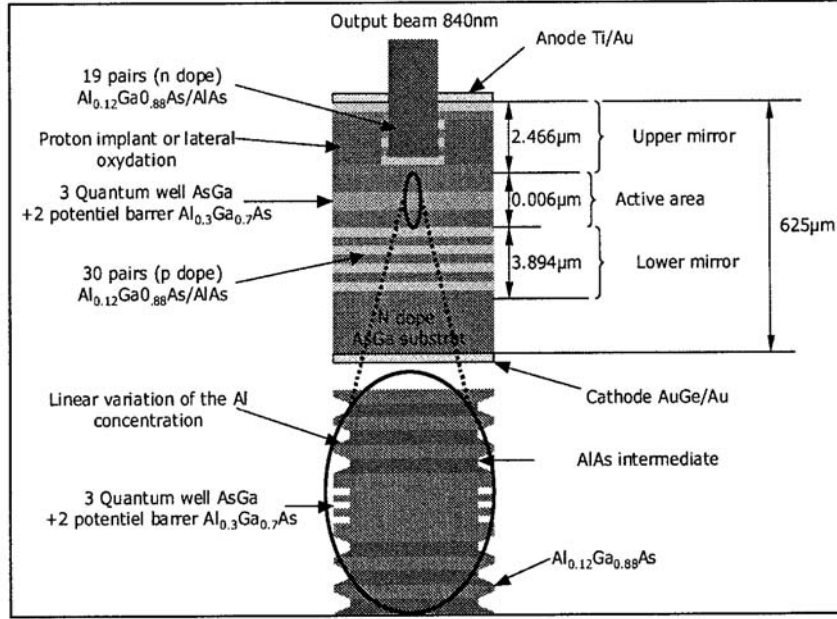


Figure 1.2: Scheme of Vertical Cavity Semiconductor Laser (VCSEL).

1.2 Epitaxial Growth

The term *epitaxy*, introduced by L. Royer in 1928 [1], is used for the growth of a crystalline layer upon (*epi*) a crystalline substrate, where the crystalline orientation of the substrate imposes an order (*taxis*) on the orientation of the deposition layer. In practice, an epitaxial growth system is characterized by two parallel contact planes of the two crystal structures and by parallel crystallographic directions within these planes. If two materials are different, the term *heteroepitaxy* is used, while for the growth of a crystalline layer on a chemically identical, crystalline substrate, the term *homoepitaxy* is commonly employed. Epitaxial growth is a very wide subject and it has been one of the key scientific issues over the last decades. Books and reviews have recently appeared, which give a good overview about the subject [2–8]. Epitaxial growth has enabled to prepare semiconductor structures with compositional or dopant properties defined in layers with thickness down to the atomic scale. The three most used epitaxial techniques will be briefly described here.

Chemical vapor phase deposition (CVD) has been extensively used, for example, for silicon epitaxial layers. These layers are grown on silicon substrates by the controlled deposition of silicon containing precursor molecules onto the surface from a chemical vapor. In one method, silicon tetrachloride reacts with hydrogen at the surface of a heated substrate, while the other reactant, HCl, is in gaseous form and is swept out of the reactor.

Liquid-phase epitaxy (LPE) is another epitaxial growth technique. A compound of the semiconductor with another element may have a melting temperature lower than that of the semiconductor itself. The semiconductor substrate is held in the liquid compound and, since the temperature of the melt is lower than the melting temperature of the substrate, the substrate does not melt. As the solution is slowly cooled, a single-crystal semiconductor layer grows on the seed crystal.

Finally **Molecular Beam Epitaxy** (MBE) is conceptually the simplest way of fabricating semiconductor heterostructures and the rest of this work will concentrate on this technique. MBE is essentially a two-step process carried out in an ultra-high vacuum (UHV) environment. In the first step, atoms or simple homoatomic molecules which are the constituents of the growing material are evaporated from solid sources in heated cells, known as Knudsen cells, collimated into beams and directed toward a heated substrate which is typically a few centimeters in size. The particles within these beams neither react nor collide with each other i.e., the deposition onto the substrate is ballistic and the particles are said to undergo molecular flow - hence the name molecular-beam epitaxy. The substrate is often rotated to achieve a more uniform deposition across the substrate. The second step of MBE is the migration of the deposited species on the surface prior to their incorporation into the growing material. This determines the profile, or morphology, of the film and its effectiveness depends on a number of factors, including the deposition rates of the constituent species, the surface temperature, the surface material, and its crystallographic orientation, to name just a few.

Through experimental techniques such as field ion (FIM) [9, 10] and scanning tunneling microscopy (STM) [11], it is possible to see the surfaces during the growth at atomic scale. Growth is a complex process and a large variety of structures can take place on the surface during this process. Examples of different structures are illustrated in Fig 1.3 where one can see the submonolayer growth for Pt on Pt(111) surfaces. Here the shape of the islands depends sensitively from the temperature and the coverage. Increasing the temperature the islands change from a fractal structure to a more compact triangular and hexagonal structure. From STM images it is also possible to get an insight on multilayer growth. As shown in Fig. 1.4, after deposition of 37.1 ML Pt with a deposition rate $F = 1.3 \times 10^{-2}$ ML/s at a partial pressure $p_{CO} = 1.9 \times 10^{-9}$ mbar of carbon monoxide at 440 K, mounds form, which are build from the terraces scattering slightly around the shape of an equal-sided hexagon. One can clearly see the atomic steps bounding the top terrace and its base terrace.

Three different types of multilayer growth [14] can be distinguished as illustrated in Fig. 1.5: the **Frank-van der Merwe** morphology [15], where one complete monolayer grows after the other (also called layer by layer mode); the **Volmer-Weber** morphology [16], where three dimensional islands are formed and the overlayer does not completely cover the exposed substrate surface; and the **Stranski-Krastanov** morphology [17], with three dimensional islands atop a thin flat wetting film that completely covers the substrate. For lattice-matched systems, the Frank-van der Merwe and Volmer-Weber morphologies can be understood from thermodynamic wetting arguments based on the interfacial free

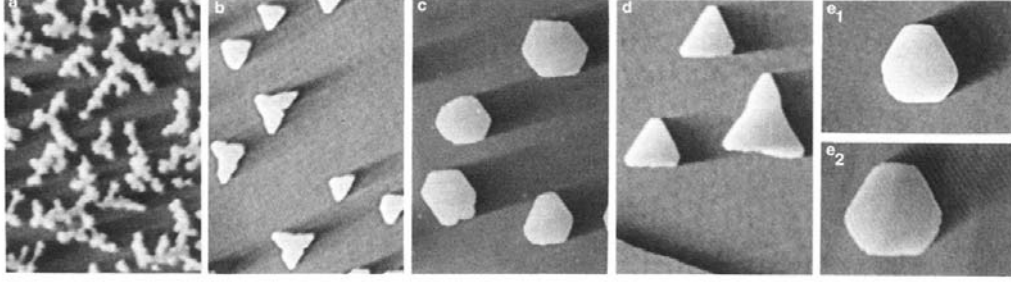


Figure 1.3: Island shapes on Pt(111) resulting at various temperatures T_s after deposition of an amount θ with a typical rate of 1×10^{-2} ML/s on images with a size S . (a) $T_s = 200$ K, $\theta = 0.2$ ML, $S = 280 \text{ \AA} \times 400 \text{ \AA}$; (b) $T_s = 400$ K, $\theta = 0.08$ ML, $S = 1300 \text{ \AA} \times 1900 \text{ \AA}$; (c) $T_s = 455$ K, $\theta = 0.14$ ML, $S = 770 \text{ \AA} \times 1100 \text{ \AA}$; (d) $T_s = 640$ K, $\theta = 0.15$ ML, $S = 2300 \text{ \AA} \times 3300 \text{ \AA}$; (e₁) $T_s = 710$ K, $\theta = 0.08$ ML, $S = 1540 \text{ \AA} \times 1100 \text{ \AA}$; (e₂) after deposition at $T_s = 425$ K ($\theta = 0.08$ ML) the sample was additionally annealed to 710 K for 1 min and than imaged ($S = 630 \text{ \AA} \times 900 \text{ \AA}$)(after [12]).

energies. The Stranski-Krastanov morphology is observed in systems where there is appreciable lattice mismatch between the epilayer and the substrate.

The first step towards a detailed understanding of the surface morphology during and after growth is to map out all relevant atomic processes. A large variety of processes can take place on the surface during growth. Fig. 1.6 illustrates the different atomic processes encountered by adatoms. After deposition (a) atoms can diffuse across the surface (b) and will eventually meet another adatom to form a small nucleus (c) or get captured by an already existing island or a step edge (d). Once an adatom has been captured by an island, it may either break away from the island (reversible aggregation) (e) or remain bonded to the island (irreversible aggregation). An atom that is bonded to an island may diffuse along its edge (f) until it finds a favorable site. As long as the coverage of adsorbed material is low (say $\theta \leq 10\%$), deposition on top of existing islands practically does not occur. However, if the step down motion (g) is hindered by an additional energy barrier, nucleation of islands on top of islands becomes likely (h).

These processes have very different time scales as illustrated in Fig. 1.7. The atoms vibrate around their stable position with a frequency of 10^{-13} s, which is the typical phonon frequency. The formation of more complicated structures as quantum dots, nanocrystals or the deposition of an entire layer on a surface can take as much as seconds. Between these two limits there is a huge interval of 13 orders of magnitude to describe.



Figure 1.4: Typical STM image of mounds appearing on the surface after the deposition of 37.1 Ml Pt/Pt(111) in a partial CO pressure of 1.9×10^{-9} mbar. Eight top terraces and the corresponding base terraces can be seen (after [13]).

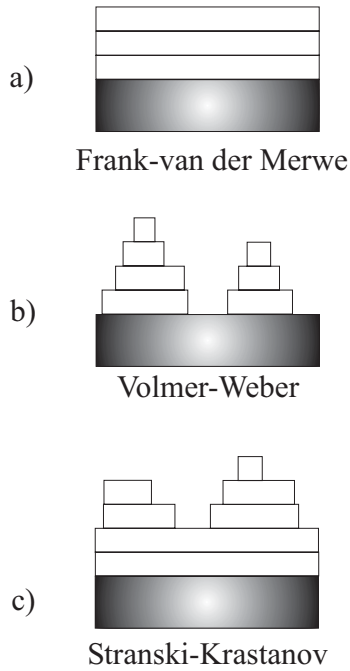


Figure 1.5: Growth modes of heteroepitaxial growth a) Frank-van der Merwe b) Volmer-Weber c) Stranski-Krastanov.

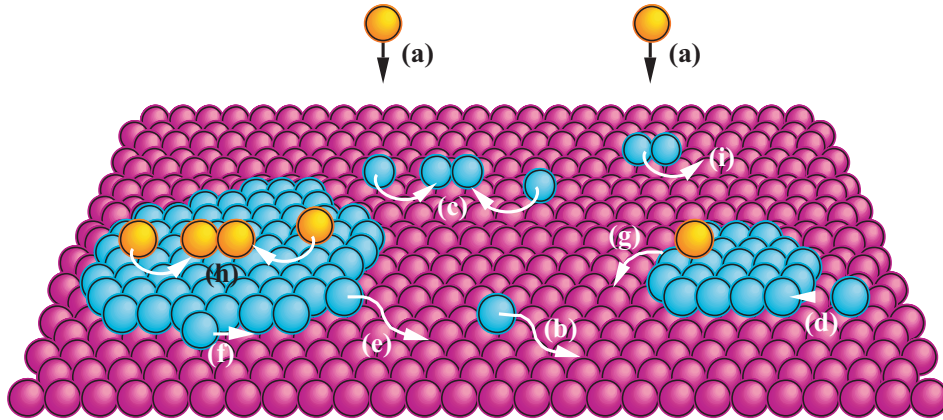


Figure 1.6: The different atomistic processes for adatoms on the surface: (a) deposition, (b) diffusion at the flat regions, (c) nucleation of an island, (d) diffusion towards and capture by the step edge, (e) detachment from an island, (f) diffusion parallel to a step edge, (g) diffusion down from an upper to a lower terrace, (h) nucleation of an island on top of an already existing island, and (i) diffusion of a dimer (or bigger island). For the processes (a), (c), (g) and (h) also the reverse direction is possible, but typically less likely.

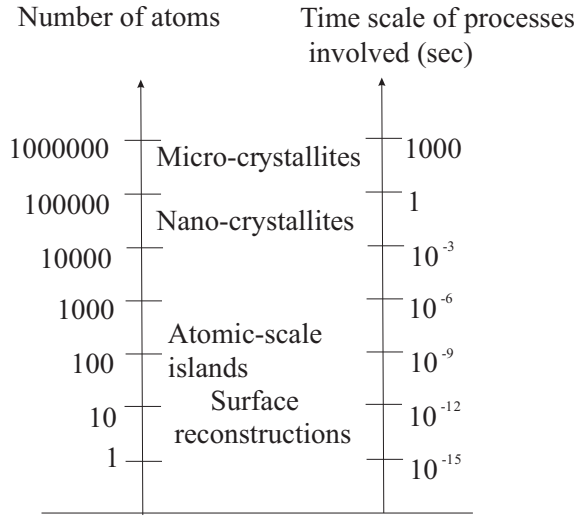


Figure 1.7: Typical time scale for growth.

1.3 Structure of the Work

The present work is devoted to the computational modeling of epitaxial growth. The processes involved in epitaxial growth range over a large number of orders of magnitudes in time and space. No computational method can describe the details of epitaxial growth from the atomic to the macroscopic scale. For this reason many different techniques have been developed, which are suited to describe the different regimes of growth. In Chap. 2 an overview of the main simulation techniques for crystal growth will be presented. First, microscopic methods as Density Functional Theory (DFT) will be described. In the second part mesoscopic methods as Rate equations, continuum methods and kinetic Monte Carlo (KMC) will be treated. In Chap. 3 the diffusion and the nucleation processes will be presented in a density picture. For the nucleation different approximations derived from concepts well known from electronic structure theory but so far never applied to describe epitaxy, as Hartree and Hartree-Fock will be tested. Also a method called Hyper Jump kinetic Monte Carlo (HJ-KMC), which can significantly reduce the simulation time of these processes compared to standard KMC, will be described. In Chap. 4 two methods for growth simulations will be discussed: the Adatom Probability kinetic Monte Carlo (AP-KMC) and its faster version the Adatom Density kinetic Monte Carlo (AD-KMC). In Chap. 5 the results for the methods presented in Chap. 4 will be given. A comparison for the island density, the island size distribution and the island shapes between AP-KMC, AD-KMC and KMC will be presented in this chapter. The development of these adatom-density based simulation techniques which allow a very efficient description of epitaxial growth is the main result presented in this work.

Chapter 2

Methods for crystal growth simulations

Due to the complexity of crystal growth, a large number of methods has been developed to simulate growth at various length and time scales. This chapter gives an overview of the simulation methods available, their present advantages, disadvantages and range of applications. Depending on the size of the system under study, these methods can be divided into microscopic and mesoscopic. A schematic classification of the different methods is given in Fig 2.1.

At the **microscopic level** (characteristic length of $\approx 10^{-9}$ m and time of the order of the phonon frequency $\approx 10^{-13}$ s) **ab initio methods** (see Sec. 2.1.1 and Ref. [18]), which apply directly to the system under study, are the method of choice. In *ab initio* calculations the principles of quantum mechanics are applied to poly-atomic systems without using any empirical or adjustable parameters. For this reason *ab initio* methods are called parameter free methods. These methods give precise results but can be applied only to systems with a rather small number of atoms ($\approx 10^2$) because they are computationally expensive. The Hartree-Fock method and the Density Functional Theory (DFT) will be described in Sec. 2.1.1. **Density Functional Theory** [19, 20] is used to provide the so-called potential energy surface (PES) as will be shown in Sec. 2.1.1. A single microscopic process on such a PES can be characterized by doing a **Molecular Dynamics** (MD) simulation. *Ab initio* MD runs usually can cover at most times of picoseconds, whereas semi-empirical MD runs may extend up to nanoseconds (at the cost of the accuracy). This is because a MD time step cannot be longer than the inverse of the highest phonon frequency. For example, a MD run simulates the entire sequence of unsuccessful attempts occurring between two successful diffusion events that may be separated by an interval of the order of nanoseconds up to seconds or even longer. Thus, for the diffusion barriers and thermal energy as characteristic for growth, MD can model only very few events and a proper statistics cannot easily be obtained for growth processes. Moreover, since growth patterns usually develop on a time scale of seconds, the inadequacy of MD is evident. Finally, the growth structures involve large numbers of particles ($\approx 10^2$ to 10^4), far beyond the reach of MD (*ab initio* simulations with 10^2 atoms are hardly feasible, and only for

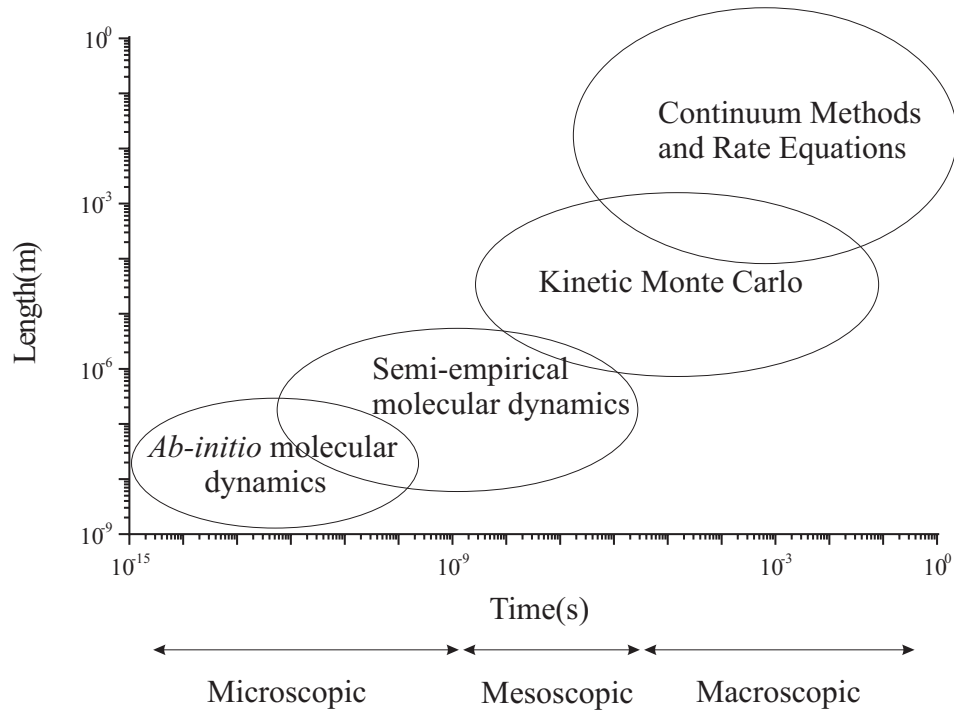


Figure 2.1: Overview of the different ranges of applications for epitaxial simulation methods. Density functional theory is for static calculations with a number of atoms $N \leq 10^3$. *Ab initio* molecular dynamics for $t \leq 10$ ps and $N \leq 10^3$. Semi-empirical MD $t \leq 1$ ns and $N \leq 10^3$. KMC is for $1 \text{ ps} \leq t \leq 1 \text{ hour}$ and length scale $L \leq 10^3 \mu\text{m}$. Rate equations for $0.1 \text{ s} \leq t \leq \infty$ and for any length scale. Continuum equations are for $1 \leq t \leq \infty$ s and $L \geq 10$ nm.

very short times). Instead of following with a MD simulation the entire trajectory of a particle moving from one minimum of the PES to another one, it can be easier to describe the process by a transition rate. This is what is done in **Transition State Theory** (TST) as shown in Sec. 2.1.2. The transition rates obtained with TST are in agreement with MD simulations as long the energy barrier is significantly larger than the thermal energy. In this case the motion of the particle on the PES is a stochastic process as mentioned in Sec. 2.1.2 and it can be correctly described by rates.

On the **mesoscopic scale** (characteristic length of $\approx 10^{-6}$ m or larger and time scales of $\approx 10^0$ s) other methods are better suited. Three main methods will be described in Sec. 2.2: Rate equations, Continuum equations, and Kinetic Monte Carlo. Approaches based on **Rate equations** (see Sec. 2.2.1 and Ref. [21]) are sufficiently fast and can be used to describe growth on the mesoscopic scale. Rate equations provide information only about the adatom density and the density of the islands but do not provide any morphological information about the growing surface. Besides this, Rate equations use empirical parameters, which are hard to relate to a microscopic picture (or to microscopic processes). Rate equations are generally used for time scales longer than 0.1 s and for arbitrary length scales. Rate equations are a deterministic method, i.e., no random numbers are used. They are often used to estimate statistical quantities such as island density and island size distributions. **Continuum equations** (see Sec. 2.2.3 and Ref. [4]) are also suited to describe growth on the mesoscopic scale. They are used for length scales larger than 10 nm. The continuum equations are solved numerically on a discrete grid and for each grid point a differential equation has to be solved. In this way the time evolution of the growing surface (surface morphology) can be directly analyzed. Continuum methods are more elaborate than Rate equations: they are stochastic equations with a noise term, and based on empirical parameters. They are often used to evaluate surface roughness. The probably most widely used method for mesoscopic growth simulations is the **kinetic Monte Carlo (KMC)** method (see Sec. 2.2.4 and [22–26]). The range of applications is between 1 ps up to hours and for system sizes smaller than 1 μ m. KMC is computationally more expensive than Rate equations and continuum methods but it has the great advantage that the parameters used are directly related to microscopic quantities/processes which can be obtained from *ab initio* calculations. KMC is a completely stochastic method.

In the last years new methods have been developed with the goal to reduce the simulation time. In Sec. 2.2.5 the **Level Set method** is described (see also Ref. [27]). It is a hybrid method that describes diffusion in a deterministic way and nucleation in a stochastic way. It is a continuous method in the x and y direction and discrete in the z direction. Another approach has been proposed in a paper by Montalenti et al. who developed a method called **Temperature Accelerated Dynamics (TAD)**. This method boosts the efficiency by several orders of magnitude with respect to ordinary molecular dynamics [28]. Noteworthy is also the work of Henkelman et al. who developed the **dimer method** (Ref. [29]) to determine the saddle points of the different processes and used this method together with KMC (Ref. [30]) to reach large-scale simulations.

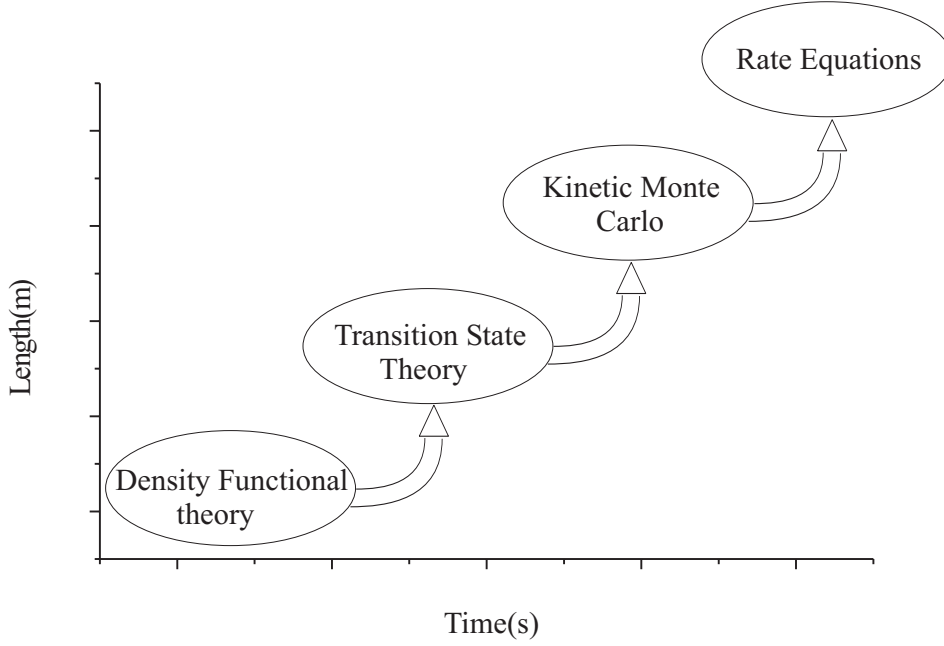


Figure 2.2: Scheme of a multiscale method. From density functional theory it is possible to calculate the kinetic parameters (diffusion barriers E_b , desorption barriers E_{dep} , etc.) which are the input for transition state theory (TST). TST provides the hopping rates Γ_i which can be used in a KMC simulation to obtain the captures numbers σ_i . Finally the capture numbers σ_i can be plugged into the Rate equations.

As epitaxial growth spans over more than 10 orders of magnitude a **multiscale method** is needed to describe the growth process as a whole. Unfortunately none of the previous methods can achieve this task. This could be possible only using different methods together as illustrate in Fig. 2.2. From DFT calculations it is possible to find the PES of the system one is interested in. The PES can be used to calculate the energy barriers for the different processes, which can be used as input for the Transition State Theory to get as output the hopping rates of the adatoms on the surface. These hopping rates are the input for KMC simulations, from which one can get e.g. the capture numbers which can be used as input for Rate equations calculations. In this way it would be possible to simulate the growth from the atomistic level up to typical length scales of devices fabrication.

2.1 Microscopic methods for crystal growth

2.1.1 Ab initio calculation

On the most fundamental level crystal growth is a dynamic many body problem. The system is composed of electrons and nuclei, which follow the principles of quantum mechanics. A system of N_e electrons with coordinates $\{\mathbf{r}_i\}$ and N_I ions (nuclei) with coordinates $\{\mathbf{R}_I\}$

will be considered here. The Hamiltonian for this system in atomic units is:

$$H = \sum_i^{N_e} \frac{\mathbf{p}_i^2}{2m_i} + \sum_I^{N_I} \frac{\mathbf{P}_I^2}{2M_I} + V_{ee}(\{\mathbf{r}_i\}) + V_{eI}(\{\mathbf{r}_i\}, \{\mathbf{R}_I\}) + V_{II}(\{\mathbf{R}_I\}) \quad . \quad (2.1)$$

The first two terms are the kinetic energies for electrons and nuclei and the last three terms are respectively the Coulomb contributions given by the electron-electron, electron-nucleus and nucleus-nucleus interaction. Further on the kinetic terms for electrons and nuclei will be respectively called T_e and T_N . The evolution in time of this many body problem is given by the time dependent Schrödinger equation:

$$-\frac{\hbar}{i} \frac{\partial \Psi(\{\mathbf{r}_i\}, \{\mathbf{R}_I\}, t)}{\partial t} = H \Psi(\{\mathbf{r}_i\}, \{\mathbf{R}_I\}, t) \quad . \quad (2.2)$$

$\Psi(\{\mathbf{r}_i\}, \{\mathbf{R}_I\}, t)$ is the many body wave function. This kind of calculations in which the entire system is treated on the basis of first principles of quantum mechanics, without the need to introduce any empirical parameters is called "*first principles*" or "*ab initio*" calculations. To solve Eq. (2.2) for large systems (such as crystal growth) is computationally way too expensive. It is therefore common to apply several (well justified) approximations. The first is based on the fact that the electron mass is orders of magnitudes ($\approx 10^3$) smaller than that of the nuclei. In such a case, where the change in the electronic state occurs fast compared to nuclear motion, the assumption that the electrons are always in the ground state holds generally. This is called the **Born-Oppenheimer** adiabatic approximation [31]. Using this approximation, one can completely separate the calculation of the electronic structure from that of the ionic motion and perform the two calculations separately at each step. This is the basis of the usual *ab initio* molecular-dynamics method. To calculate the total energy E of the system one has to solve the many body equation

$$H(\{\mathbf{r}_i\}, \{\mathbf{R}_I\})\psi(\{\mathbf{r}_i\}) = E(\{\mathbf{R}_I\})\psi(\{\mathbf{r}_i\}) \quad (2.3)$$

To solve Eq. (2.3) a number of efficient methods have been developed which tremendously simplify the many body wave function $\psi(\{\mathbf{r}_i\})$ by decomposing it into a set of one particle wave functions. In the **Hartree method** the many particle wave function is approximated as a product of one particle wave functions:

$$\psi(\{\mathbf{r}_i\}) = \prod_i \phi_i(\mathbf{r}_i) \quad . \quad (2.4)$$

This corresponds to assuming that the particles are non-interacting. Actually the electrons are fermions and they follow the Pauli principle. For this reason, a better approximation is the **Hartree-Fock** method where an antisymmetric wave function is introduced, which is given by a Slater determinant:

$$\psi(\{\mathbf{r}_1 \dots \mathbf{r}_N\}) = \frac{1}{\sqrt{N!}} \begin{vmatrix} \phi_1(\mathbf{r}_1) & \phi_2(\mathbf{r}_1) & \dots & \phi_n(\mathbf{r}_1) \\ \phi_1(\mathbf{r}_2) & \phi_2(\mathbf{r}_2) & \dots & \phi_n(\mathbf{r}_2) \\ \dots & \dots & \dots & \dots \\ \phi_1(\mathbf{r}_N) & \phi_2(\mathbf{r}_N) & \dots & \phi_n(\mathbf{r}_N) \end{vmatrix} \quad . \quad (2.5)$$

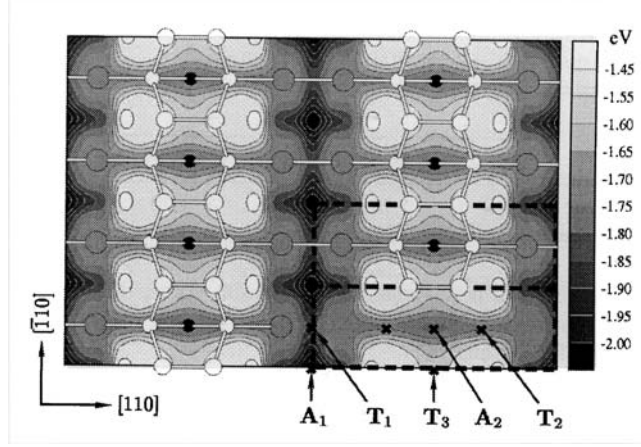


Figure 2.3: PES for an In adatom on the $\text{In}_{2/3}\text{Ga}_{1/3}\text{As}(001)-(1 \times 3)$ surface after Ref. [34].

Here N is the number of particles. A more accurate method, which takes into account the electronic interactions, is the **Density-Functional Theory (DFT)** in which the ground state properties of the electronic system are entirely determined by its electron density.

To study the diffusion of adatoms on the surface during growth it is important to calculate the **potential-energy surface (PES)** which is the potential energy experienced by an adatom diffusing on the surface. The PES has been calculated e.g. for GaAs(001) (see [32]) or for GaN(0001) and (000 $\bar{1}$) in Ref. [33]. In Fig. 2.3 the PES for InGaAs is shown. The PES can be obtained with *ab initio* methods calculating the total energy of the ground state for the system formed by the adatom and the surface on which it is diffusing:

$$E^{EPS}(X_{ad}, Y_{ad}) = \min_{Z_{ad}} \min_{\{R_I\}} E(X_{ad}, Y_{ad}, Z_{ad}, \{R_I\}) \quad (2.6)$$

where $E(X_{ad}, Y_{ad}, Z_{ad}, \{R_I\})$ is the ground-state energy of the many-electron system (also called total energy) for the atomic configuration of the adatom (X_{ad}, Y_{ad}, Z_{ad}) and of the surface atoms ($\{R_I\}$). The PES is the minimum of the total energy with respect to the z -coordinate of the adatom Z_{ad} and all the coordinates of the surface atoms $\{R_I\}$.

2.1.2 Transition state theory

When an adatom is adsorbed at a site on the surface it has a certain thermal energy. Due to this thermal energy the adatom vibrates around the adsorption site and eventually can escape from this local minima to a neighboring site. Neglecting the vibrational effects, the minima of the PES represent stable and metastable sites for the adatom. To jump from one site to another an adatom must have enough energy to overcome the saddle point between two minima. The energy difference between the minimum and the saddle point is called energy barrier E_b , as it is illustrated in Fig 2.4.

Two different time scales determine this process: the time $1/\Gamma$ an adatom waits before escaping the potential well and the characteristic period $1/\Gamma_0$ of the adatom oscillations

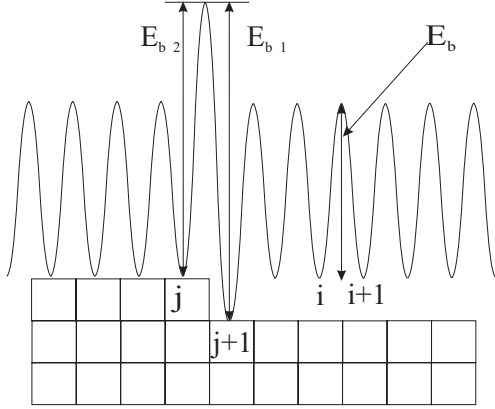


Figure 2.4: Schematic illustration of the lattice potential and its microscopic origin. The energy barrier E_b separates two stable sites.

in the well. If the energy barriers E_b are larger than the thermal energy of the particles $E_b \gg k_b T$, then $1/\Gamma \gg 1/\Gamma_0$ and the adatom motion will be a stochastic process, which can be described as a 2D random walk on a regular network Ref. [35, 36]. The sites of this network correspond to the minima of the PES. Under these conditions the diffusion can be described by rates, i.e., by the probability that the event occurs per unit time. This statistical tool, called transition state theory, has its origin in Eyring's absolute Rate Theory [37, 38]. Using **transition state theory (TST)** (see e.g. Refs. [37, 39–41]) it is possible to write the transition rate $\Gamma_{i,i+1}$ for the process of an adatom to move from site i to site $i + 1$ (see Fig. 2.4) as:

$$\Gamma_{i,i+1} = \frac{k_b T}{h} e^{-\frac{\Delta F}{k_b T}} \quad . \quad (2.7)$$

Here k_b is the Boltzmann constant, h is the Planck constant, T is the temperature and ΔF is the difference in the Helmholtz free energy between the maximum (saddle point) and the minimum (equilibrium site) of the potential curve along the reaction path of the process. The free energy ΔF of activation needed by the system to move from the initial position to the saddle point is given by:

$$\Delta F = E_b - T \Delta S_{vib} \quad . \quad (2.8)$$

Here E_b is the sum of the differences in the static total and vibrational energy of the system with the particle at the minimum and at the saddle point, and ΔS_{vib} is the analogous difference in the vibrational entropy. The rate of the process can be cast as follows:

$$\Gamma_{i,i+1} = \Gamma_0 e^{-\frac{E_b}{k_b T}} \quad . \quad (2.9)$$

Here $\Gamma_0 = \frac{k_b T}{h} e^{-\frac{\Delta S_{vib}}{k_b}}$ is the effective attempt frequency and as it will be shown in the following, it is temperature independent. The two basic quantities in Eq. (2.9) are the

attempt frequency $\Gamma_{i,i+1}$ and the activation energy E_b . The transition rate $\Gamma_{i,i+1}$ depends on the initial position i and on the final position $i+1$. In the case shown in Fig 2.4 the energy barrier E_b to move from $i \rightarrow i+1$ is the same as that from $i+1 \rightarrow i$, because the surface is flat, so that $\Gamma_{i,i+1} = \Gamma_{i+1,i}$. This is in general not the case as one can see e.g. for $\Gamma_{j,j+1}$ and $\Gamma_{j+1,j}$. Here there is a step site and the energy barriers are not the same $E_{b1} \neq E_{b2}$. The energy barriers can be calculated from the PES or by using a more crude approximation as e.g. by the bond-cutting method described in Sec. 2.2.4. The TST allows an evaluation of Γ_0 within the harmonic approximation. In this case the linear temperature dependence of Γ_0 is compensated by the term ΔS_{vib} (see Ref. [42,43]), thus, as mentioned before, Γ_0 results independent of the temperature:

$$\Gamma_0 = \frac{\prod_{j=1}^{3N} \nu_j}{\prod_{j=1}^{3N-1} \nu_j^*} \quad . \quad (2.10)$$

Here ν_j and ν_j^* are the normal mode frequencies of the system with the adatom at the equilibrium site and at the saddle point, respectively, and $3N$ is the number of degrees of freedom. Experimentally the attempt frequency Γ_0 shows a much weaker temperature dependence than the exponential and for typical growth temperatures it is of the order of $10^{12} - 10^{13}$ 1/s, which is a typical surface phonon frequency (see Ref. [44]).

2.2 Mesoscopic methods for crystal growth

On a mesoscopic scale growth can be considered as a stochastic process. Stochastic processes, stochastic variables and Markov processes are key concepts for the rest of the work presented here. A small digression will be made here to define these concepts. A stochastic variable X is defined by specifying:

1. The set of possible values (called "range", "set of states", "sample state" or "phase space");
2. The probability distribution over this set.

Once a stochastic variable X has been defined, an infinity of other stochastic variables derives from it, namely all quantities Y that are defined as function of X by some mapping f . These quantities Y may be any kind of mathematical object, in particular also functions of an additional variable t ,

$$Y_X(t) = f(X, t) \quad . \quad (2.11)$$

Such a quantity $Y(t)$ is called a random function, or, since in most cases t stands for time, a **stochastic process**. Thus a stochastic process is simply a function of two variables, one of which is the time t , and the other a stochastic variable X .

The atoms can be considered in our model as balls or cubes jumping over the surface

with a given probability. A possible configuration of the system is denoted by C and the space of all the possible configurations in a statistical mechanical model by $S = \{C\}$. S is a stochastic variable which can assume different C values/configurations. The probability that S is in the configuration C at time t is given by $P(C, t)$, which is a stochastic process. If a stochastic process has the property that the probability $P(C_t, t)$, to find the system at time t in the configuration C_t , depends only from the previous configuration C_{t-1} and not from the other configurations $C_{t-2}, C_{t-3}, \dots, C_{t-i}$, than it is a Markov process. To define more rigorously a Markov process, first the conditional probability will be defined.

The **conditional probability** $P(y_2, t_2|y_1, t_1)$ is the probability density for the stochastic variable Y to take the value y_2 at t_2 given that its value at t_1 is y_1 . More generally one may fix the values of Y at k different times t_1, \dots, t_k and ask for the joint probability at l other times t_{k+1}, \dots, t_{k+l} . This leads to the general definition of the conditional probability $P_{l|k}$:

$$\frac{P_{l|k}(y_{k+1}, t_{k+1}; \dots; y_{k+l}, t_{k+l} | y_1, t_1; \dots; y_k, t_k) = P_{k+l}(y_1, t_1; \dots; y_k, t_k; y_{k+1}, t_{k+1}; \dots; y_{k+l}, t_{k+l})}{P_k(y_1, t_1; \dots; y_k, t_k)} \quad (2.12)$$

Here $P_k(y_1, t_1; \dots; y_k, t_k)$ is the probability that the variable Y assumes the value y_k at t_k and y_{k-1} at t_{k-1} and so on till y_1 at t_1 . The subscript k indicates that the probability depends on k different times. Using this notation the conditional probability $P(y_2, t_2|y_1, t_1)$ can also be written as $P_{1|1}(y_2, t_2|y_1, t_1)$.

The **Markov processes** are a subclass of stochastic processes and they are by far the most important in physics and chemistry. A Markov process is defined as a stochastic process with the property that for any set of n successive times (i.e., $t_1 < t_2 < \dots < t_n$) one has

$$P_{1|n-1}(y_n, t_n | y_1, t_1; \dots; y_{n-1}, t_{n-1}) = P_{1|1}(y_n, t_n | y_{n-1}, t_{n-1}) \quad (2.13)$$

That is, the conditional probability density at t_n , given the value y_{n-1} at t_{n-1} , is uniquely determined and is not affected by any knowledge of the values at earlier times. A Markov process is fully determined by the two functions $P_1(y_1, t_1)$ and $P_{1|1}(y_2, t_2|y_1, t_1)$; the whole hierarchy can be reconstructed from them. Indeed, one has for instance, taking $t_1 < t_2 < t_3$,

$$\begin{aligned} P_3(y_1, t_1; y_2, t_2; y_3, t_3) &= P_2(y_1, t_1; y_2, t_2) P_{1|2}(y_3, t_3 | y_1, t_1; y_2, t_2) = \\ &= P_1(y_1, t_1) P_{1|1}(y_2, t_2 | y_1, t_1) P_{1|1}(y_3, t_3 | y_2, t_2) \quad (2.14) \end{aligned}$$

Continuing this algorithm one finds successively all P_n . This property makes Markov processes manageable, which is the reason why they are so useful in many applications.

The Markov property states that to make predictions of the behavior of a system in the future, it suffices to consider only the present state of the system and not the past history. For this reason one can say that no memory effects are present in a Markov process. The Markov processes are the next more complicated class of stochastic processes beyond the notion of fully uncorrelated processes.

If the energy barrier ΔE , that the atoms have to overcome, to move from one minimum of the PES to another one, is way larger than the thermal energy of the atoms, $\Delta E \gg k_b T$, then the atoms oscillate a long time around their equilibrium position before a successful event takes place and the atom jumps to another minimum. When the atom jumps from one position to another one the system evolves from a configuration C to a configuration C' . During the time the atom oscillates around the equilibrium position it "forgets" its previous position/configuration C_{t-1} , which will not influence the next configuration C_{t+1} . Thus, under the condition that $\Delta E \gg k_b T$, crystal growth is a Markov process. Starting from the definition of the Markov process it is possible to derive the Chapman-Kolmogorov equation, whose differential version is called Master equation. The mathematical details to derive the Master equation for a Markov process are not trivial and are briefly outlined in Appendix A (see also Ref. [45, 46]). The important result is that to any Markov process corresponds a Master equation which is given by:

$$\frac{\partial P(C, t)}{\partial t} = - \sum_{C'} w(C \rightarrow C') P(C, t) + \sum_{C'} w(C' \rightarrow C) P(C', t) \quad . \quad (2.15)$$

Here $w(C \rightarrow C')$ is the transition probability from the configuration C to the configuration C' . This can be seen as the starting point for all the statistical mechanical methods on a lattice for crystal growth at the mesoscopic scale. As shown in Refs. [47, 48] a set of continuum equations can be derived directly from the Master equation. Finally, the KMC method can be seen as a direct realization of the Master equation and repeating KMC simulation over a large number of runs it is possible to evaluate the probability distribution. The Master equation plays a central role in this work since it provides a direct handle on the time evolution of the growing surface and will be discussed in more detail in Chapters 3 and 4.

2.2.1 Rate Equations

Rate equations are applied to study the time evolution of the adatom density, n_1 , and the density of islands of size s , n_s , for growth on a flat surface in the submonolayer regime. They are commonly used/derived for large systems over long times. The theory of Rate equations derives from the work of Smoluchowski [49, 50], and has been applied extensively to analyze not just growth and nucleation, but various other diffusion-mediated processes including coagulation and chemical reactions [51]. The application to crystal growth was developed in the sixties and seventies by Walton, Zinsmeister, Venables and others [52–56]. A new interest in Rate equations started with the invention of scanning tunneling microscopy (STM) [11], which allowed a direct observation of size and shapes

of islands formed at surfaces during growth. Rate equations are a **mean-field method** Ref. [57,58]. Generally, the mean-field approach ignores certain spatial correlations in the system. In the classical mean-field treatment of nucleation and growth Ref. [55, 59, 60], as well as recent refinements Ref. [61], the crucial mean-field assumption is that the local environment of each island is independent of its size and shape. Rate equations are a set of coupled differential equations for the adatom density n_1 and for the density of islands containing s atoms n_s .

Averaged adatom density and local adatom density

Two key concepts for the present work are going to be explained here, the adatom density $n_1(t)$ and the local adatom density $\rho(x, t)$. The **adatom density** is the number of adatoms per unit surface area. It is averaged over the entire surface, i.e., the adatom density does not depend on the position at the surface but has just a temporal dependence $n_1(t)$. The **Local Adatom Density** $\rho(x, t)$ is the adatom density at time t at position x . The local adatom density will be extensively used further on. The main idea of the Rate equation model is to eliminate the explicit calculation of the position of single adatoms by just considering their surface averaged densities. For this reason it is not possible to get any local information from this method. Rate equations use the average value of the adatom density instead of the local adatom density $\rho(x, t)$:

$$n_1(t) = \overline{\rho(x, t)} = \frac{1}{A} \int \rho(\mathbf{x}, t) d\mathbf{x} \quad . \quad (2.16)$$

Here A is the surface area. In the next chapter it will be described in detail the advantages and disadvantages of this "averaged" approach for the example of the nucleation term.

Method

To describe the Rate equations the case of irreversible growth with a **critical island size** $i^* = 1$ will be considered. The **critical island size** i^* (see Ref. [21]) is defined such that islands with more than i^* atoms are stable while smaller islands can still break up (see [58] for larger i^*):

$$\frac{dn_1}{dt} = F - 2D\sigma_1 n_1^2 - D \sum_{s \geq i^*+1} \sigma_s n_1 n_s \quad , \quad (2.17)$$

$$\frac{dn_s}{dt} = D\sigma_{s-1} n_1 n_{s-1} - D\sigma_s n_1 n_s \quad s \geq i^* + 1. \quad (2.18)$$

Here F is the deposition flux on the surface, D is the adatom diffusion coefficient and σ_s denotes the capture coefficient for an island of size s . The second and third term in Eq. (2.17) represent the nucleation and the attachment term. In chapter 3 the nucleation term will be considered in detail. From Rate equations it is possible to get the island

density or the island size distribution. The island density N and the average capture coefficient $\bar{\sigma}$ are given by:

$$N = \sum_{s \geq i^*+1}^{\infty} n_s \quad , \quad (2.19)$$

$$\bar{\sigma} = \sum_{s \geq i^*+1}^{\infty} \sigma_s n_s \quad . \quad (2.20)$$

Summing over s in Eq. (2.18) one gets the differential equation for the island density. In this way the system can be described with just two equations: one for the adatom density n_1 and one for the island density N . The Rate equations can be rewritten as:

$$\frac{dN}{dt} = D\sigma_1 n_1^2 \quad (2.21)$$

and

$$\frac{dn_1}{dt} = F - 2\sigma_1 D n_1^2 - D\bar{\sigma} n_1 N \quad . \quad (2.22)$$

Eq. (2.21) states that the number of islands increases due to the fact that new islands are formed by monomer coalescence. Thus, the growth rate is proportional to the probability that a monomer meets another monomer, which is given by Dn_1^2 . Eq. (2.22) describes the variation in the number of monomers. The monomer density is fueled continuously by the deposition process, incorporated in the first term of the equation. However, the number decreases, due to the dimer formation, with a rate proportional to n_1^2 . The factor of two accounts for the fact that two monomers form a dimer which for $i^* = 1$ is stable and can thus be considered as island. The second mechanism leading to a decay in n_1 is the capture of the monomers by islands. Thus the rate is proportional to the island density and monomer density. A numerical solution for the Rate equations is given in Appendix C.

2.2.2 Scaling Laws

The fact that for different fluxes and coverages the observed island morphologies are somewhat similar suggests that scaling laws may be useful in quantitatively characterizing the model. Therefore the basic elements of a scaling theory describing the island formation and distribution will be discussed here following Ref. [62].

Island density

In order to study Eq. (2.21) and (2.22), it is convenient to write them in dimensionless units, introducing the typical length and time scales for monomer motion:

$$l_1 = \left(\frac{D}{F}\right)^{1/4} \quad , \quad t_1 = \frac{1}{(DF)^{1/2}} \quad . \quad (2.23)$$

Rewriting the Rate equations using dimensionless variables $\tilde{t} \equiv t/t_1$, $\tilde{n} \equiv nl_1^2$, $\tilde{N} \equiv Nl_1^2$, it results:

$$\frac{d\tilde{N}}{d\tilde{t}} = \tilde{n}_1^2 \quad , \quad (2.24)$$

$$\frac{d\tilde{n}}{d\tilde{t}} = 1 - 2\tilde{n}_1^2 - \tilde{N}\tilde{n} \quad . \quad (2.25)$$

For sufficiently short times such that $\tilde{t} \ll 1$ or equivalently $\theta \ll \sqrt{\frac{F}{D}}$ (it is assumed here that $\frac{D}{F} \gg 1$ so that $\theta \ll 1$ where θ is the coverage) the density of both monomers and islands is small compared to the unit in Eq. (2.25), so the last two terms in Eq. (2.25) can be neglected. This gives

$$n_1 \sim Ft = \theta \quad (2.26)$$

and Eq. 2.21 gives:

$$N \sim F^2 Dt^3 \quad (2.27)$$

At larger times, the number of monomers decreases, while the density of islands gets larger. This is supported by Eq. (2.26) and (2.27), which show that N increases much faster than n_1 . Thus one can take $n_1 < N$ and the second term in Eq. 2.22 can be neglected. These terms are relevant when they become comparable with the first term, i.e. when $Nn_1 \approx \frac{F}{D}$, so that

$$n_1 \approx \frac{F}{\bar{\sigma}DN} \quad . \quad (2.28)$$

Plugging this expression in Eq. 2.21 one gets for the island density

$$N \approx \left[3 \frac{\sigma_1}{\bar{\sigma}^2} \frac{F}{D} \theta \right]^{1/3} \quad . \quad (2.29)$$

In general, for a critical island size i^* the island density N scales as (see Ref. [63]):

$$N \sim \left(\frac{F}{D} \right)^\chi \quad . \quad (2.30)$$

Here $\chi = \frac{i^*}{i^*+2}$. This is a central result of nucleation theory. Fig. 2.5 shows the variation of the monomer and island densities, obtained with KMC simulations, as function of coverage. Four distinct regimes are found:

Low coverage regime (L): At early times, the coverage and the typical island size are both small, so the predictions of the Rate equations (2.21) and (2.22) should be valid. From Eq. 2.26, one can see that there is a linear increase in the monomer density, while the island density increases as t^3 . This regime is expected to hold if $t \ll (DF)^{-1/2}$. Indeed, as Fig. 2.5 illustrates, for early times one can see a much faster increase in N than n_1 .

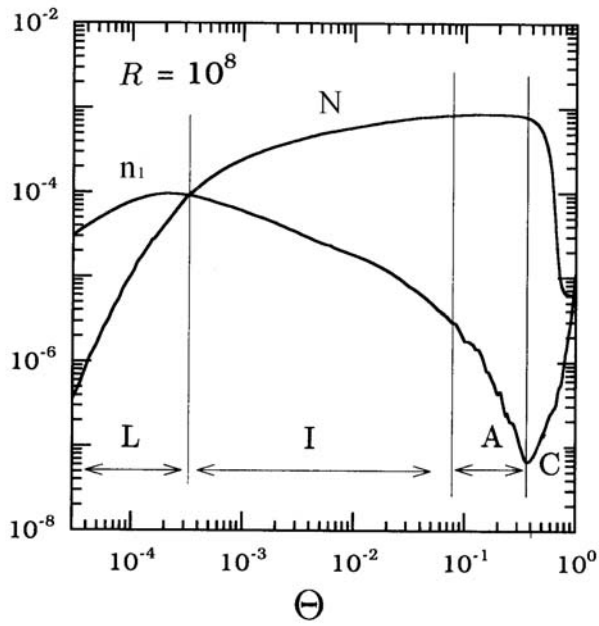


Figure 2.5: Log-Log plot of the unscaled island density N and monomer density n_1 as a function of coverage θ for $\frac{D}{F} = 10^8$ [63]. One can distinguish four different scaling regimes: low coverage (L), intermediate coverage (I), aggregation (A), coalescence (C).

Intermediate coverage regime (I): When the density of islands becomes comparable with the monomer density, the Rate equations predict a slowing down in the increase of the island density. More precisely, Eq. 2.29 implies that the island density N increases as $t^{1/3}$, while the monomer density n_1 decreases as $t^{-1/3}$. This indeed can be observed in Fig. 2.5.

Aggregation regime (A): As the size of the islands becomes comparable with the distance between them, Rate equations are insufficient to describe the scaling properties of the system. The scaling behavior in this regime is quite complicated. The onset of this regime is signaled by a rapid decrease in the monomer density, and a plateau of the island density. In this regime, it is possible to observe a "fattening" of the islands by capturing the diffusing monomers, without further island creation. However, as the islands grow, they coalesce, and eventually percolate across the entire system.

Coalescence regime (C): Finally, the number of islands decreases drastically, since they will form a single huge cluster. The coverage approaches a full layer, and cluster formation on the top of this layer becomes relevant.

Island size distribution

Here the concentration of islands n_s as a function of the island size s will be studied. In particular, the case in which the average island size \bar{s} is way larger than 1 will be considered:

$$\bar{s} = \frac{\theta}{N} \gg 1 \quad . \quad (2.31)$$

Further a coverage $\theta \ll 1$ is assumed to avoid island coalescence. For this reason the island density must be low ($N \ll \theta \ll 1$) and this is obtained for large values of D/F . The island size distribution was first calculated by Zinsmeister [52]. Bartelt and Evans were the first to propose a scaling law for the island size distribution [62]. They postulated that the dependency of the island size distribution n_s from coverage θ , diffusion D and deposition F enters only via the average island size \bar{s} . One can thus write:

$$n_s = N_c f\left(\frac{s}{\bar{s}}\right) \quad . \quad (2.32)$$

Here, N_c is a normalization constant which is determined by the following summation rules:

$$\sum_{s=i^*+1}^{\infty} s n_s \approx N_c \bar{s}^2 \int_0^{\infty} dx x f(x) = \theta \quad . \quad (2.33)$$

This is fulfilled for $N_c = \theta/\bar{s}^2$ and

$$N^{-1} \sum_{s=i^*+1}^{\infty} s n_s \approx \bar{s} \left[\int_0^{\infty} dx f(x) \right]^{-1} \int_0^{\infty} dx x f(x) = \bar{s} \quad . \quad (2.34)$$

The function f has (besides the condition 2.33) also to fulfill:

$$\int_0^\infty dx f(x) = 1 \quad . \quad (2.35)$$

Writing down the scaling function f using the normalization rules Eqs. (2.33) and (2.35) one gets:

$$n_s = \frac{\theta}{s^2} f\left(\frac{s}{s}\right) \quad . \quad (2.36)$$

It should be noted that Rate equations fail to describe the right behavior of the island size distribution. As shown in Ref. [7, 62, 64] this is due to the assumption of a constant capture coefficient.

2.2.3 Continuum methods

Crystal growth can be described by stochastic differential equations [4]. These equations give the time evolution of the epitaxial layer height $h(x, t)$ at any position x . Continuum approaches model the surface on a coarsed-grained scale, on which every property is averaged over a small volume containing many atoms. Neglecting the discrete nature of growth processes, continuum theories attempt to capture the essential mechanisms determining the growth morphology. Their predictive power is limited to length scales larger than the typical interatomic distances. They provide information on the collective nature of the growth process, such as the variation in the interface or correlation functions. An overview about continuum methods can be found in Ref. [65]. A first approach was proposed by Edwards and Wilkinson in 1982 Ref. [66]:

$$\frac{\partial h(x, t)}{\partial t} = \nu \nabla^2 h(x, t) + \eta(x, t) \quad . \quad (2.37)$$

Here ν is called the surface tension because the term $\nu \nabla^2 h$ tends to smooth the surface and η is a noise term. This equation is called **Edwards-Wilkinson (EW)** equation and it corresponds to a growth model in which the particles are randomly deposited on the surface and where they after deposition can diffuse over a finite distance. Eq. (2.37) is linear and it is valid in the small gradient approximation, i.e., $\nabla h \ll 1$. Eq. (2.37) can be extended to include non-linear contributions. This is the case for the **Kardar-Parisi-Zhang (KPZ)** equation [67]:

$$\frac{\partial h(x, t)}{\partial t} = \nu \nabla^2 h(x, t) + \lambda (\nabla h(x, t))^2 + \eta(x, t) \quad . \quad (2.38)$$

Here the non-linear term $(\nabla h)^2$ is responsible for lateral growth. These continuum models contain more information than the Rate equations because they describe the surface morphology also locally. However, the description is on a coarsed-grained scale rather than on the atomic scale. A problem of this approach is that it still relies on empirical

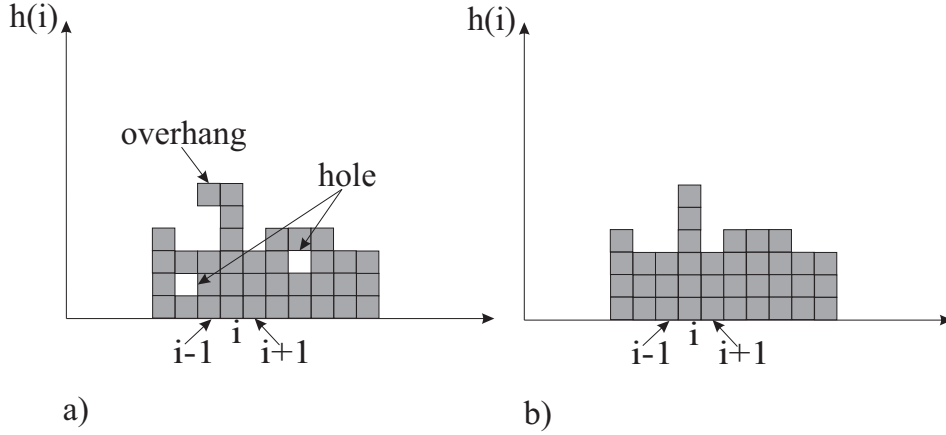


Figure 2.6: (a) Schematic side view of a general model where overhangs and holes are allowed. (b) Same for the solid on solid model - the surface is completely described by a single number (the number of atoms on site i which gives the height).

parameters that are not related to specific microscopic processes and thus cannot be calculated from *ab initio* principles. Continuum methods can be applied in the case where there is three-dimensional growth with non zero roughness. They fail e.g. to describe high temperature step flow growth or low temperature fractal growth. Modeling these growth modes would require an atomic description of the system.

2.2.4 Kinetic Monte Carlo

A powerful method for crystal growth simulations is the kinetic Monte Carlo (KMC) method. KMC is based on a statistical mechanical model for crystal growth, as described at the beginning of this section. One can schematically imagine the atoms as solid particles moving on the surface and their dynamic is described by probability rates. Many papers have been published about these methods (see e.g. Ref. [23–26, 68]). A general overview about KMC can be found in Ref. [2, 69, 70].

KMC has two main features: the geometrical part and the dynamical part. First the geometrical part will be discussed and then the dynamical part. From Eq. (2.6) one can find the minima of the PES as illustrated in Fig 2.3. KMC is a discrete method, the atoms occupy the minima of the PES. All the minima of the PES define a lattice, the atoms cannot occupy any place in space but just one of these minima. This corresponds to a lattice gas model with a lattice whose symmetry is the same as that of the crystal surface. A more crude approximation is sometimes done in KMC simulations: a simple cubic lattice is used, regardless of the symmetry of the crystal. Another approximation typically used in the implementation of KMC is the **solid on solid (SOS)** method (see Ref. [3]). This means, that each atom is sitting on top of another atom, no overhangs are allowed, and the surface can be described by a single valued function $h(i)$, which gives the number of atoms on site i , as illustrated in Fig 2.6.

The dynamics is represented by the different processes (like diffusion, deposition and

desorption) that take place on the surface. The key idea is that these processes can be described by rates. The atoms occupy lattice sites and they can jump from a site to another with a given rate. These rates are calculated using Eq. (2.9). The energy barriers in Eq. (2.9) can be obtained from the PES as calculated using Eq. (2.6). This has been done, e.g., for Al(111) by Bogicevic et al. [71]. Many different processes, with different energy barriers E_b , play a role in the growth process, as shown in Fig. 2.7. The activation temperatures for the processes involved have been calculated from the energy barriers E_b using the formula:

$$T_i = \frac{E_b/k_b}{\ln(\Gamma_0/\Gamma)} \quad . \quad (2.39)$$

The prefactor Γ has been chosen as $\Gamma = 1s^{-1}$.

KMC simulations use often a computationally simpler method —the **linear bond-cutting method**— to find the energy barriers [72]. This method is based on the idea that the energy of a many-electron system can be approximated in terms of the contributions from the individual atoms

$$E^{tot}(\{R_I\}) = \sum_I E_I \quad . \quad (2.40)$$

Here E_I is the contribution of the I -th atom. E_I depends on the local geometry of atom I . In the simplest approximation one can assume that E_I varies linearly with the coordination number (number of nearest neighbors occupied). In this way the strength of a bond is invariant with respect to the number of bonds an atom forms:

$$E_b = E_0 + nE_{\text{bond}} \quad . \quad (2.41)$$

Here E_0 is the energy barrier for the diffusion on the free surface, n is the number of nearest neighbors occupied and E_{bond} is the energy for each bond. Fig. 2.8 illustrates this concept. Using a characteristic set of parameters ($E_0 = 1$ eV, $E_{\text{bond}} = 1$ eV) the energy barriers and activation temperatures for a linear bond cutting model on a square lattice are shown.

This model is very popular and has been used e.g. in Refs. [73,74]. Γ^i are the rates for a possible surface process i , as defined in Eq. (2.9). A KMC simulation consists of 6 steps, repeated over and over again till the simulation time has been reached. The steps are shown in Fig 2.9:

1. Calculate the rate $\Gamma^i(C \rightarrow C_i)$ of all possible processes that can be realized for a given configuration.
2. Choose a random number r_1 between 0 and 1 and find the event l for which

$$\frac{\sum_{i=0}^{l-1} \Gamma^i}{\sum_i \Gamma^i} \leq r_1 < \frac{\sum_{i=0}^l \Gamma^i}{\sum_i \Gamma^i} \quad . \quad (2.42)$$

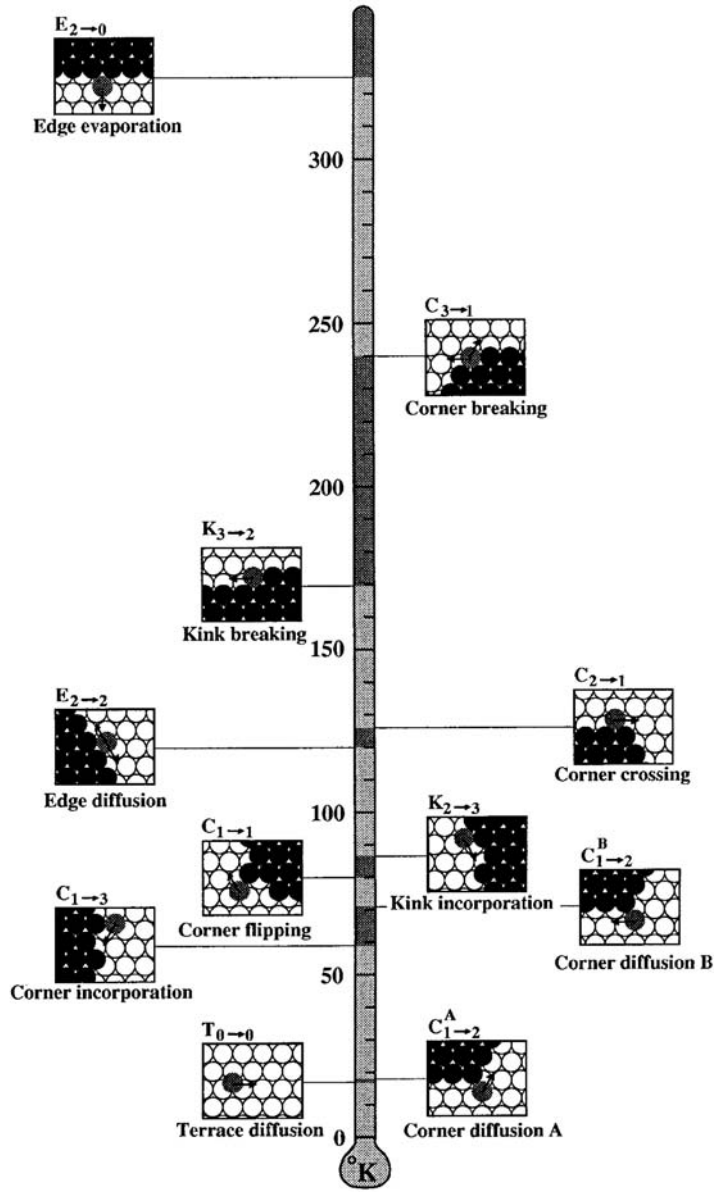


Figure 2.7: Temperature scale of Al(111) homoepitaxy of elementary diffusion processes, after Ref. [71].

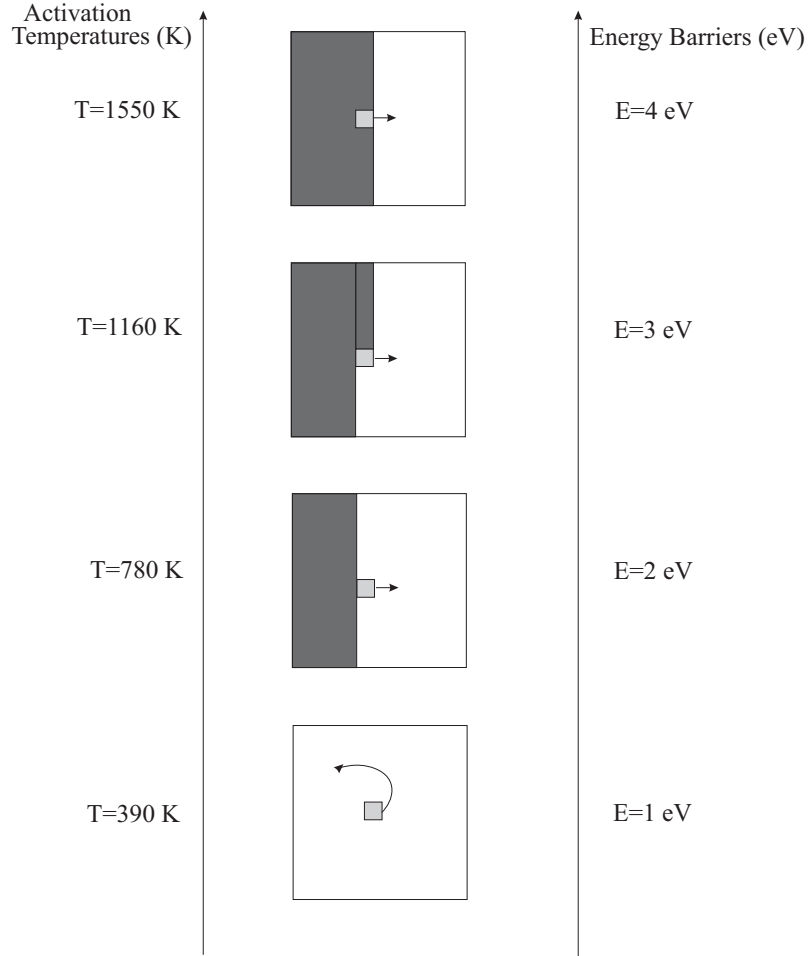


Figure 2.8: Energy barriers and activation temperatures for a linear bond cutting model on a square lattice. The parameters used here are $E_0 = 1$ eV and $E_{\text{bond}} = 1$ eV. Energy barriers and activation temperatures have been calculated according to Eqs. (2.41) and (2.39).

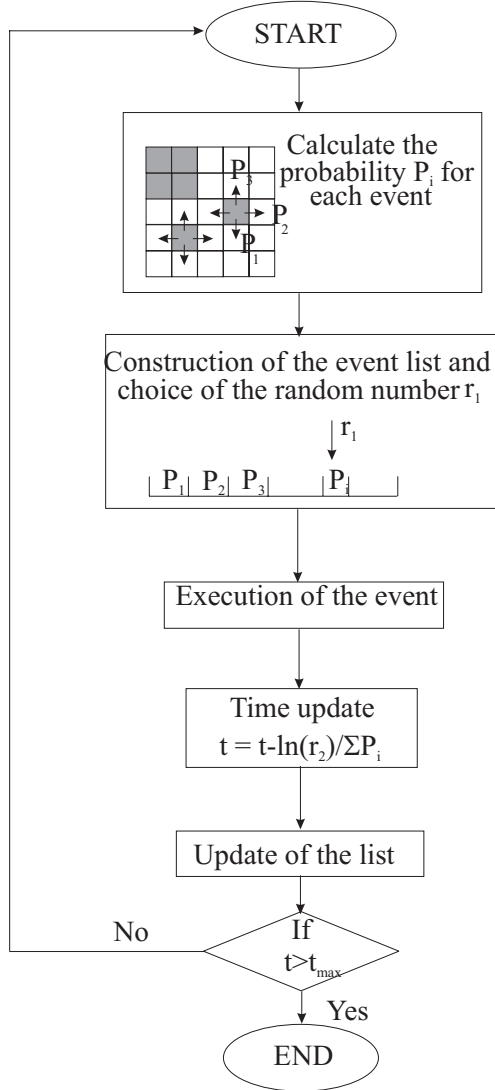


Figure 2.9: Flow-chart of a KMC simulation. First the probabilities P_i for each possible events are calculated. Then an event is selected randomly and executed. The time is incremented and the event list updated. The loop is repeated till the simulation time t_{max} has been reached.

3. Execute the event l (i.e., go from the initial configuration C to a new configuration C')
4. Increment the simulation time $t = t + \Delta t$.
5. Update of the list for the new configuration C' .
6. Check if the simulation time t_{max} has been reached.

An important issue is the choice of the **time step** Δt in step 4. Point processes will be introduced here to determine the time step. **Point processes** are processes in which at random times an event occurs such as the impact of raindrops on a surface or the impact of cosmic rays on a Geiger counter. Such processes are characterized by a sequence of random times (t_1, \dots, t_n, \dots) at which the events take place (for details see Appendix B). Also crystal growth is a point process because the diffusion, attachment and nucleation events take place at random times. In particular crystal growth is a Poisson process (see Ref. [22]). Now the following question arises: If the observation started at time $t = t_0$ how long on the average one has to wait for the next event? For a Poisson process it is known (see Appendix B) that the waiting time Δt between two events follows the distribution:

$$g(\Delta t, t_0) = \left(\sum_i \Gamma^i \right) e^{-\left(\sum_i \Gamma^i \right) \Delta t} \quad . \quad (2.43)$$

The time step Δt can be obtained applying the inverse transform method [75]. The inverse function of the integral $\int_0^{\Delta t} dt' g(t', t_0)$ yields $\Delta t = -\frac{\ln(1-\xi)}{\sum_i \Gamma^i}$ where ξ is a random number between zero and unity. To evolve in the physical time a random number $0 < \xi < 1$ is generated and the time step is calculated as:

$$\Delta t = -\frac{\ln(\xi)}{\sum_i \Gamma^i} \quad . \quad (2.44)$$

2.2.5 Hybrid methods: The Level Set Method

The Level Set technique was first introduced by Osher and Sethian (see Ref. [76–78] for details) and applied to the simulation of epitaxial growth by M.F. Gyure et al. (see Ref. [27]). The model is discrete in the growth direction, but continuum in the lateral directions and therefore, in principle, can describe growth on arbitrarily large lateral length scales. The goal of this method is to perform large scale simulations desired to optimize device fabrication, as described e.g. in Ref. [79]. The Level Set Method is based on the idea that islands and steps on a surface can be described through a curve Γ . This curve can be represented as the set $\phi = 0$, called the level set, of a smooth function ϕ , as shown in Fig. 2.10.

The evolution of ϕ in time is given by:

$$\frac{\partial \phi}{\partial t} + \mathbf{v} \nabla \phi = 0 \quad . \quad (2.45)$$

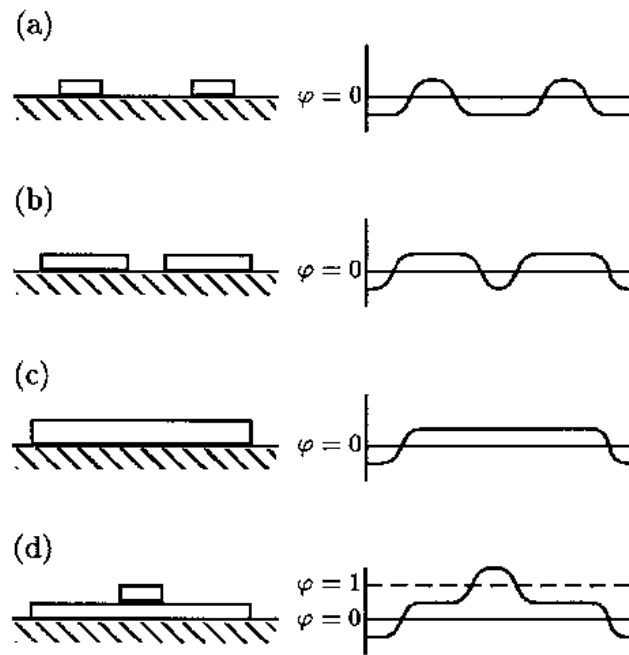


Figure 2.10: Schematic evolution of one dimensional island morphologies (left) and the corresponding level set function, ϕ (right): (a) two spatially separated islands; (b) the same islands at a later time, but before coalescence; (c) the islands after coalescence; and (d) the nucleation of a new island on top of the coalesced islands.

Here \mathbf{v} is the boundary velocity. $v = \hat{\mathbf{n}} \cdot \mathbf{v}$ is the normal component of \mathbf{v} and the vector $\hat{\mathbf{n}}$ points along the direction $\nabla\phi$. The velocity v is given by:

$$v = Da^2(\hat{\mathbf{v}} \cdot \nabla\rho^- - \hat{\mathbf{n}} \cdot \nabla\rho^+) \quad . \quad (2.46)$$

Here D is the adatom diffusion constant, a is the lattice constant, ρ is the adatom density, and the superscripts label the contributions from above (+) and below (-) the boundary (see Ref. [80]). The evolution of the adatom density is given by

$$\frac{d\rho}{dt} = F - D\nabla^2\rho - 2\frac{dN}{dt} \quad , \quad (2.47)$$

where F is the deposition flux, N is the island density and L is the system size. Further, it is assumed that $\rho = 0$ at all the island boundaries. Eq. (2.47) is a diffusion equation and it is similar to the equations derived for the adatom density as employed in Rate equations Eq. (2.22) and (2.21). The difference is that the adatom density $\rho(\mathbf{x}, t)$ in the level set method depends on the position while in Rate equations $n_1(t)$ contains just the time dependence as pointed out in Sec. 2.2.1. In Eq. (2.47) the second term describes the nucleation and it is given by the equation

$$\frac{dN}{dt} = D\sigma_1\langle\rho^2\rangle \quad . \quad (2.48)$$

Here $\langle\cdot\rangle$ defines the spatial average (i.e. $\langle\rho^2\rangle = \frac{1}{A}\int_A\rho^2(x, t)dx$). σ_1 is the adatom capture number. The nucleation term is just the same used in Rate equations except that in Rate equations no information regarding the position/arrangement of new islands exists. The position of the new island is found weighing each position by the local value of ρ^2 , other nucleation spatial dependencies have been tested in Ref. [80]. The Level Set Method is a hybrid method because it uses concepts from different methods: Rate equations, continuum methods and KMC. The adatom diffusion is described by the adatom density like in Rate equations, but at the same time it gives a local information about the surface morphology, similarly to a continuum method. Finally the nucleation is done in a stochastic way as in KMC. Extensive statistical tests have been performed for the Level Set Method in Ref. [81]. Applications of the Level Set Method to calculate capture numbers have been published in Refs. [82, 83]. A generalization of the method to include reversible growth has been presented in [84] and it has been applied to study homoepitaxial Ostwald ripening Ref. [85]. For a more fundamental discussion on Ostwald ripening see Ref. [86].

Chapter 3

An adatom density approach to nucleation and diffusion

Crystal growth involves a large number of particles (typically $\approx 10^4 \dots 9$). Instead of starting to study the entire growth process, the focus will first be set on the single processes that take place on the surface during growth. The two most important processes are diffusion and nucleation. In the previous chapter it has been shown how these elementary processes are described by the main growth simulation methods. The **aim** of this chapter is to show how to describe these two processes in an **adatom density picture**. A density approach can save CPU time when simulating these processes, compared to KMC. The results obtained here will be used in the next chapter, where density based kinetic Monte Carlo methods will be introduced. The first part of the chapter will be devoted to diffusion processes (Sec. 3.1) and the second to nucleation processes (Sec. 3.2).

The only **diffusion** process that will be treated here is the diffusion of a single adatom on the surface, the diffusion of dimers or more complicated structures will not be considered. Then, diffusion can be regarded as a single particle process because there are no interactions between two different particles that are diffusing on the surface. In this case it is straightforward to represent the diffusion process with an adatom density, in a similar spirit as used in the Level Set Method 2.2.5.

Nucleation is a process that happens when two or more adatoms come together and form a stable island. The traditional theoretical analysis of nucleation is provided by Rate equations. This is the simplest treatment of nucleation phenomena in crystal growth and it is based on the assumption (see Ref. [87]) that the nucleation rate $\frac{dN}{dt}$ is proportional to the square¹ of the stationary adatom density n_1 in the presence of a constant flux F . Eq. (2.21) presented already in the previous chapter is rewritten here:

$$\frac{dN}{dt} = D\sigma_1 n_1^2 \quad .$$

¹This is valid in the case that dimers are stable islands as introduced in Sec. 2.2.1

	Rate Equations	Level Set Method
Diffusion	averaged adatom density	local adatom density
Nucleation	averaged nucleation term	averaged nucleation term

Table 3.1: Comparison Rate Equations *vs.* the Level Set Method

Such a mean-field treatment (Ref. [88]) has been used to estimate physical parameters of materials Ref. [89–92]. The nucleation rate depends on the square of the adatom density n_1 because it is considered here that two adatoms coming together form a stable island. Recent works have appeared on the nucleation on top of islands and terraces [88,89,93–96], on the influence of the Ehrlich-Schwobel barrier [97,98], on the nucleation rate and on the limits of the mean-field approach to describe nucleation [13,96,99,100].

Besides Rate Equations another method based on an adatom density approach, is the Level Set Method (see Sec. 2.2.5). The Level Set Method uses a local adatom density $\rho(\mathbf{x}, t)$ to describe the diffusion processes but for the nucleation it uses the mean-field approach given in Eq. (2.21). In Table 3.1 a comparison between Rate Equations and the Level Set Method is shown: while Rate equations use an averaged adatom density to describe both processes (diffusion and nucleation) the Level Set Method uses a local adatom density for diffusion and an averaged for nucleation. To go a step further than the Level Set approach a method called Adatom Probability Kinetic Monte Carlo (AP-KMC) will be introduced here, in which both diffusion and nucleation will be treated with a local adatom density. This method is a density based KMC method. In this chapter the AP-KMC will be described for the diffusion and nucleation processes and in the next chapter it will be extended to construct a complete growth simulation.

The main results of this chapter will be:

1. The CPU time comparison between AP-KMC and KMC for diffusion processes, which shows that AP-KMC allows to significantly speed up the simulation.
2. The introduction of a local nucleation term based on the single adatom density. This nucleation term gives the probability for a nucleation event on each site on the surface. This is the first time to our knowledge that such a local nucleation term has been used.

In addition to the density approach, diffusion and nucleation will be treated with another method called Hyper Jump KMC (HJ-KMC). This method, which has been inspired by the density approach, is very promising and allows a further speed up of the simulation compared to AP-KMC.

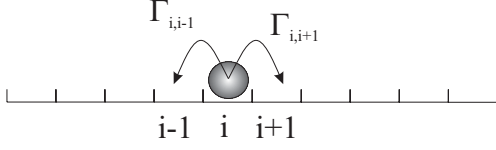


Figure 3.1: Schematic representation of the hopping process of an adatom. This can be described by a random walk. The particle can jump only to the next nearest lattice sites. $\Gamma_{i,i\pm 1}$ is the particle transition rate.

3.1 A Probability interpretation of Adatom Diffusion

In this section first the AP-KMC method for diffusion processes for the one-dimensional case will be derived from the Master equation. A CPU time comparison will show the advantage of AP-KMC over KMC. The method will then be extended to the two-dimensional case. In Sec. 3.1.4 the HJ-KMC will be presented.

3.1.1 Diffusion coefficient

To study adatom diffusion a model will be considered that consists of a single particle moving on a one- and two-dimensional discrete lattice as illustrated in Fig 3.1 for the one-dimensional case.

It is further assumed that the particle is executing a random walk. Then, if the position of the particle at time t is called $x(t)$ one gets (see for instance Ref. [101]):

$$\langle \Delta x(t) \rangle \equiv \langle x(t) - x(0) \rangle = 0 \quad (3.1)$$

and

$$\langle |\Delta x|^2 \rangle = a^2 N(t) \quad . \quad (3.2)$$

Here a is the step length and $N(t)$ the number of diffusion steps in time t . In two dimensions, assuming steps in the x and y directions to be independent of each other, one has

$$\langle (\Delta r)^2 \rangle \equiv \langle |r(t) - r(0)|^2 \rangle = a_x^2 N_x(t) + a_y^2 N_y(t) = a^2 N_{tot}(t) \quad . \quad (3.3)$$

Here N_x is the number of steps in the x direction and N_y in the y direction. If $a_x = a_y = a$ it results:

$$\langle (\Delta r)^2 \rangle = a^2 \Gamma t \quad (3.4)$$

where Γ is the transition rate (or jump rate). The diffusion coefficient D is defined as:

$$\langle (\Delta r)^2 \rangle = Dt \quad (3.5)$$

or in terms of Γ :

$$D = a^2 \Gamma \quad . \quad (3.6)$$

Using Eq. 2.9 D becomes

$$D = a^2 \Gamma_0 e^{-\frac{E_b}{k_b T}} \quad . \quad (3.7)$$

If the step length a is chosen equal to the unit length 1 than:

$$D = \Gamma \quad . \quad (3.8)$$

The calculation of the diffusion coefficient for a one-dimensional random walk and for more complicated cases in two and three dimensions on regular and disordered lattices is presented in Refs. [35,102,103]. For the further discussion the energy barrier E_b is assumed to be $E_b = 1.0$ eV. The value of the prefactor is $\Gamma_0 = 10^{13} \text{ s}^{-1}$ and the step length is set $a = 1$, thus $\Gamma = D$.

3.1.2 Master equation for diffusion processes

The diffusion of an adatom along a step can be represented by a random walk in one dimension. The adatom jumps from one minimum to a neighboring one of the PES. At each minimum it vibrates around the equilibrium position trying to overcome the energy barriers by which it is surrounded, as pointed out in Sec. 2.2. As the position of the adatom at time t depends only from the position the adatom had at time $t - \Delta t$ and not from the previous time steps, this process is a Markov process and it is described by the **Master equation** introduced in its general form in Eq. 2.15:

$$\frac{\partial P(C, t)}{\partial t} = - \sum_{C'} w(C \rightarrow C') P(C, t) + \sum_{C'} w(C' \rightarrow C) P(C', t) \quad .$$

The Master equation will be now written for the particular case of an adatom diffusing on the one-dimensional lattice. A configuration C is uniquely determined by the position of the adatom thus, $P(C, t) = \rho(i, t)$ where i gives the position of the adatom on the lattice. The nearest neighbor configurations are characterized by the adatom occupying the position $i - 1$ and $i + 1$. The transition rate from one configuration to another $w(C \rightarrow C')$ is given by the probability for the adatom to jump from site i to a nearest neighbor site Γ_i

$$w(C \rightarrow C') = \Gamma_i \quad (3.9)$$

and it can be calculated using Eq. (2.9). The Master equation for this model becomes:

$$\frac{\partial \rho(i, t)}{\partial t} = [\Gamma_{i+1} \rho(i + 1, t) + \Gamma_{i-1} \rho(i - 1, t) - 2\Gamma_i \rho(i, t)] \quad . \quad (3.10)$$

In the case the coefficients Γ_i are the same all over the surface (which is e.g. the case for an unreconstructed atomically flat surface) the previous equation can be written as:

$$\frac{\partial \rho(i, t)}{\partial t} = \Gamma [\rho(i + 1, t) + \rho(i - 1, t) - 2\rho(i, t)] \quad . \quad (3.11)$$

If the length of the vector is called L one can introduce the distance $\Delta x = \frac{(i+1)-i}{L}$. In case Δx is very small ($\Delta x \rightarrow 0$) x_i can be replaced by a continuum variable x . In the continuum limit Eq. (3.11) becomes the well known diffusion equation (for details see [45] p.286):

$$\frac{\partial \rho(x, t)}{\partial t} = \Gamma \nabla^2 \rho(x, t) \quad . \quad (3.12)$$

It will be further assumed that at time $t = 0$ an adatom is put on site $x = 0$, i.e., $P(x, 0) = \delta_{x,0}$. Then, Eq. (3.12) can be analytically solved (for details see Appendix D):

$$\rho(x, t) = \frac{1}{\sqrt{4\pi\Gamma t}} \exp^{-\frac{x^2}{4\Gamma t}} \quad . \quad (3.13)$$

This expression is a solution of Eq. (3.11) in the continuum limit case. Solutions of Eq. (3.11) in the discrete form can be obtained by solving numerically the set of equations (one for each lattice site) assuming e.g. periodic boundary conditions or by simulating the diffusion process with **KMC** over a large number of runs.² To solve numerically Eq. (3.11) one has to discretize the time to get:

$$\frac{\rho(i, t) - \rho(i, t - \Delta t)}{\Delta t} = \Gamma [\rho(i + 1, t) + \rho(i - 1, t) - 2\rho(i, t)] \quad . \quad (3.14)$$

Three different schemes to solve numerically this kind of equation are available: explicit, implicit and Crank-Nicholson (for details see Appendix E). The explicit scheme is the easiest to implement. The value of $\rho(i, t)$ at time t can be calculated from the values of $\rho(t - \Delta t)$ at time $t - \Delta t$. The disadvantage is that this method can become unstable and that a stability condition has to be considered for the time step Δt . The implicit method is more complicated than the explicit. The value of $\rho(i, t)$ depends also from the values of $\rho(i - 1, t)$ and $\rho(i + 1, t)$. For this reason a system of linear equations has to be solved. The advantage of the implicit method is that the solutions are stable for any Δt . This is the method we used for the simulations presented here. Finally the Crank-Nicholson method is also stable for any Δt and it is more accurate than a normal implicit method. In the present work the explicit method has been used.

3.1.3 Adatom Probability KMC for diffusion processes

The Adatom Probability KMC (**AP-KMC**) approach will be described here for the diffusion processes. In the next chapter other processes will be included in AP-KMC so that it can be applied to perform crystal growth simulations. The AP-KMC consists essentially of two steps:

1. Solve the difference equation for the adatom density
2. Collapse the adatom density

²As mentioned in Sec. 2.2 the KMC method can be used to solve the Master equation.

The **difference equation** can be **solved** to find the probability distribution for the adatom, as described in the previous section. The solution in the continuum limit is a Gaussian, if the diffusion coefficient D is constant everywhere or it can assume more complicated shapes in case D is position dependent.

To make a working approach it is necessary to use the calculated adatom density to find the final position of the adatom. This is done by **collapsing** the adatom density onto a single lattice site. This process is similar to a measurement process in quantum mechanics. Before the observation/measurement of the position of an electron, for example, the electron is described by a wave function $\psi(x, t)$ and the probability to find the electron at certain positions in space is given by $\psi(x, t)\psi^*(x, t)$. After measuring the position of the particle the wave function collapses—it is one at the measured position of the electron and zero anywhere else. This is valid in general for the measurement of any quantity in quantum mechanics, not only for the position of an electron. The collapse is performed by using a random number r between zero and one and finding the collapse site i so that:

$$\sum_{l=1}^i \rho(l) \leq r < \sum_{l=1}^{i+1} \rho(l) \quad . \quad (3.15)$$

Thus AP-KMC represents an alternative method to KMC to find the position of a particle after a given time t .

The time step in KMC is proportional to the inverse of the particle's diffusion coefficient (Eq. 2.44), which depends exponentially from the temperature (Eq 2.9). Thus, the CPU time of a KMC simulation scales exponentially with the temperature. Note that the CPU time of a KMC simulation does not depend on the size of the lattice that is considered, but just on the number of particles (in this case one) on the surface and their diffusion coefficients.

The solution of the difference equation for the adatom density is independent from the temperature because solving the equation with an implicit method the solutions are always stable. The CPU time scales linearly with the size of the lattice considered. For higher temperature larger lattices have to be considered because the particle is spreading out more and more. To have a lattice large enough to include all the significant part of the probability distribution, the lattice size L has to be proportional to the square root of D , $L \approx \sqrt{D}$ (times a factor two to include the 96% of the distribution) . Based on this scaling analysis it is expected that for temperatures high enough AP-KMC will be faster than KMC, because KMC is proportional to D while AP-KMC is proportional to \sqrt{D} .

To check the above analysis, the CPU times of KMC and AP-KMC have been compared. Fig. 3.2 shows the CPU times for the two methods for diffusion coefficients going from $5 * 10^6 \dots 4 * 10^8 \text{ s}^{-1}$. From this picture it is possible to see how the CPU time for KMC scales linearly with the diffusion coefficient. For AP-KMC the required CPU-time is clearly lower and scales also faster (better) than linear with the diffusion coefficient.

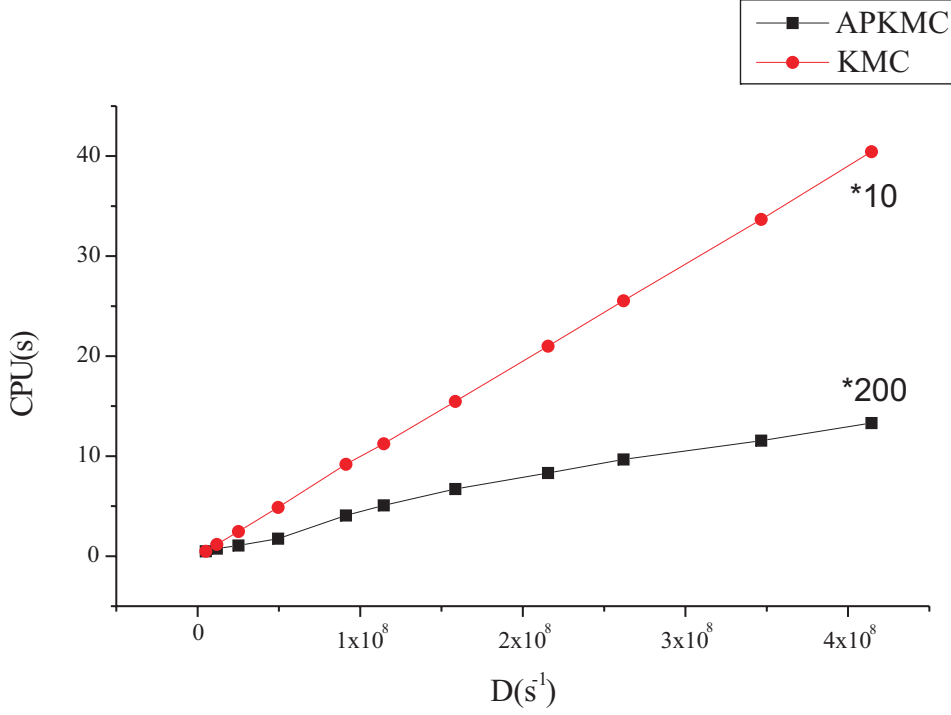


Figure 3.2: Comparison of the CPU times for the one-dimensional diffusion process. The diffusion coefficient is ranging between $D = 5 * 10^6 \dots 4 * 10^8 \text{ s}^{-1}$. The simulation time is $t = 0.01 \text{ s}$. The CPU times are multiplied by a factor 10 for KMC and by a factor 200 for AP-KMC. The size of the matrix increases with temperature (see text).

In Fig. 3.3 the CPU times are plotted for simulations done at temperatures between $800 \dots 1150 \text{ K}$ and for a total simulation time $t = 0.01 \text{ s}$. As expected, KMC is increasing exponentially with the temperature. To obtain a CPU time measurable by the internal clock of the computer the KMC simulation were performed over 10 runs and the AP-KMC over 200 runs, for this reason in Fig. 3.3 and 3.2 the CPU times are multiplied by a factor of 10 for KMC and by a factor of 200 for AD-KMC. As obvious from both figures AD-KMC drastically speeds up the simulation.

3.1.4 Hyper Jump KMC

Most of the CPU time in an AP-KMC simulation is spend to solve the set of difference equations for the adatom probability. A more efficient scheme to evaluate the adatom probability is thus desirable. Actually, the full adatom distribution provides much more information than needed. What can be learned from the probability distribution is that in general the probability for an adatom to jump to the next nearest neighbors is way smaller than the probability to jump to any other site further away. This observation gave us the idea for a further improvement of AP-KMC. The possibility to include in a

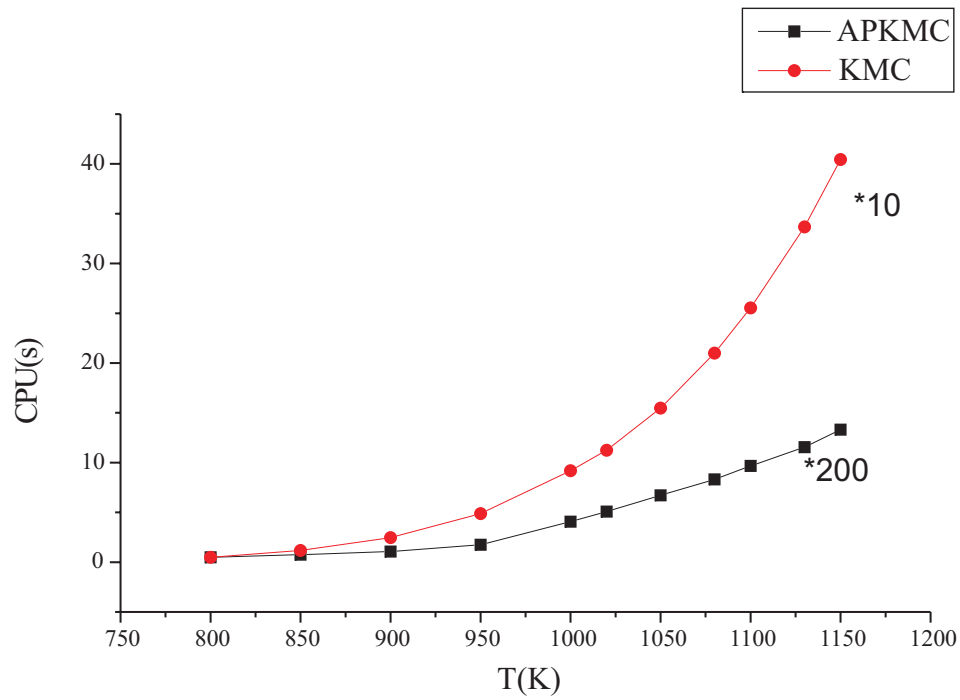


Figure 3.3: Comparison of the CPU times for the one-dimensional diffusion process. The temperatures ranging between $T = 800 \dots 1150$ K. The simulation time is $t = 0.01$ s. The CPU times are multiplied by a factor 10 for KMC and by a factor 200 for AP-KMC. The size of the matrix increases with temperature.

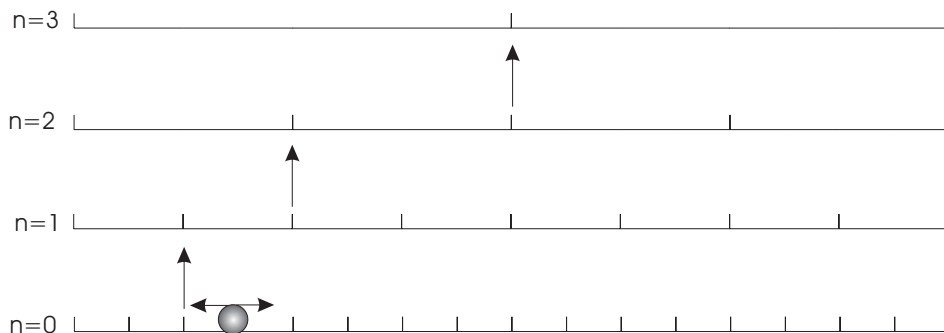


Figure 3.4: Multilevel scheme for Hyper Jump KMC. The particle starts at the level $n = 0$ and can jump to higher levels and descend than to lower levels when the simulation's end is approaching.

KMC simulation larger jumps—in contrast to jumps to the nearest neighbor site—will be considered here. A multigrid approach for KMC has been developed in which the length of the jump depends on the order/level of the grid the adatom is. This method has been called Hyper Jump KMC (HJ-KMC). In this section HJ-KMC will be described, its results will be compared with KMC results to test its reliability, and finally the CPU times will be compared with KMC and AP-KMC.

A model will be considered in which an adatom is diffusing on a one-dimensional lattice with a spacing Δx between sites—its position on the lattice is given by x . Here, for simplicity Δx is set equal to one ($\Delta x = 1$). As soon as the adatom reaches a site that is a multiple of two, it can be promoted to a coarser lattice where the lattice spacing is twice larger than the previous. A number n can be introduced to distinguish between the two lattices, which assumes the value 0 for the original lattice and 1 for the coarser lattice. n gives the level of the lattice. The jumps of the adatom on the coarser lattice are twice larger than on the original lattice. From the level 1 lattice the adatom can be further promoted to an even coarser grid, when the adatom reaches a site that is multiple of two (just in the same way as applied at level 0). This process of promoting the adatom to the next higher level grid can be continued further. For a lattice of level n the spacing between sites increases like $\Delta x = 2^n$. The jumps an adatom can do are always equal to the spacing of the lattice in which the adatom is. The larger the jumps an adatom can do, the larger the time steps Δt associated with the jumps. Thus the time step of the adatom depends on the level in which the adatom is:

$$\Delta t = \frac{(4)^n}{2\Gamma} \quad . \quad (3.16)$$

This model can be imagined as a stack of lattices one over the other with increasing site spacing Δx and increasing level n , as shown in Fig. 3.4.

When the simulation starts, the adatom is at level $n = 0$ and time $t = 0$. The simulation time is t_{sim} , thus $0 < t < t_{\text{sim}}$. If $\Delta t_{n=0}$, the time step at level $n = 0$, is way smaller

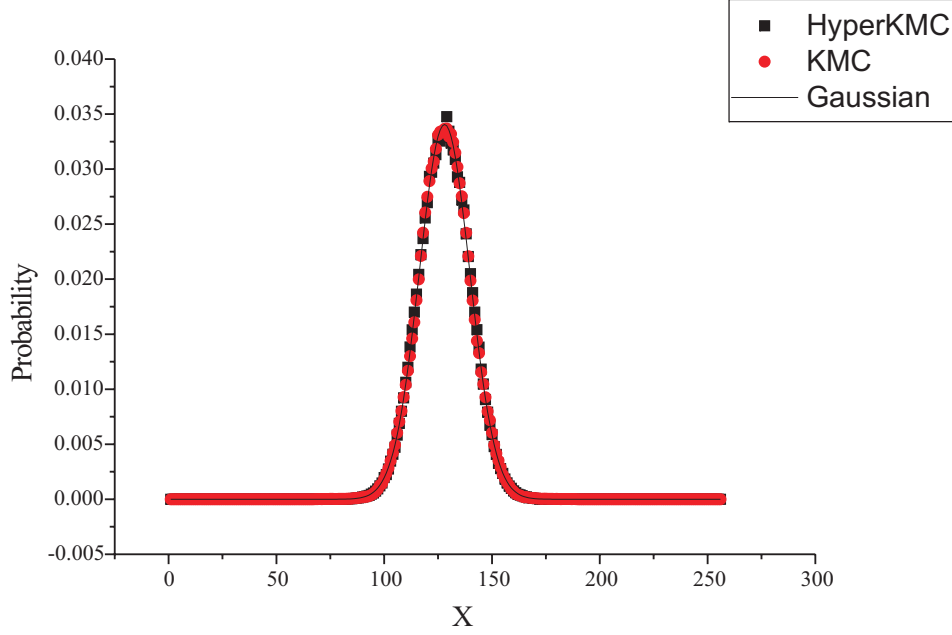


Figure 3.5: Comparison between KMC, HJ-KMC for a simulation done at $T = 550$ K for $t = 0.01$ s on a 256 vector. The solid line is a gaussian.

than the simulation time t_{sim} , $\Delta t_{n=0} \ll t_{\text{sim}}$ than the adatom starts an ascending process. The time step of the level reached by the adatom has to be always compared with the total simulation time t_{sim} . The time step $\Delta t_{n_{\text{max}}}$ of the highest level reached has thus to obey the relation $A\Delta t_{n_{\text{max}}} < t_{\text{sim}} - t$, where A is the ascending factor, which should be chosen such that the adatom has sufficiently time to relax on the n_{max} lattice. When $t = t_{\text{sim}}$ the adatom has to be in the lowest level ($n = 0$). When t is approaching t_{sim} the adatom starts to descend. Introducing the descending factor B , if $t + B\Delta t_n > t_{\text{sim}}$ the adatom has to move from the level n to the level $n - 1$. As the development of the HJ-KMC is still in an initial stage, the optimum values for the coefficients A and B are still explored. For the results presented here a value of $A = 15$ and $B = 10$ has been used. The HJ-KMC has thus three main stages. In a first step the adatom has to find its optimal level, which should be high enough to perform rapidly the diffusion events without exceeding the simulation time t_{sim} . Once the highest level has been attained, the diffusion events are performed. Finally, when the end of the simulation approaches the adatom starts a descending process, which will bring it at the level $n = 0$ at $t = t_{\text{sim}}$.

To check the accuracy/reliability of this approach a comparison with KMC has been performed. The results are shown in Fig. 3.5. Here the simulation has been done at $T = 550$ K for $t = 0.01$ s on a 256 vector. The solid line in the figure is a Gaussian. As can be seen the differences between the two methods are negligible.

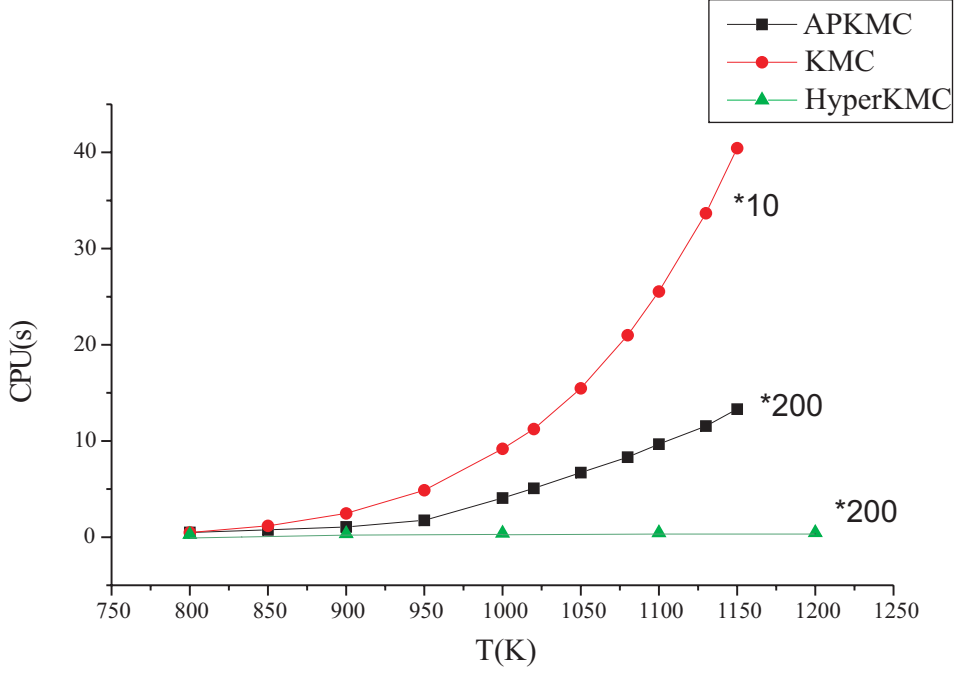


Figure 3.6: Comparison of the CPU times for the one-dimensional diffusion process. The temperatures range between $T = 800 \dots 1200$ K. The simulation time is $t = 0.01$ s. The CPU times are for 10 runs for KMC and 200 runs for AP-KMC and HJ-KMC.

In Fig. 3.6 the CPU times for the three methods are compared for a simulation of $t = 0.01$ s at temperatures between $T = 800 \dots 1200$ K. The CPU times for KMC are obtained over 10 runs and for AP-KMC and HJ-KMC over 200 runs. The simulation for HJ-KMC were performed over 200 runs to obtain a CPU time large enough to be measured by the internal clock of the computer. This method is clearly faster than normal KMC and it is even significantly faster than AP-KMC.

An interesting result emerged when studying the scaling with respect to the temperature: The CPU time for HJ-KMC is increasing less than linear with the temperature (see Fig 3.7). In Sec. 3.2.4 the HJ-KMC will be extended also to the nucleation process.

3.1.5 2D diffusion

The same system as before will be now considered expect that the particle should be moving on a two-dimensional array. The Master equation for this system can be written as:

$$\frac{\partial \rho(i, j, t)}{\partial t} = [\Gamma_{i+1, j} \rho(i+1, j, t) + \Gamma_{i-1, j} \rho(i-1, j, t) + \Gamma_{i, j+1} \rho(i, j+1, t) + \Gamma_{i, j-1} \rho(i, j-1, t) - 4\Gamma_{i, j} \rho(i, j, t)] \quad . \quad (3.17)$$

Here $\rho(i, j, t)$ is the probability to find the particle at time t on site (i, j) . If the transition rate $\Gamma(i, j)$ is constant everywhere the Master equation simplifies to:

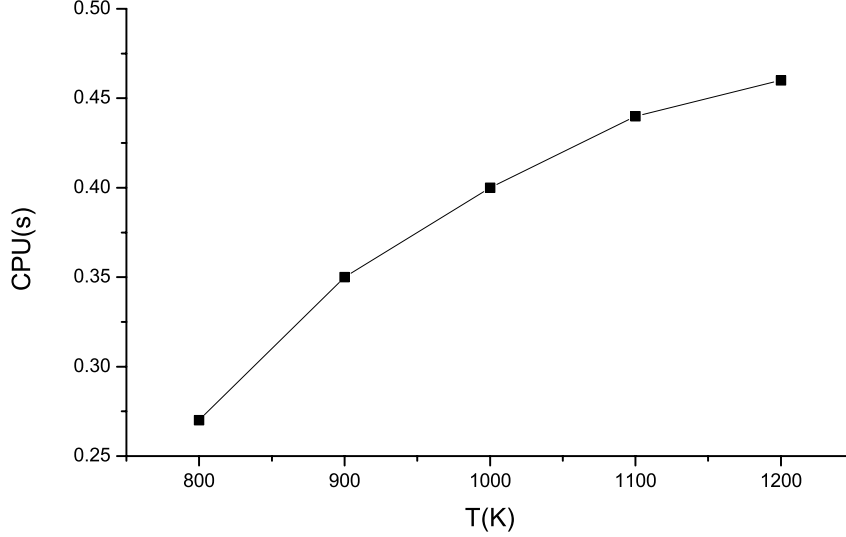


Figure 3.7: CPU times of HJ-KMC for the one-dimensional diffusion process. The temperatures range between $T = 800 \dots 1200$ K. The simulation time is $t = 0.01$ s.

$$\frac{\partial \rho(i, j, t)}{\partial t} = \Gamma[\rho(i+1, j, t) + \rho(i-1, j, t) + \rho(i, j+1, t) + \rho(i, j-1, t) - 4\rho(i, j, t)] \quad . \quad (3.18)$$

Fig. 3.8 shows the probability distribution on a 2 dimensional lattice for two different cases. First a constant diffusion coefficient D all over the surface has been considered. The results are shown in Fig. 3.8 a) and c) as 3 dimensional plot and as contour plot respectively.

In the second case the diffusion coefficient is constant all over the surface except along the lower-left/upper-right diagonal of the surface where it is set to zero. This means that once the particle has reached the diagonal it cannot escape: The diagonal acts like an attractor. Figs. 3.8 b) and d) show the 3 dimensional and the contour plot for this case. As it will be shown in Sec. 3.2 this 2 dimensional model provide direct insight into how nucleation can be efficiently described in a density approach. For the first case the result is a Gaussian distribution: the contour plot of the adatom density is completely spherical. However, in the case of an attractor on the diagonal the adatom probability is no longer spherical but gets deformed and an additional maximum along the diagonal appears. The simulations were done for $t = 0.1$ s and at $T = 450$ K.

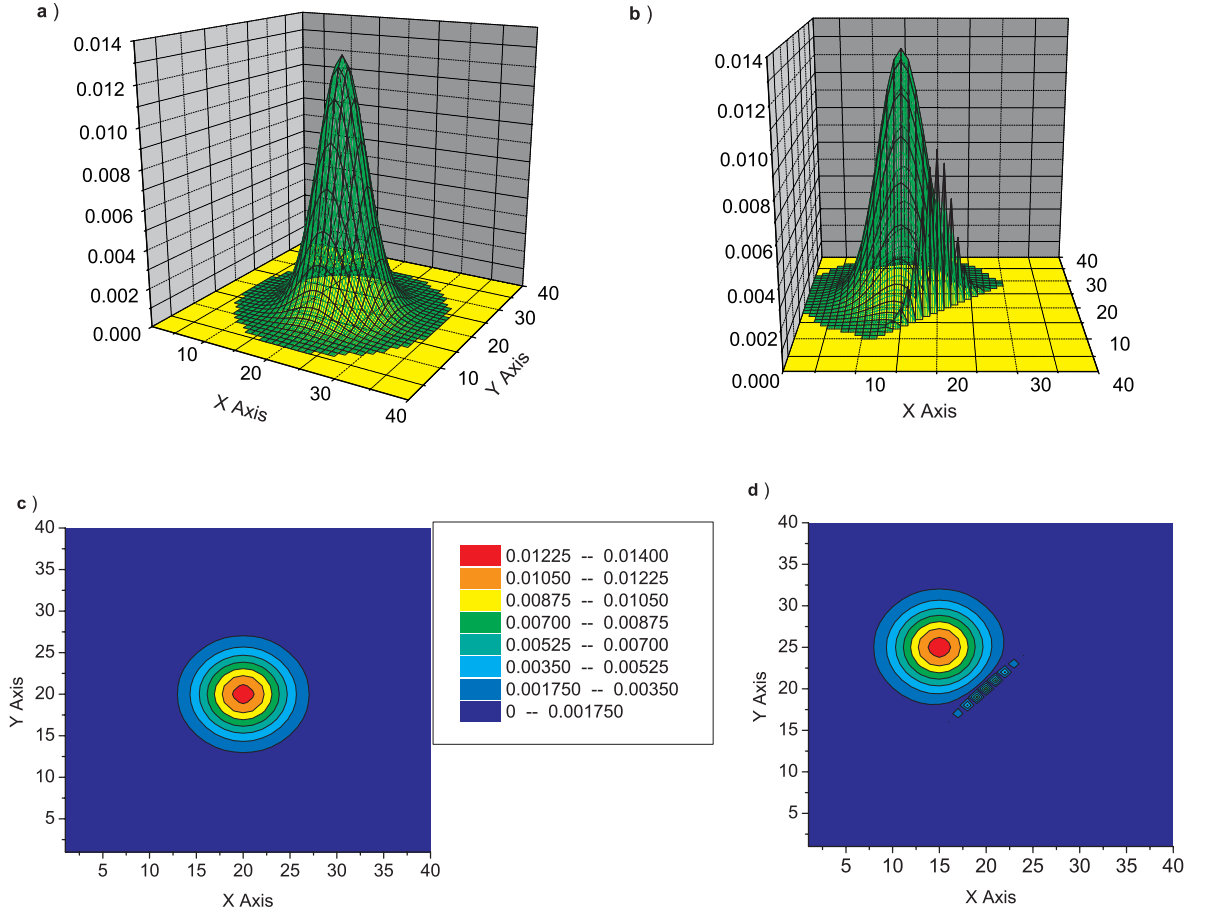


Figure 3.8: Probability distribution $P(i, t)$ for a particle on a two-dimensional array as 3 dimensional plot (a) and as contour plot (c) for the case of a constant diffusion coefficient D over the surface. b) and d) show the 3 dimensional and the contour plot for the case the diffusion coefficient is constant all over the surface except along a diagonal where it is set to $D = 0$. The simulations were done for $t = 0.1$ s and $T = 450$ K.

3.2 Nucleation

To construct a density based method for growth simulations, a density description of the nucleation is needed, similarly to what has been done in the previous paragraph for diffusion. To study nucleation, the case of two particles moving on a one-dimensional vector will be considered here. Even if this could seem a too simple model, it corresponds to the crucial case of nucleation along a step. Usually when an adatom arrives at a step or island edge it starts to diffuse along the edge until it finds a stable position, which could be a kink site, or it nucleates with another adatom, which is also diffusing along the edge. As a first model it will be assumed that the two adatoms nucleate when they are on the same site. In a second step the model will be extended to the case where the two adatoms nucleate if they occupy nearest neighbor sites. Here and in the following it is assumed that once the nucleus has formed it cannot break up anymore i.e., detachment will not be considered. This model for nucleation can be described by the Master equation Eq. (2.15), which is rewritten here:

$$\begin{aligned} \frac{\partial \rho(i, j, t)}{\partial t} = & \Gamma_{i+1 \rightarrow i, j} \rho(i+1, j, t) + \\ & \Gamma_{i-1 \rightarrow i, j} \rho(i-1, j, t) + \Gamma_{i, j \rightarrow j+1} \rho(i, j+1, t) + \\ & \Gamma_{i, j \rightarrow j-1} \rho(i, j-1, t) - [\Gamma_{i \rightarrow i+1, j} + \\ & \Gamma_{i \rightarrow i-1, j} + \Gamma_{i, j \rightarrow j+1} + \Gamma_{i, j \rightarrow j-1}] \rho(i, j, t) \end{aligned} \quad (3.19)$$

As the transition rate is constant everywhere and one-point islands are considered, one can write for the transition rates:

$$\Gamma_{i, j} = \begin{cases} \Gamma & \text{if } i \neq j \\ 0 & \text{if } i=j \end{cases} \quad (3.20)$$

It is interesting to note that the problem of the two particles diffusing on a one-dimensional vector is equivalent to study the diffusion of a single particle on a two-dimensional vector (in fact Eqs. 3.17 and 3.19 are equivalent). In the 2D case $\rho(i, j)$ can be interpreted as the probability to find the particle on site (i, j) and $\Gamma_{i \rightarrow i+1, j}$ as the transition rate from site (i, j) to $(i+1, j)$. If the adatom reaches the diagonal $i = j$ it stops diffusing, because the transition rates on the diagonal are zero. The points along the diagonal correspond in the one-dimensional system to the nucleation, when two particles are on the same site.

An exact solution for this problem can be obtained by solving numerically Eq. 3.19 (as shown in Fig. 3.9 a)) or by performing a large number of KMC simulations. In Fig. 3.9 a) the results obtained by solving Eq. 3.19 are plotted as a two-dimensional contour plot $P(i, j)$. This result is equivalent to that shown in Fig. 3.8 d) for a single particle in two dimensions. The calculations were done for a temperature $T = 450$ K and a time $t = 0.1$ s on a 40 sites long matrix. The two particles were set at $t = 0$ s at position 15 and 25.

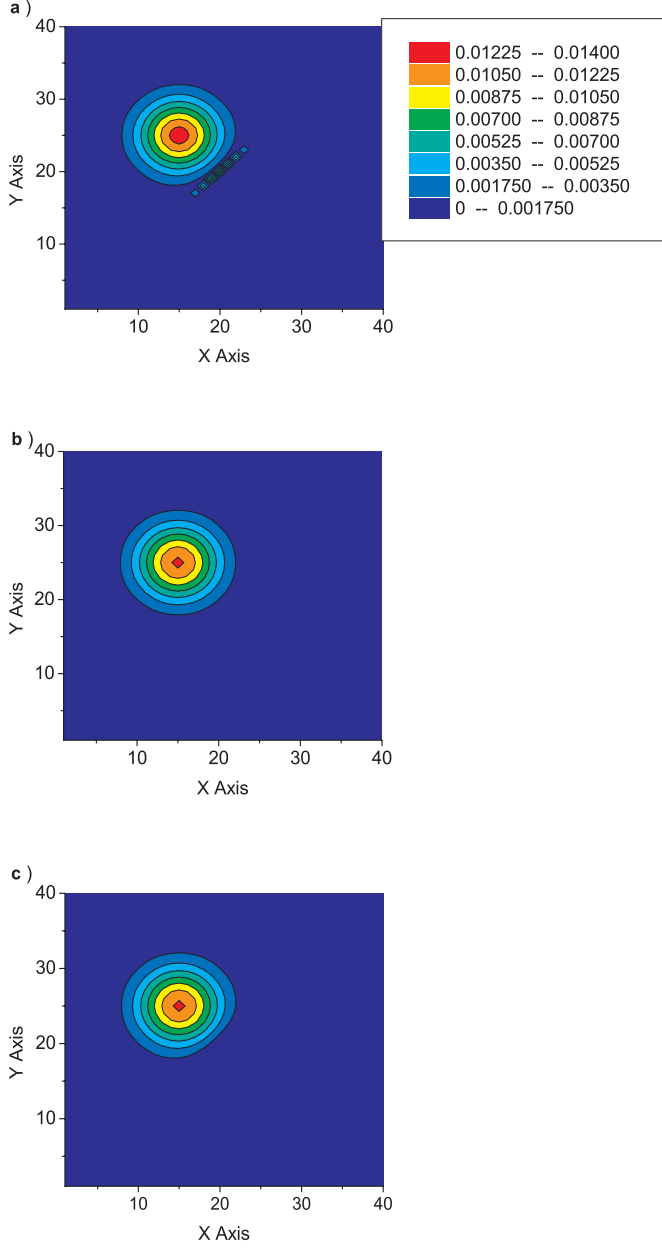


Figure 3.9: Contour plot of the two particle probability $P(i, j, t)$ for a simulation done at $T = 450$ K for $t = 0.1$ s on a 40 sites long vector. At $t = 0$ s the two particles are at position 15 and 25. In a) we have the exact solution, b) the Hartree approximation and c) the Hartree-Fock approximation (see text).

Along the diagonal $i = j$ a strong accumulation of the adatom density appears due to the nucleation processes.

The nucleation can be described exactly using the two-particles density $\rho(i, j)$. A problem with this approach is that the calculation of a two-particle density is computationally rather expensive. Therefore, in the following different approaches will be tested with respect to replacing the two-particle density by a one-particle density of single adatoms $\rho_l(i)$ and $\rho_m(j)$. The key step is then to identify a function f which allows to calculate/approximate the two particle density by single particle densities: $\rho(i, j) = f(\rho_m(i), \rho_l(j))$. In general the exact expression of f is unknown and approximations have to be introduced. Thus, the results are no longer exact as for the case of the two-particle density.

A key problem to express the two-particle density in terms of single particle densities is commonplace in many-bodies theory and in electronic structure theory. For example electronic structure theory treats the general problem how to write the many-electron wave function $\Psi(x_1, x_2, \dots, x_n, t)$, where x_i is the coordinate of the i -th electron, as a function of the single electron wave functions $\psi_i(x_i, t)$:

$$\Psi(x_1, x_2, \dots, x_n, t) = f(\psi_1(x_1, t), \psi_2(x_2, t), \dots, \psi_n(x_n, t)) \quad . \quad (3.21)$$

There are many similarities between the two-adatom system on a surface and a two-electron system. Besides the external potential, the electrons are subject to their repulsive Coulomb interaction. As the electrons are Fermions they obey the Pauli principle, that states that the wave function of a system of Fermions must be antisymmetric with respect to interchange of any two Fermions. This implies that two electrons with the same spin have zero probability of being found at the same point in the three-dimensional space. Thus the Pauli antisymmetry principle forces electrons of like spin to keep apart from one another, this is often called the Pauli repulsion. The position of the electrons in the potential can be described by the electron density $|\psi(x, t)|^2 = \psi(x, t)\psi^*(x, t)$ where $\psi(x, t)$ is the wave function. The electron density gives the probability to find an electron at a given position in space. In the same way the two adatoms on the surface are subject to the Potential Energy Surface (PES, see Sec. 2.1.1). The adatoms have just a very short range interaction in the model considered here. If they are at the same position they stick together and form a stable nucleus, otherwise if the two adatoms are not at the same site, there is no interaction between them. Thus, the type of interaction between the electronic system and the adatoms is quite different. Long range and repulsive interactions determine the electronic system while short range and attractive the adatom system. The adatom density gives the probability to find an adatom at a given position similarly to the electron density. As already described for the diffusion in Sec. 3.1.3, the position of the adatom can be found collapsing the adatom density in one point, in the same way it is done for the measurement process in quantum mechanics. Thus, in the following methods typically used in electronic structure like Hartree, Hartree-Fock approximation will be applied to the nucleation of the adatoms.

3.2.1 Hartree approximation

To study a many electron system in an external potential a first approximation would be to simplify the interactions between the electrons. Instead of considering the interactions between each single electron i and all the other it would be easier to consider the average electrostatic repulsion exerted on the electron i by all the other electrons. This is what is done in the Hartree approximation (as mentioned in Sec. 2.1.1) where the wave function is written as the product of single electron wave functions. Within the Hartree approximation the Pauli principle is not respected and it can happen that two electrons with the same spin occupy the same position. The Hartree approach can be applied to adatom nucleation by writing the two particle probability $\rho(i, j)$ as product of single adatom densities:

$$\rho(i, j, t) \approx \rho_1(i, t)\rho_2(j, t) \quad . \quad (3.22)$$

Here, the indices 1 and 2 distinguish between the two particles. The two adatoms are independent, there is no interaction between them. The only interaction the adatoms feel is the one with the surface on which they are diffusing. In fact, the diffusion rates of the adatoms depend on the PES. If the two adatoms are on the same place, no nucleation takes place because the two adatoms do not "see" each other. With the Hartree approximation for an adatom system it is not possible to describe the nucleation just as for an electron system it was not possible to respect the Pauli principle. Indeed, the Hartree approximation is a very crude approximation. If $\rho(i, j, t)$ as given in Eq. 3.22 is substituted into Eq. 3.19 one gets:

$$\frac{\partial \rho_\alpha(i, t)}{\partial t} = \Gamma[\rho_\alpha(i + 1, t) + \rho_\alpha(i - 1, t) - 2\rho_\alpha(i, t)] \quad . \quad (3.23)$$

Here, the index α is 1 or 2. This equation corresponds to Eq. 3.11 for the free particle diffusion. In Fig. 3.9 b) the results for the Hartree approximation are plotted in a 2 dimensional contour plot. On the x and y axes the position of the two particles are plotted. The result is a two-dimensional Gaussian as expected.

The Hartree approximation can well describe the adatom densities far away from the $i = j$ diagonal, which also in the following will be called nucleation line because it is where the nucleation events take place. Far from the nucleation line the adatom distributions in Fig. 3.9 a) and b) look the same, because this region corresponds to the case where the two adatoms are far away from each other and they do not interact. Under these condition the Hartree approximation is in good agreement with the exact solution.

From Fig. 3.9 a) it is possible to see that the probability distribution is different from zero only above the diagonal in the upper left. Further, along the diagonal are peaks due to nucleation. Within the Hartree approximation it can happen that also the lower part below the diagonal becomes different from zero. This adatom density below the diagonal corresponds to an unphysical case. As a 1 dimensional simulation is considered here, at $t = 0$ one adatom occupies a larger x coordinate than the other. This non zero density below the diagonal means that at the end of the simulation time $t = t_{\text{sim}}$, the adatom that

had the higher coordinate at the beginning has now the lower coordinate and the adatom which had the lower one has now the higher. The positions of the adatoms are inverted. This can happen only if the two adatoms have been on the same position at the same time, but did not nucleate. Thus, within this approximation it is not possible to obtain any information about the nucleation.

3.2.2 Hartree-Fock approximation

As the electrons are Fermions the Hartree approximation can be extended by including the Pauli principle in the method. This is what is done by the Hartree-Fock approximation (see Sec. 2.1.1). The Pauli principle states that the wave function of a system of electrons must be antisymmetric with respect to interchanging any two electrons:

$$\Psi(x_1, x_2, \dots, x_n, t) = -\Psi(x_2, x_1, \dots, x_n, t) \quad . \quad (3.24)$$

Antisymmetric wave functions are obtained by solving the Slater determinant (see Sec. 2.1.1) and for the case of two electrons the wave function looks like:

$$\Psi(x_1, x_2, t) = \psi_1(x_1, t)\psi_2(x_2, t) - \psi_1(x_2, t)\psi_2(x_1, t) \quad . \quad (3.25)$$

If $x_1 = x_2$ the wave function $\Psi(x_1, x_2)$ is equal zero, thus it is impossible for the two electrons to be at the same position.

The adatoms do not have of course to follow the Pauli principle but there is an analogy between the Pauli principle for the electrons and the nucleation for the adatoms. If one considers that two adatoms nucleate when they are on the same position, one could say that the probability to find two different adatoms on the same position is zero, because as soon as they occupy the same position they are no longer adatoms but form a nucleus. For this reason the two-adatom density $\rho(i, j, t)$ can be written as an antisymmetric function of $\rho_1(i, t)$ and $\rho_2(j, t)$:

$$\rho(i, j, t) \approx \rho_1(i, t)\rho_2(j, t) - \rho_1(j, t)\rho_2(i, t) \quad . \quad (3.26)$$

Here the position of the adatoms is given by the discrete variables i and j instead of the continuum ones x_1 and x_2 used for the wave functions. To express the analogy with the electronic system, Eq. 3.26 which has been derived for the adatoms will be called Hartree-Fock approximation. Within this approach the adatom density is zero along the diagonal $i = j$ as shown in Fig. 3.9 c).

The shape of the adatom density has changed compared to the one obtained from the Hartree approximation. The adatom density is now deformed close to the diagonal $i = j$ this is similar to the correct solution of Fig. 3.9 a). The Hartree-Fock approximation describes not only the region far away from the nucleation line properly, as it was the case for the Hartree approximation, but also close to this region. It is also possible to get some information about the nucleation from the Hartree-Fock approximation. In fact,

the sum of the total adatom density on the surface is now less than one. The difference between the sum of the adatom density on the surface and one gives the probability that the particles have nucleated:

$$nuc = 1 - \sum_{i,j} \rho(i,j) \quad . \quad (3.27)$$

From the Hartree-Fock approximation it is not possible to know how the nucleation is distributed on the surface, as it is the case of the exact solution shown in Fig. 3.9 a).

If Eq. 3.26 is plugged into Eq. 3.19 it gives Eq. 3.23 which was obtained using the Hartree approximation. In the continuum case ($x = \frac{i}{L}$ with $\Delta x = \frac{(i+1)-i}{L} \rightarrow 0$) the two-particle density is then given by a superposition of two Gaussians:

$$\frac{1}{4D\pi t} \left(\exp^{-\frac{(x-x_0)^2 + (y-y_0)^2}{4Dt}} - \exp^{-\frac{(x-y_0)^2 + (y-x_0)^2}{4Dt}} \right) \quad . \quad (3.28)$$

Here (x_0, y_0) are the initial conditions. In Fig. 3.9 c) only the positive part of the solution has been plotted, omitting the part with negative density. This is similar to what is commonly done in electrostatics when applying the image method (see Ref. [104]), where a problem with boundaries (for example a metal slab at a given potential) is replaced by an enlarged region with fictitious charges and no boundaries. This method has been applied to nucleation in Ref. [88].

3.2.3 Hartree approximation with a nucleation term

To have a local description of nucleation it is necessary to further improve the approaches proposed in the last two sections. A possible idea is to introduce a nucleation term which is position dependent. Equation (3.19) is a good starting point to find a possible nucleation term. In fact from this equation one can evaluate the probability $\rho(i, i, t)$ to find the two adatoms at the same position, which will be called $n(i, t)$. The nucleation rate is then given by:

$$\frac{\partial n(i, t)}{\partial t} = \Gamma [\rho(i+1, i, t) + \rho(i-1, i, t) + \rho(i, i+1, t) + \rho(i, i-1, t)] \quad . \quad (3.29)$$

As each density term on the right hand side of Eq. (3.29) involves always different sites, the diffusion rate is $D = \Gamma$ for all the sites. The key issue is now how to express the two-adatom density terms appearing on the right hand side as function of the single-adatom densities. Here again the first possibility coming to mind is to substitute the two-adatom density by a product of the respective single-adatom densities (i.e. Hartree-like approximation). Of course, in principle more complicated approaches could be used to express the two-adatom density, like for example adopting an antisymmetric function as done for the Hartree-Fock approach (see previous section). As shown there it gives better results than the Hartree approach. However, since in this first derivation the main concern is on keeping things as simple as possible, the discussion will be restricted to the Hartree approximation. Performing it the nucleation term writes:

$$\frac{\partial n(i, t)}{\partial t} = \Gamma[\rho_1(i+1, t)\rho_2(i, t) + \rho_1(i-1, t)\rho_2(i, t) + \rho_1(i, t)\rho_2(i+1, t) + \rho_1(i, t)\rho_2(i-1, t)] \quad . \quad (3.30)$$

This term is added to Eq. (3.23) used in the Hartree approach, resulting in the following two equations for the adatom densities:

$$\frac{\partial \rho_1(i, t)}{\partial t} = \Gamma[\rho_1(i+1, t) + \rho_1(i-1, t) - 2\rho_1(i, t)] - \Gamma\rho_1(i, t)[\rho_2(i+1, t) + \rho_2(i-1, t)] \quad (3.31)$$

$$\frac{\partial \rho_2(i, t)}{\partial t} = \Gamma[\rho_2(i+1, t) + \rho_2(i-1, t) - 2\rho_2(i, t)] - \Gamma\rho_2(i, t)[\rho_1(i+1, t) + \rho_1(i-1, t)] \quad . \quad (3.32)$$

In the following the performance of this approximation for the nucleation term will be checked.

As a first test it will be compared with the Hartree-Fock approach. As mentioned in the previous section, from the Hartree-Fock approach it is possible to get the total nucleation N_{HF} correctly. The total nucleation from Hartree-Fock can be compared with the total nucleation given by the nucleation term N_T . This has been done for different temperatures in Fig. 3.10.

Here the relative difference for the total nucleation between the exact Hartree-Fock results and the Hartree plus the nucleation term have been plotted for temperatures between 490 K and 540 K. The relative error plotted in Fig 3.10 is:

$$\Delta E_{rel} = \frac{2(N_{HF} - N_T)}{N_{HF} + N_T} \quad . \quad (3.33)$$

Around 540 K the relative difference is less than 0.2. For higher temperatures (which are particularly interesting because they correspond to the step flow regime) the difference is expected to decrease further. Simulations at higher temperatures were not performed in this work because of the long computational time needed. For low temperatures the difference in nucleation increases but it is still smaller than a factor 2. Around $T = 490$ it gets as large as 0.6. At high temperatures the distribution functions are smoother and thus the approximations introduced give better results. The spatial distribution for the nucleation and the adatom density obtained with the Hartree approach plus nucleation term have been plotted in Fig. 3.11 for three different temperatures.

The simulations were done on a 500 vector for a simulation time $t_{sim} = 1.0$ s. The two adatoms were located at $t = 0$ at position 200 and 300. Increasing the temperatures the adatom densities get smoother and the nucleation distribution gets higher. From Fig. 3.10 one can see that the relative error between the Hartree-Fock approach and the nucleation term decreases for increasing temperatures. This is due to the fact that for high temperatures the adatom distribution gets smoother so that the variation of the adatom density at each site is better approximated by a constant value. To test the correctness of

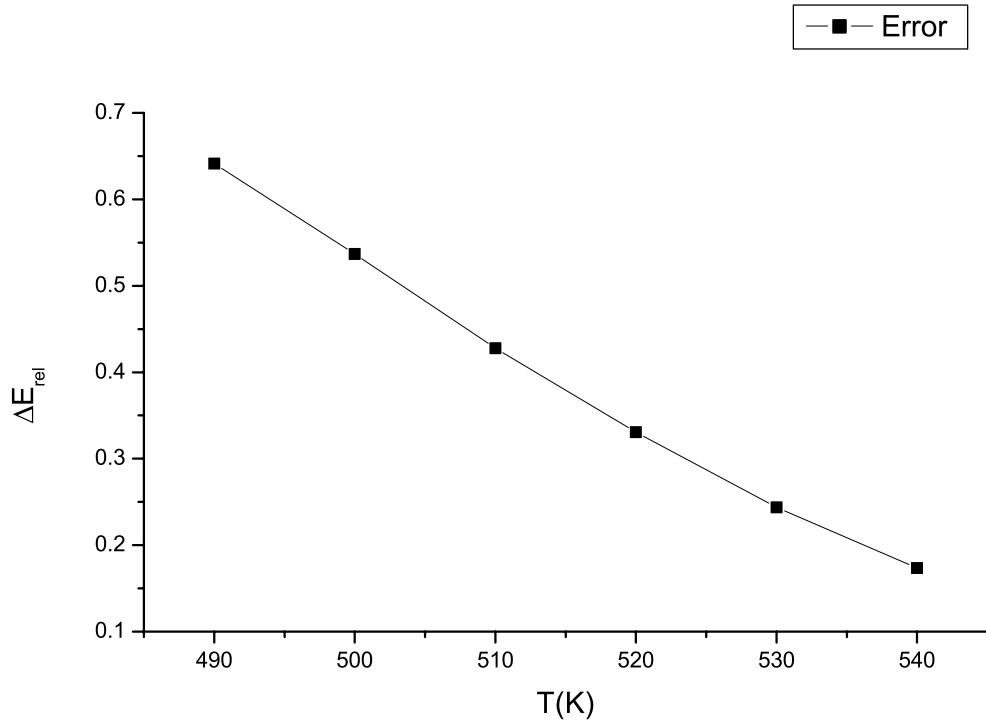


Figure 3.10: Relative difference between Hartree-Fock and Hartree plus nucleation term as defined in Eq. (3.33) versus simulation temperature. ΔE_{rel} as defined in Eq. 3.33 is a real number. The lattice consists of 500 sites and the initial positions of the two adatoms are 200 and 300.

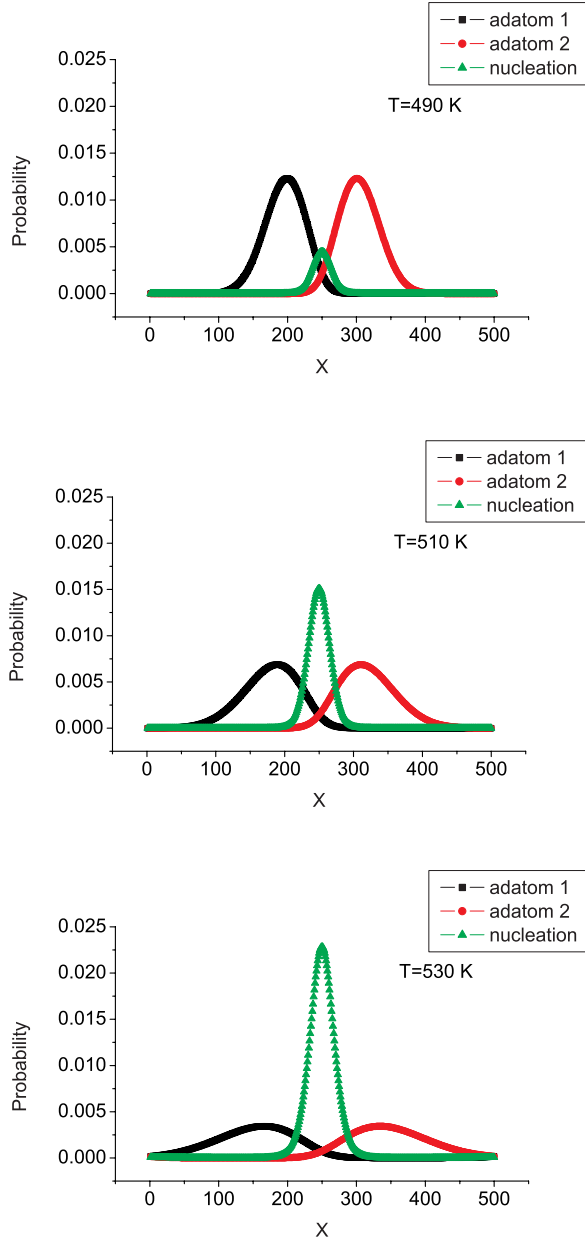


Figure 3.11: Adatom densities and nucleation distribution at different temperatures calculated using the Hartree approach plus nucleation term. The lattice consists of 500 sites and the initial positions of the two adatoms are 200 and 300.

the spatial dependence of the nucleation term it would be necessary to compare it with a KMC simulation or with the solution of the full two-particle equation. Both methods are computationally demanding because to get a reasonable statistics KMC simulations have to be performed for millions of runs and for the solution of the two-particle problems the number of equations to solve is equal to the square of the length of the surface considered. These tests are still under work and we are not yet at a stage to present some results. As a further research, other local nucleation terms could be considered, for example starting from an Hartree-Fock approach.

To simulate the more realistic case of two-point islands the following equations might be used. The equations used are similar to Eq. (3.31) with a slightly different nucleation term:

$$\frac{\partial \rho_1(i, t)}{\partial t} = \Gamma[\rho_1(i+1, t) + \rho_1(i-1, t) - 2\rho_1(i, t)] - \Gamma\rho_1(i, t)[\rho_2(i+2, t) + \rho_2(i-2, t)] \quad (3.34)$$

$$\frac{\partial \rho_2(i, t)}{\partial t} = \Gamma[\rho_2(i+1, t) + \rho_2(i-1, t) - 2\rho_2(i, t)] - \Gamma\rho_2(i, t)[\rho_1(i+2, t) + \rho_1(i-2, t)] \quad (3.35)$$

These equations are given here just to show the way one has to go to develop more realistic models, but no tests have been performed based on this set of equations.

3.2.4 Nucleation with Hyper Jump KMC

The Hyper Jump KMC (HJ-KMC) will be here applied to nucleation. In Sec. 3.1.4 the HJ-KMC had already been described for the diffusion processes. In the case of nucleation the interactions between the two adatoms should be taken into account. At $t = 0$ the two adatoms are at the level $n = 0$ and if they are sufficiently far away from each other, they start an ascending process. Now there are two limiting conditions for this ascending process of the adatoms. One is that the time step Δt_n at the level n reached by the adatom, should not get larger than the total simulation time t_{sim} , as was also the case for the diffusion. The second condition is that the spacing Δx_n at level n , where the adatom is, should not get so large to include the second adatom in it. If the positions of the two adatoms on the lattice are i and j , it should be always valid that $|i - j| > \Delta x_n$ where Δx_n is the spacing of the highest occupied level of the two adatoms. The two adatoms can occupy different levels as long as they are far away. This is particular important in the case of a simulation where more than two adatoms are involved, which is not the case here, but that is what normally happens in a complete growth simulation of a surface. In fact it could happen that two adatoms are close to each other, thus they can occupy only a low level, while another adatom is far away isolated and it can reach a high level. As soon as two adatoms occupy two nearest neighbor sites they are moved to the next lower level they occupy, unless they are already at the lowest level $n = 0$. A nucleation process can take place only at the level $n = 0$. At each time step the relative distance of the two adatoms has to be checked.

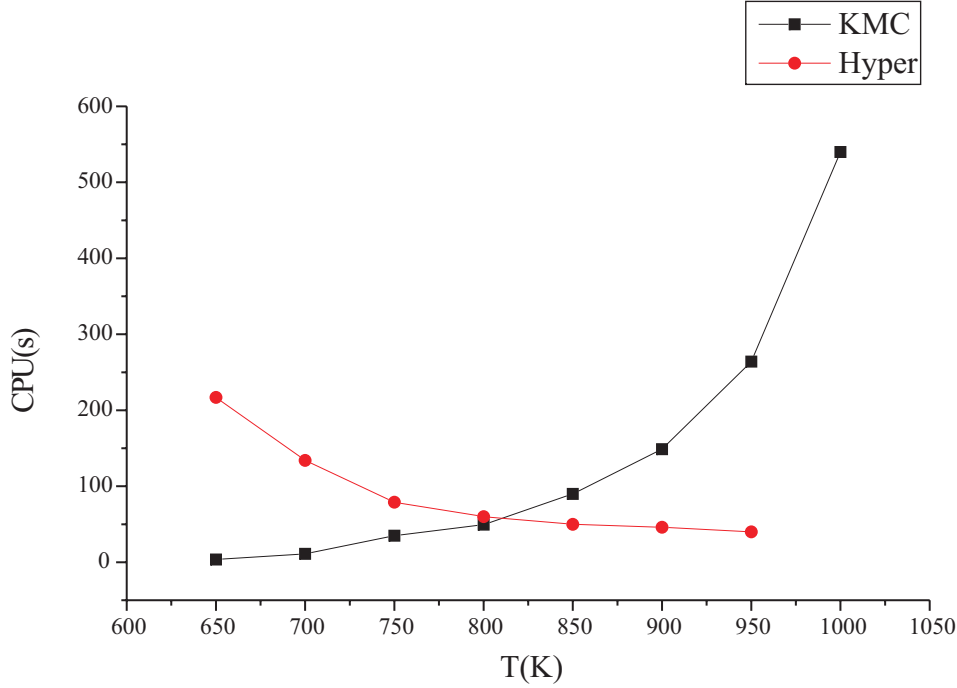


Figure 3.12: CPU time comparison for the nucleation between KMC and HJ-KMC. The simulations were done for a two-particle system on a one-dimensional vector long 256 sites. The simulation has been done for $t = 0.01$ s.

To check the speed of the method a CPU time comparison has been performed between HJ-KMC and KMC for nucleation events. A system is considered in which two particles are on a one-dimensional vector. The vector is 256 sites long and at $t = 0$ s the two particles are at site 114 and 142. The simulation is done for $t = 0.01$ s. Once the two particles nucleate the simulation stops. In Fig. 3.12 the CPU time as function of the temperature for both methods has been plotted. The CPU time is increasing exponentially as was the case also for diffusion. For HJ-KMC the CPU time is even decreasing with temperature. This is due to the fact that by increasing the temperature the probability that the two particles nucleate gets higher and the simulation stops before the final time is reached, if the nucleation takes place. The algorithm used for the HJ-KMC is more complicated than the normal KMC because it includes the management of particles on different levels. This means that at every time step the relative distance has to be checked and the time step has to be compared with the total simulation time. For these reasons the HJ-KMC is slower than the normal KMC for low temperatures, but it gets faster for high temperatures.

3.3 Conclusions

Diffusion and nucleation are the two main processes occurring during growth. They are Markov processes and can be described by a Master equation. A standard way to handle this Master equation is to realize randomly the processes included into it and following from configuration to configuration the evolution of the system. This is exactly what the KMC methods do. It is a straightforward way to approach the problem, but it is not the most efficient. In particular the diffusion processes are responsible for the slow down of the simulation at high temperatures. In this chapter it has been shown, that the density approach is a more efficient way to describe the diffusion processes. The AP-KMC method has been presented for diffusion. This has been a good starting point to describe the technique, which will be extended in the next chapter for a general epitaxial growth simulation. The comparison of the CPU times for the diffusion between AP-KMC and KMC has been presented. The tests have been restricted to the one dimensional case, which is computationally easier. It would be also very interesting to perform tests for the two dimensional case, this was not done here because of time limitations. Besides AP-KMC also HJ-KMC has been presented for diffusion. HJ-KMC can be even faster than AP-KMC. The second part of the chapter has been dedicated to nucleation. A system of adatoms on a surface has been compared to a system of electrons in an external potential and techniques typically used in electronic structure theory have been applied to the nucleation. A Hartree-like and an Hartree-Fock-like approach to nucleation has been investigated and a nucleation term to describe the nucleation has been introduced. As the nucleation term presented in Sec. 3.2.3 is the only one which can describe locally the nucleation it will be used in the next chapters to derive a schema which allows a complete growth simulation. Finally the HJ-KMC has been also applied in the case of nucleation.

Chapter 4

Density Based KMC methods (AP-KMC): Fundamentals and Definitions

4.1 Master equation for crystal Growth

In the previous chapter a density approach has been presented for the diffusion and nucleation processes. These results will be used here to extend this approach to describe epitaxial growth in general. Crystal growth is a stochastic process and can be described by a Master equation (as said already in Sec. 2.2, see also [2, 3]). A SOS model (see Sec. 2.2.4), will be used to describe the growing surface so that it can be represented by a vector:

$$C = \{h_1, h_2, \dots, h_M\} \quad . \quad (4.1)$$

Here M is the number of sites and h_i gives the number of atoms on site i . Other models with more complicated structures than the cubic SOS structure or also including vacancies can be implemented but for simplicity the treatment will be limited here to the SOS model. The Master equation will be presented here for the one-dimensional case and the adatoms can hop only to nearest neighbors sites. As in the Master equation there are contributions of many different configurations, to reduce its length a couple of abbreviations will be introduced. The probability to have a configuration $P(C, t) = P(\{h_1, \dots, h_i, \dots, h_M\}, t)$ will be just written as $P_{(h_i)}$ or if the heights of some particular sites are important, as h_{i-1} and h_i in $P(\{h_1, \dots, h_{i-1} + 1, h_i - 1, \dots, h_M\}, t)$, than it will be used $P_{(h_{i-1}+1, h_i-1)}$. The transition rates between two different configurations as $w(\{h_1, \dots, h_{i-1} + 1, h_i - 1, \dots, h_M\} \rightarrow \{h_1, \dots, h_{i-1}, h_i, \dots, h_M\})$ will be written as $w_{(h_{i-1}+1, h_i-1) \rightarrow (h_{i-1}, h_i)}$. The Master equation looks like:

$$\frac{\partial P_{(h_i)}}{\partial t} = \sum_{i=1}^M [w_{(h_{i-1}, h_{i+1}+1) \rightarrow (h_i, h_{i+1})} P_{(h_{i-1}, h_{i+1}+1)} + w_{(h_{i+1}, h_{i+1}-1) \rightarrow (h_{i-1}, h_i)} P_{(h_{i+1}, h_{i+1}-1)}]$$

$$\begin{aligned}
& +w_{(h_{i-1}+1, h_i-1) \rightarrow (h_{i-1}, h_i)} P_{(h_{i-1}+1, h_i-1)} + w_{(h_{i-1}-1, h_i+1) \rightarrow (h_{i-1}, h_i)} P_{(h_{i-1}-1, h_i+1)}] \\
& - \sum_{i=1}^M [w_{(h_{i-1}, h_i) \rightarrow (h_{i-1}-1, h_i+1)} + w_{(h_{i-1}, h_i) \rightarrow (h_{i-1}, h_{i+1}+1)} + w_{(h_{i-1}, h_i) \rightarrow (h_{i-1}+1, h_i-1)} \\
& + w_{(h_{i-1}, h_i) \rightarrow (h_i+1, h_{i+1}-1)}] P_{(h_i)} + \sum_{i=1}^M w_{(h_i-1) \rightarrow (h_i)} P_{(h_i-1)} \quad (4.2)
\end{aligned}$$

The terms in the first summation are all positive. They correspond to the probability that the system is in a configuration C' , which is a nearest neighbor configuration of $C = (h_i)$. C' is a nearest neighbor configuration of C if moving one-adatom to a nearest neighbors site, C' becomes C . The four terms in the first summation correspond to the probability that the system, being in a configuration C' , moves to the configuration C thanks to a diffusion process. These different contributions have been graphically represented in Fig. 4.1 for a configuration C taken as example. The first term $P_{(h_{i-1}, h_{i+1}+1)}$ for example corresponds to Fig. 4.1 b), in fact the value of $i+1$ is one unit higher than in the configuration C and the value of i one unit lower, if the adatom in $i+1$ hops to i it becomes the configuration C . The other three terms in this first summation correspond to Fig. 4.1 c-e). In the second summation there are four negative terms which correspond to the probability that the system already is in the configuration C and it moves away from it, becoming one of the four configurations represented in Fig. 4.1 b-e). The term in the last summation corresponds to the deposition as shown in Fig. 4.1 a). No desorption has been considered here.

The Master equation includes all the information about the dynamics of the SOS system considered. The challenging problem is now how to solve the Master equation. In principle the Master equation describes the dynamics of any possible configuration of the system. If the system is composed by 10^4 adatoms or more, as it is generally the case for epitaxial growth, the numbers of possible configurations gets huge and the problem is not treatable. Two different approaches are available to treat the Master equation reducing the number of configurations. One possibility is to derive from the Master equation a set of continuum equations and the second is to simulate the system with KMC, which corresponds to follow just one possible configuration. In this section the first approach will be investigate, while the KMC will be the object of the next section.

A number of papers appeared [47, 48, 105] that derived a set of continuum stochastic equations from the Master equation. The basic idea of all these methods is that, instead of using the probability for each configuration $P(\{h_1 \cdots h_i, \cdots h_M\})$ to describe the system, how it is done by the Master equation, a set of equations for the height of each site h_i is used. This reduces considerably the complexity of the problem because the system can be described with M equations which is way smaller than the number of possible configurations. To do this, a two step procedure is applied. A brief summary of the technique will be given here, for details see [45, 48]. First, the Master equation is approximated by the Fokker-Planck equation using a Kramers-Moyal expansion at the second order (see

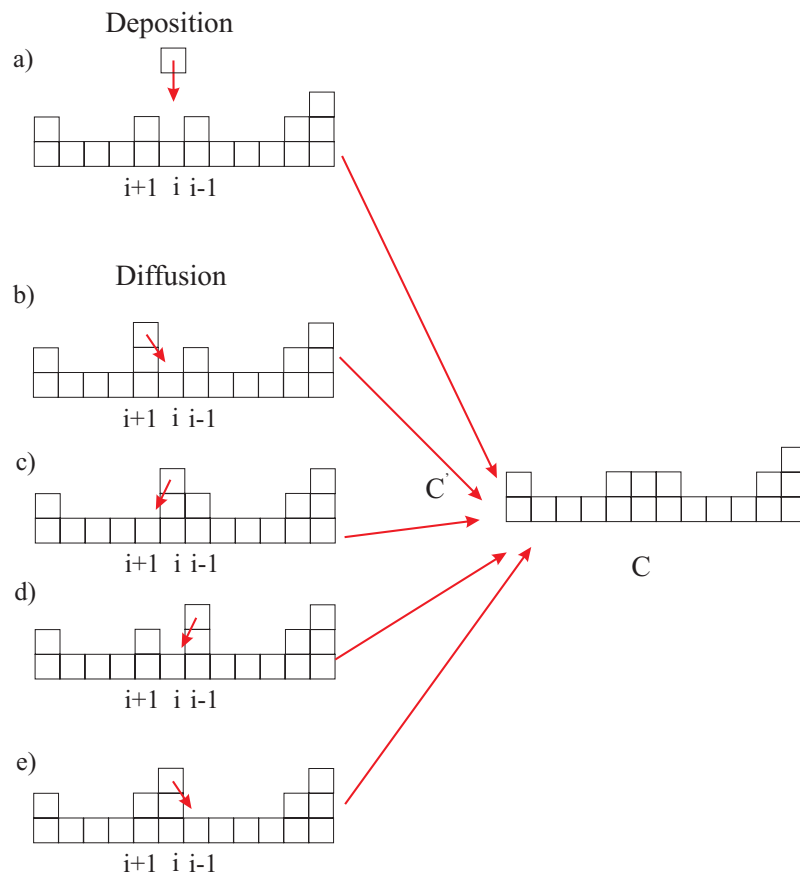


Figure 4.1: Graphical representation of the Master Equation given in 4.2. In Fig a) is represented the contribution due to deposition and from b) to e) the contributions due to diffusion.

Ref. [45])

$$\frac{\partial P(C, t)}{\partial t} = - \sum_i \frac{\partial}{\partial h_i} [K_i^{(1)} P(C, t)] + \sum_{i,j} \frac{1}{2} \frac{\partial^2}{\partial h_i \partial h_j} [K_{i,j}^{(2)} P(C, t)] \quad . \quad (4.3)$$

where

$$K_i^{(1)} = \sum_{C'} (h'_i - h_i) w(C \rightarrow C') \quad (4.4)$$

is the first moment and

$$K_{ij}^{(2)} = \sum_{C'} (h'_i - h_i)(h'_j - h_j) w(C \rightarrow C') \quad (4.5)$$

is the second moment of the transition matrix. Then the equivalent Langevin equation is:

$$\frac{\partial h_i(t)}{\partial t} = K_i^{(1)} + \eta_i(t) \quad (4.6)$$

where η_i represents white Gaussian noise with zero mean and covariance given by the second transition moment

$$\langle \eta_i(t) \rangle = 0 \quad , \quad (4.7)$$

$$\langle \eta_i(t) \eta_j(t') \rangle = K_{ij}^{(2)}(H) \delta(t - t') \quad . \quad (4.8)$$

In a second step one has to go from this discrete set of equations to a continuum equation. To obtain the Langevin equation for the function $h(x)$ of the continuous variable x one needs some smoothing procedure. It is made the assumption that there exists a smooth function $h(x)$ that is obtained from a function interpolating through the points $h_i(t)$. The continuum Langevin equation is than:

$$\frac{\partial h(x, t)}{\partial t} = K_i^{(1)}(h(x, t)) + \eta(x, t) \quad . \quad (4.9)$$

From this equation it is possible to have the time evolution of the height of each site on the surface. In the last years new papers appeared about the subject (see Ref. [106, 107]). In Ref. [106] the set of discrete Langevin equations 4.6 is used to evaluate the surface roughness and the results are compared with KMC simulation. To our knowledge the set of discrete equations given in 4.6 has never been used for applications to real systems. Continuum equations like the one given in Eq. 4.9 are generally used for large scale simulations in which the value of x is not related to a particular site and the parameters used cannot be related to microscopic parameters.

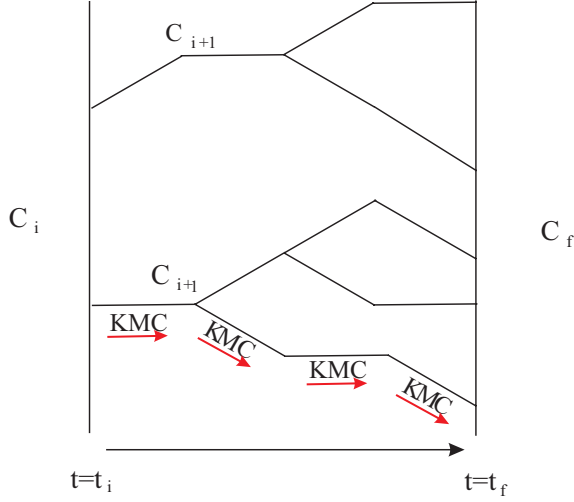


Figure 4.2: Phase space representation of a given system between $t = t_i$ and $t = t_f$. KMC is just following one of these paths, while the Master equation keeps track of all of them.

4.2 Kinetic Monte Carlo

An alternative method to the continuum equations to solve the Master equation is the KMC method. A KMC simulation starts from an initial configuration C_i of the system and at each time step it evolves to a new configuration till the simulation time t_{sim} is reached and the system is in a final configuration C_f . Each configuration of the system can be seen as a point in the configuration space and a KMC simulation as a time dependent path connecting the different phase space points as represented in Fig. 4.2. A KMC simulation follows just one of the possible paths that brings the initial configuration C_i to a final one C_f . Solving the Master equation for an initial configuration C_i instead corresponds to consider all the possible paths starting with C_i and find the probability of each final configuration C_f . If KMC runs are repeated a large number of times it is also possible to map the configuration space of the system. In this way every KMC runs can follow a new path and from the frequency of the final configurations C_f over a large number of runs it is possible to find the probability distribution $P(h_1, \dots, h_i, \dots, h_M)$ as for the Master equation. Generally the probability distribution for all the possible configurations is not needed and a single KMC run is enough to see how the surface looks like. Nevertheless many KMC runs are needed every time that one has to calculate some statistical values as the island density or the island-size distribution.

KMC follows the trajectories of each adatom diffusing on the surface. Each event corresponds to a new configuration. At high temperatures diffusion events play an important role and the adatoms' trajectories can get very complicated as shown in Fig. 4.3.

The simulation of such complicated trajectories requires a great computational effort. The time step for KMC simulation is given by Eq. 2.43 that it is reported here in its

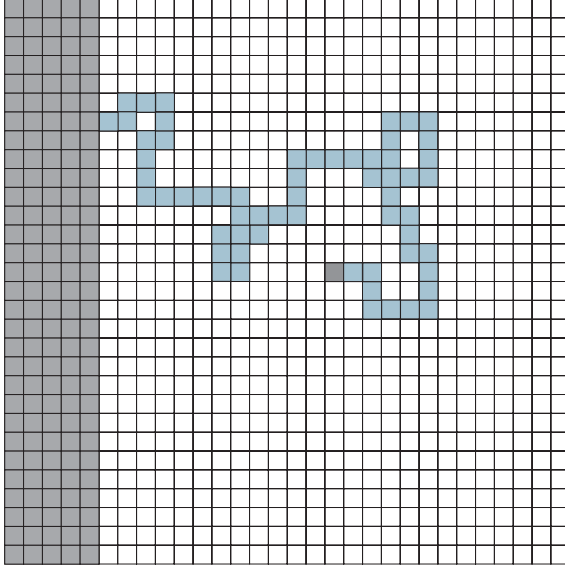


Figure 4.3: Here it is shown the path followed by an adatom diffusing on a surface before attaching to the step edge. This trajectory can be obtained with KMC. The calculation of these trajectories can get very complicated for high diffusion coefficients.

explicit form:

$$\Delta t = -\frac{\ln(\xi)}{\sum_i \Gamma_i} \quad .$$

Here Γ_i are the transition rates for the different processes. The diffusion coefficients depend exponentially on the temperature see Eq. 2.9. This implies that the time step decreases exponentially with the temperature. In Table 4.1 the diffusion mean free path per atom and the average time between two diffusion events are shown for KMC simulations on a 100×100 matrix for a simulation time of 0.1 s with a flux of 1 monolayer (ML)/s. A linear bond cutting model (see 2.41) was used with $E_0 = 1$ eV and $E_b = 1$ eV. The simulations were done for temperatures varying between 500 K and 1150 K. As expected, the number of jumps an adatom is doing before it is incorporated increases exponentially and the time step between two jumps decreases exponentially.

It is important here to distinguish between two very different types of processes that take place on the surface. On one side there are **growth processes** like nucleation and attachment which contribute to the growth of the surface and than there are **diffusion processes**, which do not produce any morphological change of the surface. The number of growth events is much smaller than the number of diffusion events. The number of growth events is of the same order as the number of adsorbed adatoms. Let us define $\Delta t_{\text{diffusion}}$ as the average time interval between two diffusion events and Δt_{growth} as the average time interval between two growth events. For the simulation considered in Table 4.1 there are roughly 1000 adatoms reaching the surface, thus the average time step between growth

Temperature (K)	$d_{\text{MFP}}/\text{atom}$ (d_{lat})	$\Delta t_{\text{diffusion}}$ (s)
500	30	$3.3 \cdot 10^{-5}$
750	470	$2.1 \cdot 10^{-6}$
1000	1800	$5.6 \cdot 10^{-7}$
1150	60000	$1.7 \cdot 10^{-8}$

Table 4.1: Diffusion mean free path (d_{MFP}) per atom and average diffusion time step Δt_{diff} , for temperatures ranging between 500 and 1150 K. d_{lat} is the distance between nearest neighbor sites. The results have been obtained employing KMC on a 100×100 matrix (for more details see text).

events is $\Delta t_{\text{growth}} \approx 10^{-4}$. In general it is possible to write $\Delta t_{\text{growth}} = \frac{1}{FL^2}$, where F is the flux (in ML/s) and L^2 is the total number of sites on the surface. As can be seen from Table 4.1, for higher temperatures the time scale for growth events (which one is eventually interested in) becomes orders of magnitude larger than that of the diffusion events. For example comparing the results for 1150 K it appears that $\frac{\Delta t_{\text{growth}}}{\Delta t_{\text{diffusion}}} \approx 10^4$. For this reason at high temperature KMC is getting exceedingly slow. Due to the different time scale between diffusion and growth events, the diffusion events will be called **fast events** and the growth events **slow events**. In the following a method, called Adatom Probability Kinetic Monte Carlo (AP-KMC), will be introduced to separate these two different time scales to improve the efficiency of the simulation. It is an extension of the one used in Chap. 3 for full growth simulation. The separation of the two time scales is obtained using a time step of the order of Δt_{growth} instead of Δt_{diff} as in KMC and treating the diffusion processes, which are not interesting for the growth, with a diffusion-like equation instead of following each trajectory.

To better understand the main ideas behind AP-KMC, a comparison will be done between KMC and Molecular Dynamics (MD) as illustrated in Fig. 4.4. In a) the AP-KMC method is just describing the important events for growth (attachment and nucleation). A part of the surface is enlarged in b) to show how the KMC method simulates these processes by following each single jump of the adatom. Finally in c) the surface is further enlarged to see how MD would describe all the atomic vibrations of an adatom around each stable site. As the KMC method does not follow the motion of an adatom around its equilibrium position and just considers the diffusion events where the adatom can escape from the energy's minimum, in the same way the AP-KMC method does not follow the diffusion processes of the adatom on the surface but it describes only the growth processes. MD, KMC and AP-KMC work on three different time scales, as illustrated in Fig. 4.5. The typical time step Δt used in MD is of the order of the phonon frequency, for the KMC it is of the order of the hopping rate and for AP-KMC it is of the order of the growth process rate. The value shown in Fig. 4.5 for the hopping rate is for the particular case of $T = 1000$ K as shown in Table. 4.1. The growth event rate follows from the previous discussion.

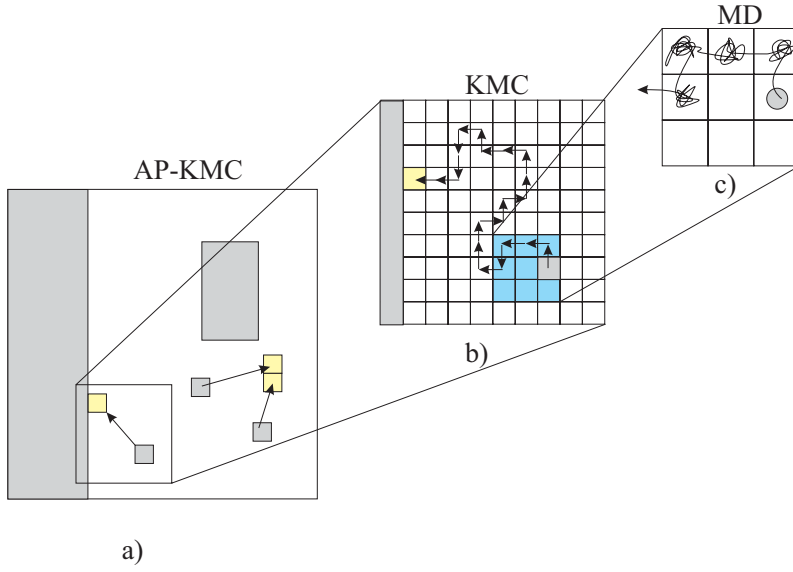


Figure 4.4: Schematic comparison between AP-KMC, KMC and MD is shown. In a) one can see a simulation done with AP-KMC, where only the growth processes are taken into account. In b) it is shown an enlargement of a part of the surface shown in a). Here one can see how KMC describe each single adatom hop. In c) it is presented a further enlargement of a part of the surface shown in b) and it is possible to see how a MD simulation describes all the adatoms vibrations around a stable site before jumping to a neighboring site.

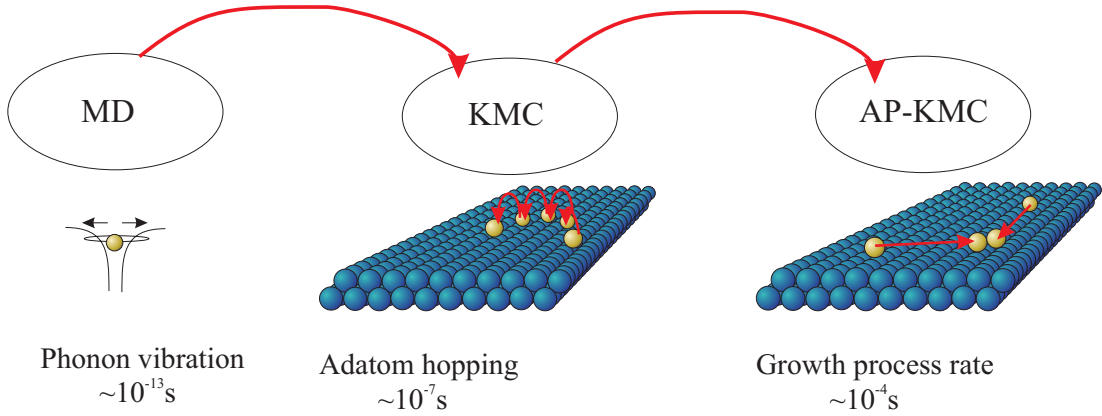


Figure 4.5: Schematic picture of the three different time scales used by MD, KMC and AP-KMC. MD works on the time scale of the phonon frequency, KMC on the time scale of the adatom hopping rate and AP-KMC on the growth process rate. The values for the hopping rate and growth process rate are taken from Table 4.1.

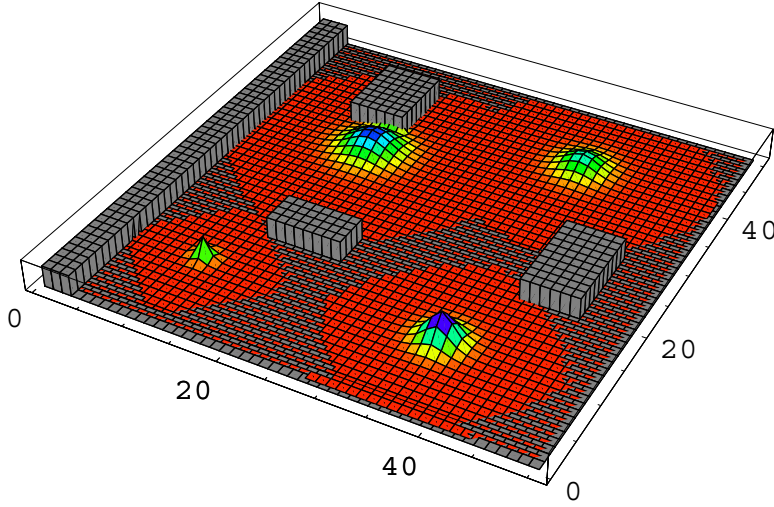


Figure 4.6: Picture of the surface with islands and steps where the adatoms are represented by their adatom densities. The shapes of the adatom densities can be peaked or smooth depending on how much time they had to spread out since the deposition moment.

4.3 Description of AP-KMC

As mentioned in the last two sections, it is possible to solve the Master equation using two different approaches: first using a set of continuum equations, and second using KMC simulations. A number of approximations have to be done to obtain the continuum equations and a large number of runs are necessary with the KMC method to solve the Master equation. Here a new hybrid approach to solve the Master equation is presented. This approach is a density based KMC and it is a mix of the previous two: the main idea is to describe the adatoms' dynamic on the surface through an adatom density, avoiding in this way the need to follow the trajectory of each adatom, as it is done for KMC. It is important to notice that the density approach affects only the adatoms, while the surface and the islands on the surface will be treated as in a KMC approach. For this density approach it is necessary to switch from the normal surface where the adatoms occupy a given position to a **density picture** where the adatoms have a certain probability to be in a given site. This is shown in Fig. 4.6 which shows a surface with steps and islands and the adatoms are described through densities.

From the density picture it is possible to go back to the surface by collapsing each single adatom density on the surface as it will be described in detail in Sec. 4.3.2. At each time step it is necessary to switch from the surface to the adatom density picture and back to the surface with the collapse procedure. Two methods will be proposed which use this density based approach. Here first the adatom probability Kinetic Monte Carlo (AP-KMC) and in Sec. 4.6 the Adatom density Kinetic Monte Carlo (AD-KMC) will be described.

4.3.1 Model Structure

In order to separate the two time scales (for growth events and diffusion events) the configuration C is rewritten in two parts: (i) the index S describing the surface without the adatoms and (ii) the index (i_1, i_2, \dots, i_N) which gives the position of the adatoms on the surface:

$$C \rightarrow \{(i_1, i_2, \dots, i_N), S\} \quad . \quad (4.10)$$

i_α gives the site index of the α -th adatom, the total number of adatoms is N . For the index S a SOS model is used as before. To each adatom is associated a number so it is possible to distinguish them and follow the evolution of every single adatom. The Master equation will be solved for a time $t = \Delta t_{\text{growth}}$. During this time it is assumed that the surface S does not change, while the adatoms are moving around and (i_1, i_2, \dots, i_N) is changing rapidly. Under these conditions the index for the surface S can be taken out of the Master equation and it can be written as function of the adatoms configuration only:

$$P(C, t) = P_{\text{ad}}(i_1, i_2, i_3, \dots, i_N, t) P_S(t) \quad (4.11)$$

Here, $P_{\text{ad}}(i_1, i_2, i_3, \dots, i_N, t)$ is the probability to find the adatoms in the configuration $(i_1, i_2, i_3, \dots, i_N)$ at time t and $P_S(t)$ is the probability to have the surface in the configuration S at time t . As during Δt_{growth} the surface does not change it results $P_S(t) = 1$, than:

$$P(C, t) = P_{\text{ad}}(i_1, i_2, i_3, \dots, i_N, t) \quad . \quad (4.12)$$

4.3.2 Non-Interacting adatoms

Let us first consider the case of non-interacting adatoms. This means that two adatoms do not see each other. No nucleation events can take place on the surface. The adatoms diffuse as free particles on the surface and they interact only with the surface. They can be attracted by steps and kinks on the surface. Three types of processes are involved in this situation: **adsorption**, **diffusion** and **attachment**. Each of these processes will be considered in detail. The probability function can be rewritten as:

$$P^{\text{non-int}}(i_1, i_2, i_3, \dots, i_N, t) = \prod_{\alpha} \rho_{\alpha}(i_{\alpha}, t) = \rho_1(i_1, t) \rho_2(i_2, t) \dots \rho_N(i_N, t) \quad . \quad (4.13)$$

Here $\rho_l(i_l, t)$ gives the probability to find the particle number l at position i_l at time t .

Adsorption

The incoming flux of particles is F (in ML/s). The **adsorption time step** $\Delta t_{\text{ads}} = \frac{1}{L^2 F}$ is the average time step between two adsorption events, and L^2 is the total number of adsorption sites on the surface. The adsorption time is chosen deterministically:

$$t_{\alpha}^{\text{ads}} = \alpha \Delta t_{\text{ads}} \quad (4.14)$$

where α is an integer number. It would also be possible to use a random time step for adsorption but for simplicity a constant one has been used here. Deterministic time steps have been used already in other methods as the Level Set Method giving good results. The adsorption site i_{ads} is chosen randomly on the surface. A random number r_{rand} is picked so that $1 \leq r_{rand} \leq L^2$ and it results:

$$i_{ads} \leq r_{rand} \leq i_{ads} + 1 \quad . \quad (4.15)$$

At the adsorption time t_{α}^{ads} the adatom density is given by:

$$\rho_{\alpha}(i, t_{\alpha}^{ads}) = \delta_{i, i_{ads}} \quad (4.16)$$

where $\delta_{i, i_{ads}}$ is the Kronecker symbol. The implementation of the adsorption process is local because a particular site of the surface is chosen for the adsorption. The adsorption process is treated locally also by the KMC method, but other methods like Rate equation or the level set method consider it homogeneous all over the surface.

Diffusion

Substituting Eq. 4.13 into Eq. 4.2 one gets a set of single adatom equations:

$$\frac{\partial \rho_{\alpha}(i, t)}{\partial t} = \sum_{\delta} [\Gamma_{i+\delta, i} \rho_{\alpha}(i + \delta, t) - \Gamma_{i, i+\delta} \rho_{\alpha}(i, t)] \quad . \quad (4.17)$$

Here, $\Gamma_{i+\delta, i}$ is the transition probability of an adatom to go from site $i + \delta \rightarrow i$ and δ is an index which goes over all nearest neighbor sites. The initial condition for Eq. 4.17 is given by Eq. 4.16 for adsorption. In this way each adatom is described by an adatom density. This is what was also done in the previous chapter. In Fig. 4.7 it is illustrated how the adatom density profile is changing during the time. Here a model system with $D = 10 \text{ s}^{-1}$ is used and the differential equation is solved for different times $t = 0.0025 \dots 0.2 \text{ s}$.

To discuss the diffusion process in more detail let us consider a single adatom in front of a surface step. This is shown in Fig. 4.8 for a temperature of 500 K and in 0.03 s time intervals on an array of 40×40 . At $t = 0 \text{ s}$ the adatom density is unity at the deposition site and zero everywhere else (see Eq. 4.16 and Fig. 4.8 a)). In the next two time steps the adatom density spreads out on the surface (Figs. 4.8 b) and c)) and eventually reaches the step. Since the probability to move away from the step is low (the barrier for jumping from the step to the terrace is 2 eV compared to 1 eV for the jump from the terrace to the step; see (Eq. 2.41)) the adatom density accumulates at the step edge (Figs. 4.8 d) and e)). In the last figure of this sequence the initial peak at the deposition site completely disappears and almost all the density is concentrated along the step edge. It should be noted that the density correctly describes all relevant processes: diffusion on the terrace, attachment and detachment at steps, and diffusion along the step.

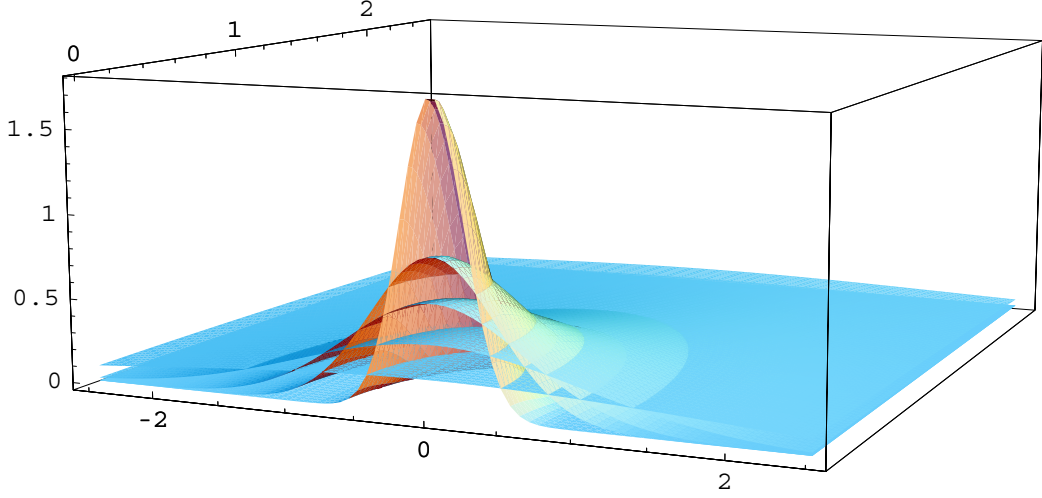


Figure 4.7: Adatom density profiles for a diffusing adatom on a flat surface. In the beginning the adatom density is sharply localized on the initial position $(0,0,0)$ of the adatom and then it becomes more and more delocalized. The calculations were done for $D = 10$ and $t = 0.0025, 0.01, 0.02, 0.05, 0.2$ s.

Collapse

When $t = \Delta t_{\text{growth}}$ it is necessary to go back from this density picture to a surface in which an adatom is occupying a given position. This is done by collapsing the adatom density. The **collapse** of the **adatom density** is a key point of the method. It is important to note that from the single particle density $\rho_\alpha(i, t)$ it is possible to obtain the position of the adatom at each time. To this end the single particle density has to be collapsed on a single site which can be done by choosing a random number p_{rand} in the interval $[0, 1]$ and selecting the site l such that:

$$\sum_{i=0}^l \rho_\alpha(i, t) \leq r_{\text{rand}} \leq \sum_{i=0}^{l+1} \rho_\alpha(i, t) \quad . \quad (4.18)$$

Note that the integrated density is

$$\bar{\rho}_\alpha = \sum_{i=0}^{L^2} \rho_\alpha(i, t) \equiv 1 \quad . \quad (4.19)$$

It should be noted that the collapse is *not a deterministic process* but stochastic in analogy to a measurement process of a quantum mechanical wave function. To be more specific, let us again consider the evolution of the single particle density of an adatom in front of a surface step. This is shown in Fig. 4.9. The simulations were done at a temperature of $500K$ and the collapse took place after a time interval of $\Delta t = 0.01s$. As can be seen the adatom attaches to the step already after three collapses/simulation steps.

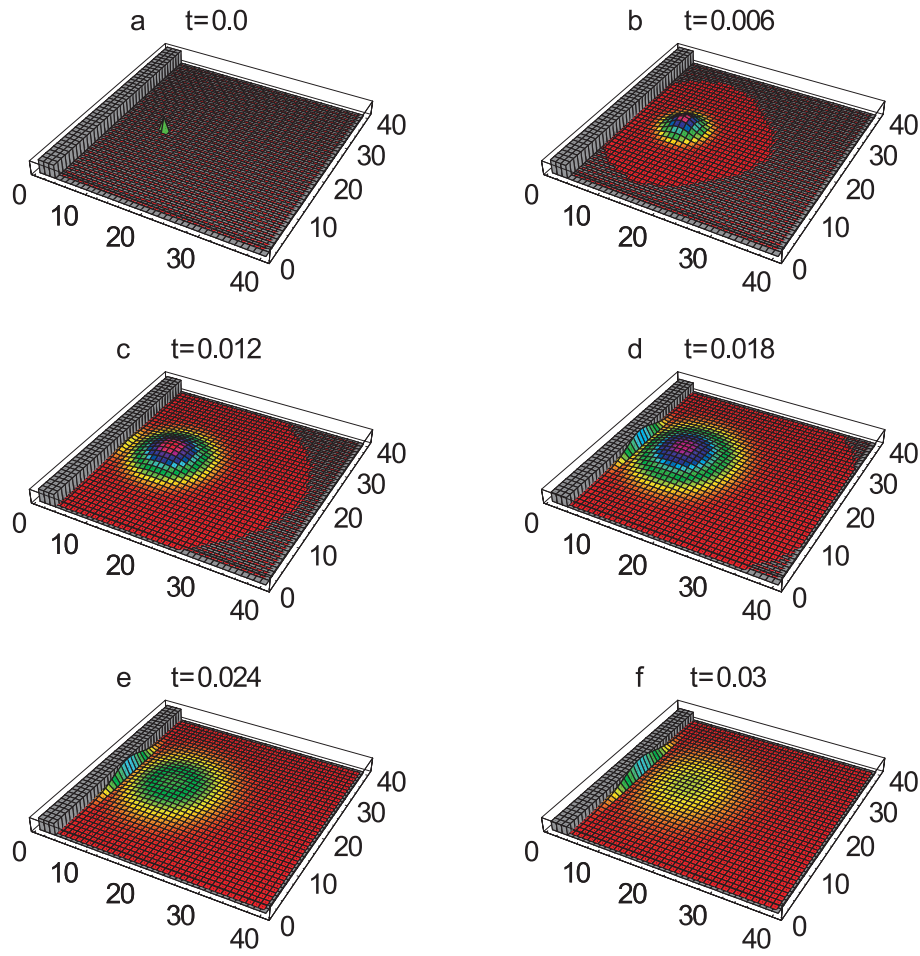


Figure 4.8: Time evolution of the adatom density for an adatom close to a step. The snapshots are taken between $t = 0.00$ s and $t = 0.03$ s for $T = 500$ K. For $t > 0$ the adatom density has been multiplied by an arbitrary scaling factor for ease of viewing.

Using KMC, where each individual jump is described, a much larger number of time steps would have been required (for the specific case shown in Fig. 4.9 approx. 800 steps), i.e., this approach indeed allows to dramatically reduce the number of time steps. To perform simulations for $t > t_{\text{growth}}$ one has to repeat this procedure by switching between the adatom density picture and the collapse. If one starts with a surface, first one has to go to the adatom density picture, solve the set of differential equations for the adatom density and then collapse the system to go back to the surface and start a new cycle again. This sequence of switches between the adatom and its density is shown in Fig. 4.10 for the case of a single adatom. Starting from the deposition moment the adatom is alternatively treated as density or adatom until it nucleates or gets attached to a step edge.

Some similarities between the KMC method and the density based KMC regarding the time step and the collapse will be pointed out here. In KMC the characteristic/average time step is of the order or smaller than Δt_{diff} . The time step in KMC is chosen in such a way that only one event takes place in a time interval. In density based KMC the time step is chosen in such a way that only one growth event (nucleation or attachment) can take place, and not any event as it was the case for KMC. The density based KMC time step is orders of magnitude larger than the one used by KMC.

In KMC at each time step a list of the probabilities of all the new possible configurations is built and then randomly a configuration is chosen. In the density KMC method it is possible to evaluate the probability for each configuration of the system. This can be done knowing the single adatom densities. When the adatom densities are randomly collapsed, one of the possible configuration is chosen. The collapsing procedure in the density KMC method is similar to the random choice of a possible configuration from the probability list done in KMC. It should be noted here that if in the density KMC a time step as small as in KMC is used, then the density KMC method is equivalent to KMC.

Attachment

To understand how the attachment process works it is useful to look at Fig. 4.8. Here one can see how after the deposition the adatom density starts to diffuse and eventually reaches the step edge where it accumulates because it is unfavorable for the adatom density to move away from the step edge. After a certain time almost all the adatom density is located along the step edge. The probability that the adatom density is collapsed along the step is very high. If the adatom is collapsed along the step it becomes part of the surface and it will not move anymore. This assumption corresponds to the case of irreversible growth, which is made at this point for simplicity. The method could be easily extended to include also detachment processes but this argument will not be discussed here. The surface is updated, i.e. if i is the site where the attachment event takes place the following relation holds:

$$S = (...h_i, ...) \Rightarrow S' = (...h_i + 1, ...). \quad (4.20)$$

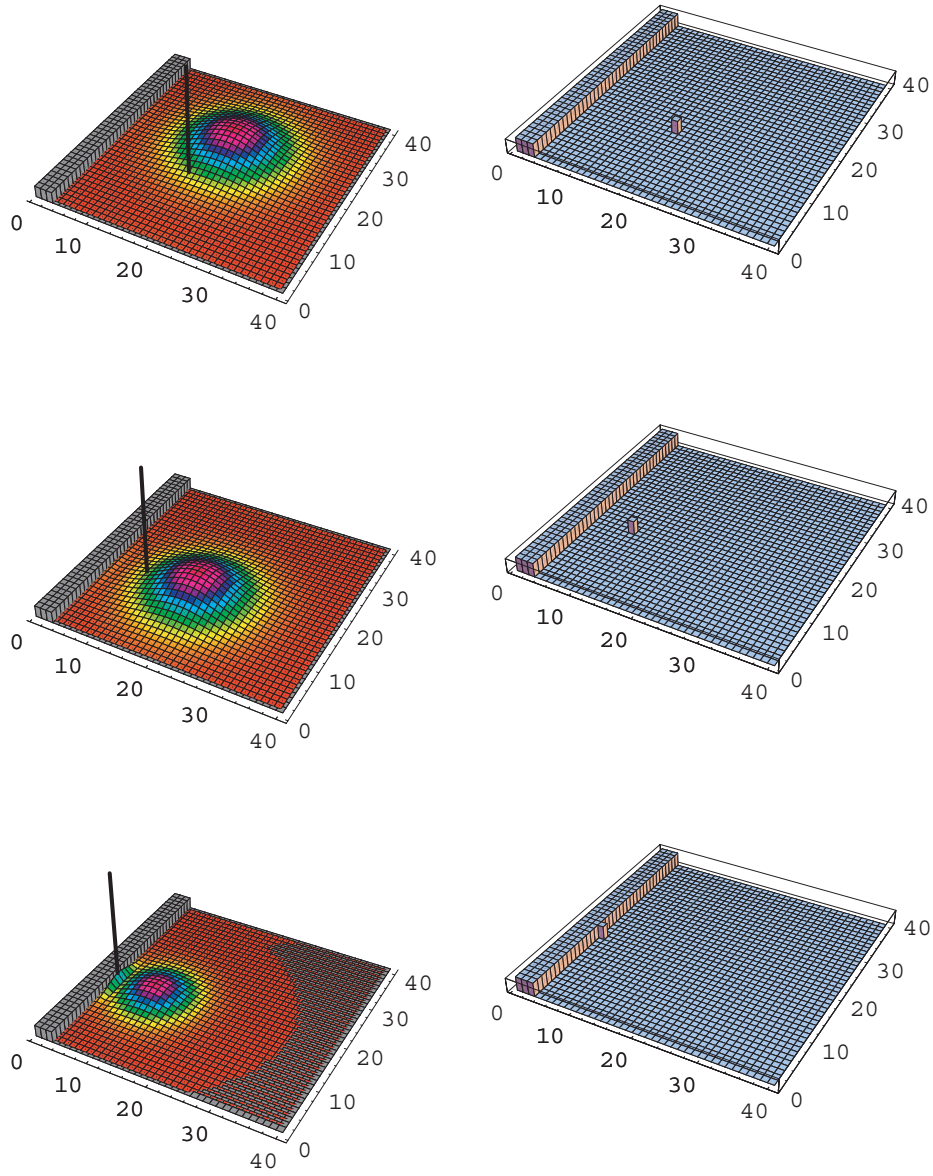


Figure 4.9: Surface before (left) and after (right) a collapse of the adatom density. The collapse is performed at equal time intervals of $\Delta t = 0.01$ s. The simulation has been performed at a temperature of $T = 500$ K. The adatom density has been scaled for ease of viewing.

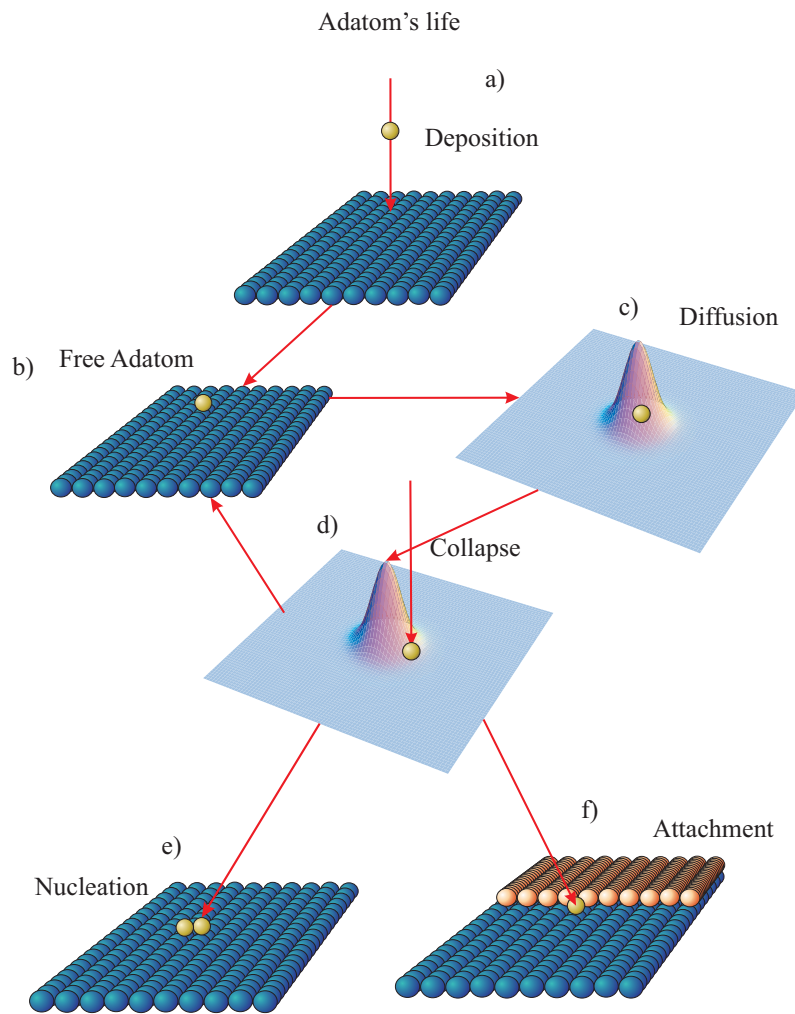


Figure 4.10: Schematic view of the "life" of an adatom. First there is a deposition event a), which creates a free on the surface b). To describe the diffusion the adatom is treated as an adatom density c) and which is collapsed at d). The lifetime of an adatom ends if the collapse places the adatom at a step edge (attachment) f) or next to another adatom (nucleation) g), otherwise if it is still a free adatom a new cycle is started.

The adatom density that was collapsed disappears. In general an attachment event happens when the adatom density is collapsed in a site where at least one nearest neighbor site is already occupied. If the adatom is collapsed on a site where all the other nearest neighbor sites are unoccupied, than in the next time step the adatom will be treated again as an adatom density.

4.3.3 Interacting adatoms

The method proposed for the non-interacting model in the previous section is in principal correct. This means it would give the same results as the direct solution of the Master equation or a KMC simulation. The interactions between the adatoms play a very important role during crystal growth. In particular, they are responsible for nucleation events on the surface. The interactions between adatoms is mainly due to their chemical bond. If two adatoms occupies two neighboring sites, they form a strong chemical bond, so that long range interactions due to elastic and/or electrostatic interactions can be often neglected. For the simplified energy functional used here (Eq. 2.41) this assumption is always fulfilled. In the following it will be assumed that only adatoms on nearest neighbor sites interact with each other. Since interaction is restricted between adatoms on neighboring sites it means that once interaction occurs, a cluster/nucleus consisting of 2 or more adatoms on the surface is formed. Depending on the growth parameters (temperature, fluxes) the minimum size of such a cluster to form a stable nucleus may vary (see e.g. Ref. [6]). In order to keep the following discussion simple it is assumed that already a nucleus consisting of two atoms is stable and represents an island. This means that the critical island size is $i^* = 1$ (see Chap. 3). A generalization to larger critical island sizes is straightforward and will be described elsewhere [108]. Due to the interactions between the adatoms now it is not possible to rewrite the probability function as the product of the single adatom densities as it was done in Eq. 4.13. Because of the choice of the time step $\Delta t \approx \Delta t_{\text{growth}}$, the probability that more than two adatoms interact at the same time is very small and can be neglected. This means that if there are three adatoms on the surface, the probability to find them at a given position is $P(i_1, i_2, i_3)$ and as just two adatoms can interact together the third one is not correlated to the other two. For this reason it is possible to write:

$$\rho(i_1, i_2, i_3) = \rho(i_1, i_2)\rho(i_3) \quad . \quad (4.21)$$

Here it was assumed that the adatoms one and two are interacting and adatom three is independent. For this reason it is possible to describe all the system using a two-particle density:

$$P^{\text{AD-AD Int.}}(i_1, i_2, i_3, \dots, i_N, t) = \prod_{\alpha, \beta} \rho_{\alpha, \beta}(i_{\alpha}, i_{\beta}, t) \quad (4.22)$$

If this expression for the probability function is plugged in the Master equation Eq. 4.2, it is possible to get a set of two-particle density equations:

$$\begin{aligned} \frac{\partial \rho_{\alpha,\beta}(i,j,t)}{\partial t} = & \sum_{\delta_i} \Gamma_{i+\delta_i,i} \rho_{\alpha,\beta}(i+\delta_i,j,t) + \\ & \sum_{\delta_j} \Gamma_{j+\delta_j,j} \rho_{\alpha,\beta}(i,j+\delta_j,t) \quad . \end{aligned} \quad (4.23)$$

δ_i, δ_j describe neighboring sites around sites i and j . i and j are nearest neighbors. To reduce the complexity of the equation it is useful to write the two-particles density as a function of the one-particle densities. If one uses now the Hartree approximation as it was done in Chap. 3 the previous set of equations can be written as:

$$\begin{aligned} \frac{\partial \rho_{\alpha,\beta}(i,j,t)}{\partial t} = & \sum_{\delta_i} \Gamma_{i+\delta_i,i} \rho_{\alpha}(i+\delta_i,t) \rho_{\beta}(j,t) + \\ & \sum_{\delta_j} \Gamma_{j+\delta_j,j} \rho_{\alpha}(i,t) \rho_{\beta}(j+\delta_j,t) \quad . \end{aligned} \quad (4.24)$$

This is the same nucleation term used in Eq. 3.30 for the two point island, so to describe the system one can use the following set of equations:

$$\begin{aligned} \frac{\partial \rho_1(i,t)}{\partial t} = & D[\rho_1(i+1,t) + \rho_1(i-1,t) - 2\rho_1(i,t)] - \\ & D\rho_1(i,t)[\rho_2(i+2,t) + \rho_2(i-2,t)] \quad . \end{aligned} \quad (4.25)$$

To perform a growth simulation including adatom-adatom interaction is then straightforward and very similar to solving the non-interacting adatom-adatom system. The only difference is that in addition to solving (Eq. 4.17) after each time step also all nucleation probabilities $p_{\alpha,\beta}(i,j,t)$ have to be calculated.

Similarly as for the collapse of the single particle densities one can perform also a collapse for the nucleation density to decide whether and where a nucleation takes place. It is possible therefore to calculate the nucleation time by:

$$t_{\text{nuc}} = -\frac{\ln r_{\text{rand}}}{n_{\text{tot}}} \quad . \quad (4.26)$$

Here, $n_{\text{tot}} = \frac{1}{2} \sum_{\alpha,\beta,i,j} p_{\alpha,\beta}(i,j,t)$ is the total probability of a nucleation event (j is restricted to be a nearest neighbor of i). If t_{nuc} is larger than the simulation time step Δt_{growth} no nucleation event occurs. If, however, t_{nuc} is smaller a nucleation event is performed by applying a further collapse (in analogy to Eq. 4.18) to select the pair of atoms (α and β) and the nucleation sites i, j . On the site where the nucleation occurs the surface is updated, i.e.:

$$S = (...h_i, h_j, ...) \Rightarrow S' = (...h_i + 1, h_j + 1...). \quad (4.27)$$

After the nucleation event the two-adatom densities involved in the process are eliminated.

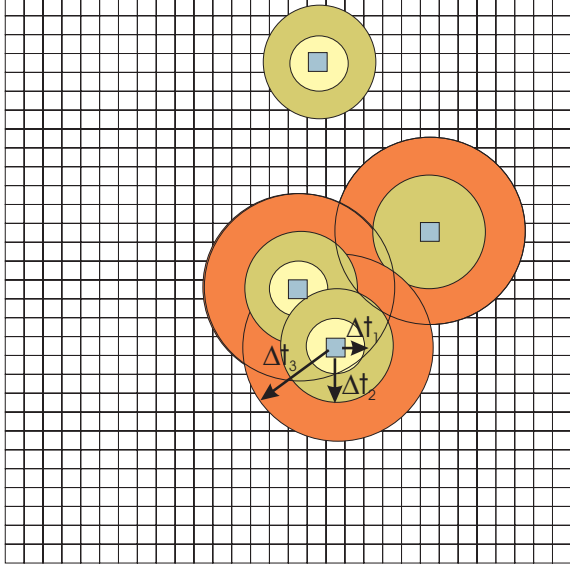


Figure 4.11: The interaction areas for the adatoms are plotted at different times. Increasing the time step the overlapping of the interaction areas for different adatoms are increasing and higher density terms have to be taken into account.

4.4 Longer time steps and higher density terms

In the previous section the choice for the time step was $\Delta t = \Delta t_{\text{growth}}$. Here the possibility to develop new methods which use a time step Δt larger than Δt_{growth} will be briefly discussed. In this case there are more events that happen in a time step Δt and in particular more than one growth event can take place within Δt . For example two adatoms can nucleate together and afterwards another adatom can attach to the new islands. To take into account the correlation between the three adatoms, the three particle density $\rho_{\alpha,\beta,\gamma}(i, j, k, t)$ should be considered and Eq. 4.13 can be rewritten as:

$$P^{\text{int.}}(i_1, i_2, i_3, \dots, i_N, t) = \prod_{\alpha,\beta,\gamma} \rho_{\alpha,\beta,\gamma}(i_\alpha, i_\beta, i_\gamma, t) \quad (4.28)$$

As the time step is increasing the number of particles interacting with each other is increasing as illustrated in Fig. 4.11, where it is shown how the interaction area of a particle is increasing with time.

For longer time steps one has to include higher order adatom densities till the moment when all the particles are interacting and the distribution probability $P(i_1, i_2, i_3, \dots, i_N, t)$ cannot be reduced anymore to lower order terms and the Master equation must be solved for the full probability distribution. Even if a larger time step allows to reduce the number of time steps needed to perform the simulation, the complexity of the method to take into account larger time steps also increases, thus one should pay attention to the fact that a larger time step could finally slow down the simulation. Concluding one should find the time step which can perform the best for the system under study. In the present work

only the two particle density was used because it was the easiest model to test. This means that, referring to Fig 4.11, the time step Δt has to be chosen in such a way that $\Delta t \approx \Delta t_2 = \Delta t_{\text{growth}} \ll \Delta t_3$, where Δt_2 is the time for two particles to interact and Δt_3 for the three particles interaction.

4.5 Implementation of AP-KMC

To understand the implementation of AP-KMC a flow chart of the method will be presented in Fig 4.12. The method is composed by 7 steps:

1. the simulation starts at $t = 0$ with a given surface.
2. If there are adatoms on the surface they are going to be converted into adatom densities.
3. The time step must be of the order of Δt_{growth} . To do this one gets Δt equal to the minimum between the deposition time step $\Delta t_{\text{dep}} = \frac{1}{FL^2}$ and the nucleation time step $\Delta t = \frac{1}{N}$ where N is the probability that a nucleation event takes place on the surface, as it will be shown in the following.
4. Check for deposition events. If $\Delta t FL^2 > 1$ than there is a deposition event and this is done randomly on the surface as described in Sec 4.3.2.
5. The system of differential equations for the adatom density is solved.
6. If the nucleation term $\sum_{\alpha,\beta} D\rho_\alpha(i,j)\rho_\beta(i,j) > 1$ there is a random nucleation event on the surface
7. Collapse all the densities on the surface

The solution of the differential set of equations is the most time consuming part of the method. Different approaches are possible to solve the system. On one side there are the explicit methods in which to calculate $\rho_i(t + \Delta t)$ one just needs to know the values of $\rho(t)$. This approach is easy to implement and fast, but it gives unstable solution for large time steps (see App. E). On the other side implicit methods can be applied, which are more complicated to implement, because one has to solve a system of difference equations to find the solution, but they have the big advantage that they are stable for any time step (for more details see App. E).

4.6 AD-KMC

Even if the method described in the previous section successfully decouples the “fast” time scale of the diffusion events from the “slow” time scale of the growth events it is numerically still very expensive. The most expensive computations are those of the single particle density and of the nucleation probability (which is a two-particle density and scales thus with the square of the number of adatoms).

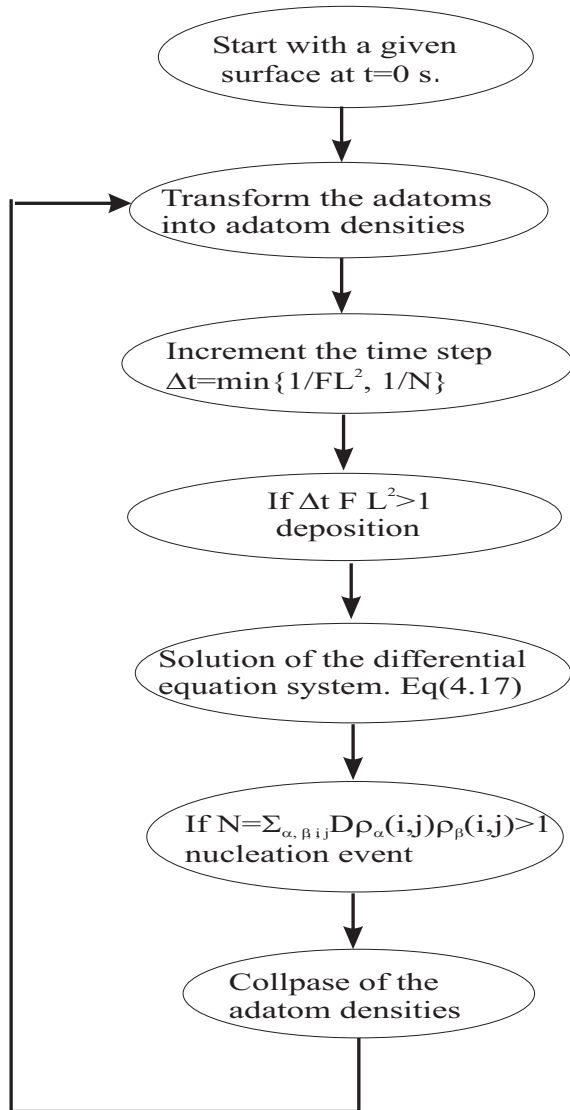


Figure 4.12: Flow chart for AP-KMC, see text for the description of each single step.

In order to discuss further optimizations it will be considered the case of high growth temperatures, which is particularly relevant for realistic growth simulations. Since the diffusivity (the jump probability) of an adatom increases exponentially with temperature at high temperatures an adatom quickly explores a large part of the surface and gets quickly trapped on energetically favorable sites (such as surface steps or kinks). Under these conditions the total adatom density and thus the nucleation rate will be small. With other words, the one-particle density will be rather delocalized and will quickly “lose” the information about the initial adsorption site (see e.g. Fig. 4.8 f)). In the limit of infinite diffusivity each adatom can explore the entire surface, i.e., the single particle density will be infinite and describe the *thermodynamic* probability to find an adatom on a certain site. This probability function is of course identical for all adatoms. For conditions close to thermodynamic equilibrium the densities are not identical but similar.

If the one-particle densities are (at least in a local region) similar to each other and largely delocalized the adatoms can be described by the *total adatom density*

$$\rho(i, t) = \sum_{\alpha} \rho_{\alpha}(i, t) \quad (4.29)$$

rather than by the complete set of single particle densities. Using the same arguments as in the previous section one then obtains a method which it will be called adatom-density KMC (AD-KMC) and which completely avoids the calculation of the single particle densities. To keep the following discussion simple aggregated growth is assumed (as it has also been done for the AP-KMC), i.e., once an adatom has been incorporated it can not be dislodged to become an adatom again. The equation describing the time evolution is similar to (Eq. 4.17)

$$\begin{aligned} \frac{\partial \rho(i, t)}{\partial t} = \sum_{\delta} [\Gamma_{i+\delta, i} \rho(i + \delta, t) - \Gamma_{i, i+\delta} \rho(i, t)] - \\ n_{\text{nuc}}(i, t) - n_{\text{att}}(i, t) + F(i, t) \quad . \end{aligned} \quad (4.30)$$

except that nucleation $n_{\text{nuc}}(i, t)$, attachment $n_{\text{att}}(i, t)$ and adsorption $F(i, t)$ are now explicitly included. For the further discussion a constant and homogeneous flux ($F(i, t) = F$) will be assumed. Attachment is described by a deterministic event, i.e., it occurs once the adatom density at site i_0 and at time t_0 is unity ($\rho(i_0, t_0) = 1$). If such an event occurs, $n_{\text{att}}(i, t) = \delta_{i, i_0} \delta_{t, t_0}$, i.e. the density on this site is reset to zero. Also, the surface and thus the transition probabilities $w_{i+\delta \rightarrow i}$ around the attached atom are modified:

$$S = (...h_i...) \Rightarrow S' = (...h_i + 1...) \quad . \quad (4.31)$$

For a nucleation event on a terrace away from steps and for realistic growth parameters (Eq. 4.24) can be further simplified. On a free terrace all transition rates are identical and are given by the surface diffusion constant D :

$$\Gamma_{i+\delta, i} = D/l_0^2 \quad . \quad (4.32)$$

Here, l_0 is the distance between two nearest neighbor sites. If it is further assumed that the adatom density around the nucleation site is approximately constant, then the probability that a nucleation event takes place on site i at time t is given by:

$$p_{\text{nuc}}(i, t) \approx D l_0^2 \rho^2(i, t) \quad , \quad (4.33)$$

which is a well known relation often applied in Rate equations [6]. To calculate the nucleation rate $n_{\text{nuc}}(i, t)$ needed to solve (Eq. 4.30) it is assumed:

$$n_{\text{nuc}}(i, t) \equiv \bar{p}_{\text{nuc}}(t) = \int_{t-\Delta t_{\text{growth}}}^t \sum_i p_{\text{nuc}}(i, t) dt \quad . \quad (4.34)$$

The replacement of a localized nucleation term by a delocalized term is well justified for the high temperature conditions assumed here and avoids the formation of localized regions with negative adatom density. For the modification of the surface and the transition states the non-averaged nucleation term according to (Eq. 4.33) is used. As can be seen from the above equations all quantities entering (Eq. 4.30) are either explicitly given (like the flux F) or can be directly calculated from the total adatom density $\rho(i, t)$. Thus, in contrast to AP-KMC the explicit calculation of single particle densities and two-particle nucleation terms is avoided making AD-KMC computationally much more efficient. Applications of the method and a discussion about the validity of the underlying assumptions will be given in the next chapter.

4.7 Conclusion

KMC is the standard method for atomistic growth simulations. It is very efficient and it has been applied in many studies on different systems. Nevertheless improvements of the method are still possible. In this chapter alternative methods within an adatom density approach have been proposed. This allows a better description of the diffusion processes. Two different methods have been presented here, the adatom probability kinetic Monte Carlo (AP-KMC), in which each adatom on the surface is described by an adatom density and the adatom density kinetic Monte Carlo (AD-KMC), in which just one-adatom density is used for all the adatoms present on the surface. In the next chapter a comparison between density based KMC and standard KMC will be shown.

Chapter 5

Statistical Tests for the Submonolayer growth

In this chapter the results of an extensive comparison between AD-KMC and AP-KMC with KMC are presented. Simulations to check the island density, the island size distribution, and the island shape in the submonolayer regime have been performed. For all three approaches identical simulation parameters have been chosen: The simulations have been performed on a square lattice (mesh size 80×80), the transition rates are calculated according to (Eq. 2.9) using a prefactor $\Gamma_0 = 10^{13} \text{ s}^{-1}$ (Eq. 2.10) and the diffusion barrier according to (Eq. 2.41) [109,110]. The flux of incoming adatoms is $F = 1 \text{ ML/s}$. The total simulation time is 0.1 s, i.e., a total of 0.1 ML is deposited on the surface. It is further assumed that already a dimer forms a stable nucleus. This is explicitly enforced in the KMC calculations and allows to approximate the nucleation in AD-KMC by (Eq. 4.33). The growth temperature has been varied over a large range of temperatures (from 500 to 1000 K). Finally the application of AD-KMC to capture numbers are presented. The comparison with the KMC simulation is the result of a collaboration with R. Kunert and E. Schöll, who performed the KMC calculations. The results of this joined work have been published in Ref. [111].

5.1 Island nucleation density

The first quantity which will be discussed is the island nucleation density (see Sec. 2.2.2) which is simply the number of islands formed on the surface. Rather than using directly the temperature as variable the ratio of $D(T)/F$ is used as free variable to allow a direct comparison with previous studies (see e.g. [63,112]). The calculated island nucleation density as function of D/F is shown in Fig. 5.1. As can be seen, AD-KMC and KMC give virtually identical results: With increasing D/F ratio the island density rapidly decreases.

Employing rate equations the slope of this curve can be described analytically by Eq. 2.30 that it is reported here:

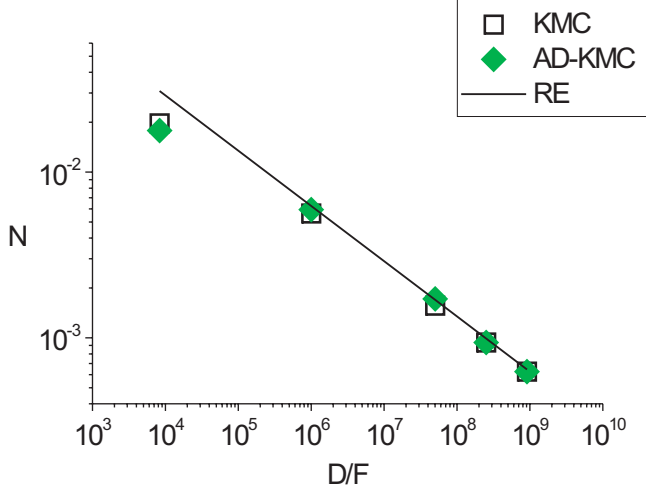


Figure 5.1: Island density N obtained with AD-KMC and KMC as a function of D/F between 10^4 and 10^9 at a coverage of $\theta = 0.1$. The solid line (RE) is an analytic approximation based on rate equations and a critical nucleus size of two atoms (see text). Fig. from Ref. [111].

$$N \sim \left(\frac{D}{F} \right)^{-\frac{i^*}{i^*+2}}.$$

Since for our system already a dimer forms a stable nucleus $i^* = 1$, i.e., the nucleation density should follow a scaling law with power $-1/3$. This scaling relation has been also included in Fig. 5.1. Since an analytical solution of the proportionality factor in the scaling relation (Eq. 2.30) is not known it has been fitted to the KMC result for $D/F = 10^9$. As can be seen the scaling relation correctly approximates the slope of the KMC and AD-KMC results except for very low D/F ratios. Under these conditions the adatom diffusivity is negligible and nuclei are no longer formed by two adatoms moving together but by adsorption of an adatom next to an existing adatom.

5.2 Island size distribution

Having verified that the nucleation density is correctly described we will now focus on spatial information. To this purpose the island size distribution has been calculated. In Sec. 2.2.2 it is shown that over a large range of fluxes, temperature, and diffusion barriers the island size distribution approximately follows a universal scaling law given by Eq. 2.36, that it is reported here:

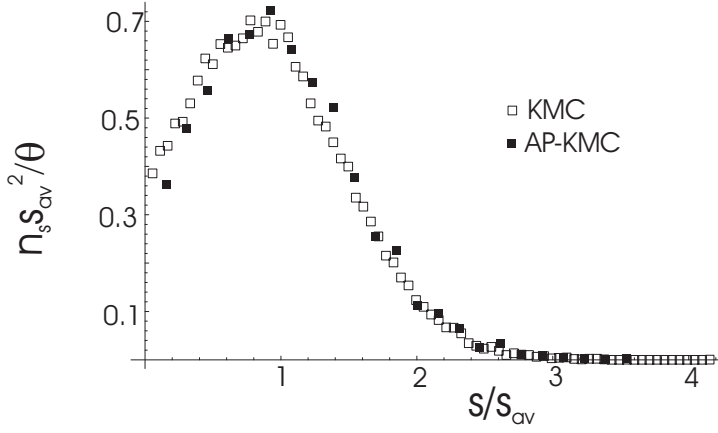


Figure 5.2: Island size distribution obtained from KMC (filled squares) and AP-KMC (empty squares) for $T = 630$ K, $D/F = 10^6$, with a coverage of $\theta = 0.1$ ML. Under these conditions fractal islands are formed (see Fig. 5.4). Fig. from Ref. [111].

$$n_s = \frac{\theta}{\bar{s}^2} f\left(\frac{s}{\bar{s}}\right) \quad .$$

This scaling law was confirmed by experiments (e.g. Ref. [113]) and by KMC simulations (e.g. Ref. [64]). These studies showed also that the scaling function depends also from the critical island size i^* . Amar and Family (Ref. [64, 112]) proposed the following expression for the scaling function

$$f_{i^*}(x) = C_{i^*} x^{i^*} \exp[-i^* a_{i^*} x^{1/a_{i^*}}] \quad . \quad (5.1)$$

Here, a_{i^*} and C_{i^*} are determined by:

$$\frac{\Gamma[(i^* + 2)a_{i^*}]}{\Gamma[(i^* + 1)a_{i^*}]} = (i^* a_{i^*})^{a_{i^*}} \quad (5.2)$$

$$C_{i^*} = \frac{(i^* a_{i^*})^{(i^* + 1)a_{i^*}}}{a_{i^*} \Gamma[(i^* + 1)a_{i^*}]} \quad (5.3)$$

Γ is the Gamma function.

As a first comparison between KMC and AP-KMC the island size distribution is considered. A temperature $T = 630$ K has been chosen and the results are shown in Fig. 5.2. At this temperature both methods show the formation of fractal islands. The agreement is excellent demonstrating the accuracy of AP-KMC. Fig. 5.3 shows the island size distribution for all three approaches. A total of 45 runs on a 300×300 matrix has been performed to obtain a reliable statistics. As it can be seen (see also Fig. 5.2) the island size distribution as calculated by KMC and AP-KMC are identical within the statistical error bars.

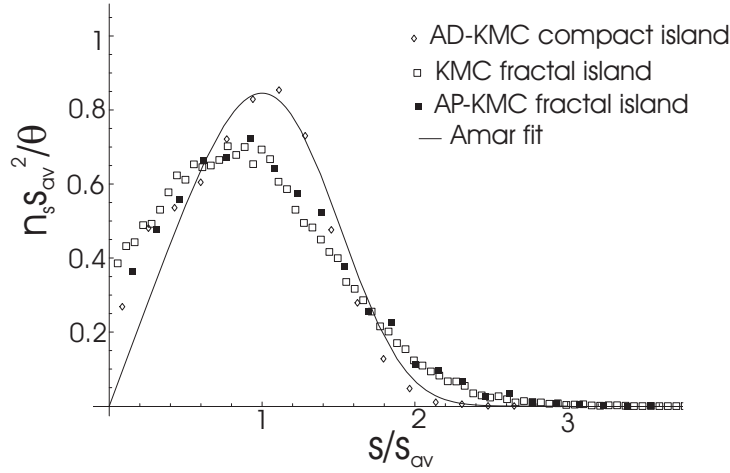


Figure 5.3: Island size distribution as obtained by KMC (empty squares), AP-KMC (filled squares) and AD-KMC (diamonds) for $T = 630$ K and a ratio $D/F = 10^6$. The solid line is the universal scaling relation eq. 2.36, as given in Ref. [64]. Fig. from Ref. [111].

However, AD-KMC exhibits rather large deviations: The maximum is larger and shifted towards larger island sizes. Also, the distribution function is narrower than for KMC and AP-KMC. An interesting behavior shown in from Fig. 5.3 is that the universal scaling law (Eq. 2.36) describes the KMC and AP-KMC results only rather poorly, indicating the limits of this model. Interestingly, however, it correctly reproduces the AD-KMC results.

In order to understand this puzzling behavior morphology and shape of the islands have been analyzed in more detail. Fig. 5.4 shows example surfaces for each of the three approaches. As can be seen both KMC and AP-KMC exhibit fractal growth, indicating that the flux ratio chosen here corresponds to rather low temperatures. AD-KMC shows a very different shape: islands are not fractal but more compact. The obvious failing of AD-KMC is related to the fact that to derive this scheme it was assumed that the system is close

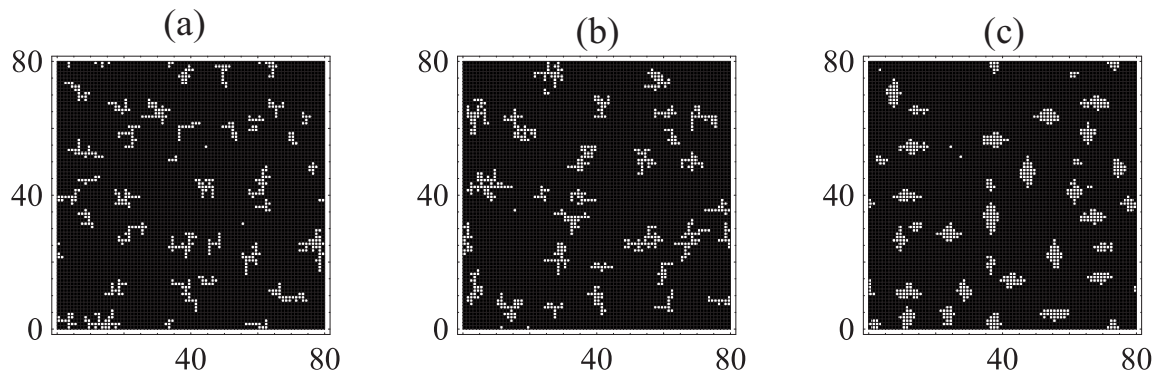


Figure 5.4: Example of a growth simulation applying (a) KMC, (b) AP-KMC, and (c) AD-KMC for 630 K. Fig. from Ref. [111].

to thermodynamic equilibrium, i.e., temperatures are high enough to realize delocalized adatom densities. Based on the discrepancy in the island size distribution, but also in the island shapes (see Fig. 5.4) the temperature chosen here is much too low.

5.3 Island shapes

Let us now focus on a comparison of the different growth simulations at high temperatures. The calculations of the island size distribution with reliable statistics at high temperatures is computationally rather expensive and therefore the discussion will be focused here on the island shapes. Fig. 5.5 shows characteristic surfaces as obtained from KMC and AD-KMC simulations for temperatures between 1000 and 1200 K. For temperatures above 1100 K the agreement is excellent: Both methods show compact islands with similar features such as density of kinks. Also, both methods show that with increasing temperature the deviations from the equilibrium shape (which is a square for the parameters and lattice chosen here) become smaller. Only for the lowest temperature, where KMC shows the formation of fractal like structures AD-KMC gives too compact islands as already found for the low temperature case. One can therefore conclude that for high temperatures (where KMC becomes exceedingly expensive) AD-KMC is an efficient and accurate tool. It will be now checked the choice of the time step Δt that was made to obtain the picture in Fig. 5.5. For the results at $T = 1100$ K a time step $\Delta t = 6.7 \cdot 10^{-4}$ has been used. The typical growth time step for this simulation is $\Delta t_{\text{growth}} = 1.56 \cdot 10^{-3}$, so the time step chosen Δt is roughly a factor 2 smaller than the Δt_{growth} . In Fig. 5.6 it is shown the same simulation for $T = 1100$ K done with Δt ranging between $10^{-3} \dots 1.7 \cdot 10^{-4}$. As one can see the simulations done with a time step Δt smaller than the one used before look totally the same. Instead for larger time steps ($\Delta t = 10^{-3}$) the number of island is increased. This is probably due to the fact that with such a large time step the adatom density does not arrive to find the right place along the islands edges. This would cause a higher nucleation rate.

5.4 Capture zones

An important quantity to analyze in growth simulations are capture zones. The capture zone of an island defines the region around an island where adsorbing adatoms on the average diffuse to that island and are incorporated there. An interesting feature of the density based KMC methods described in this work is that they give direct insight into the capture zones. As an example let us discuss Fig. 5.7 which shows a characteristic adatom density as calculated by AD-KMC. Clearly visible are the adatom depleted regions (dark areas) around all islands which mark the capture zones. From the picture it becomes also clear that some capture zones coalesce (these islands compete for the same adatoms and will grow more slowly) while others are open to higher density regions (those islands will grow faster).

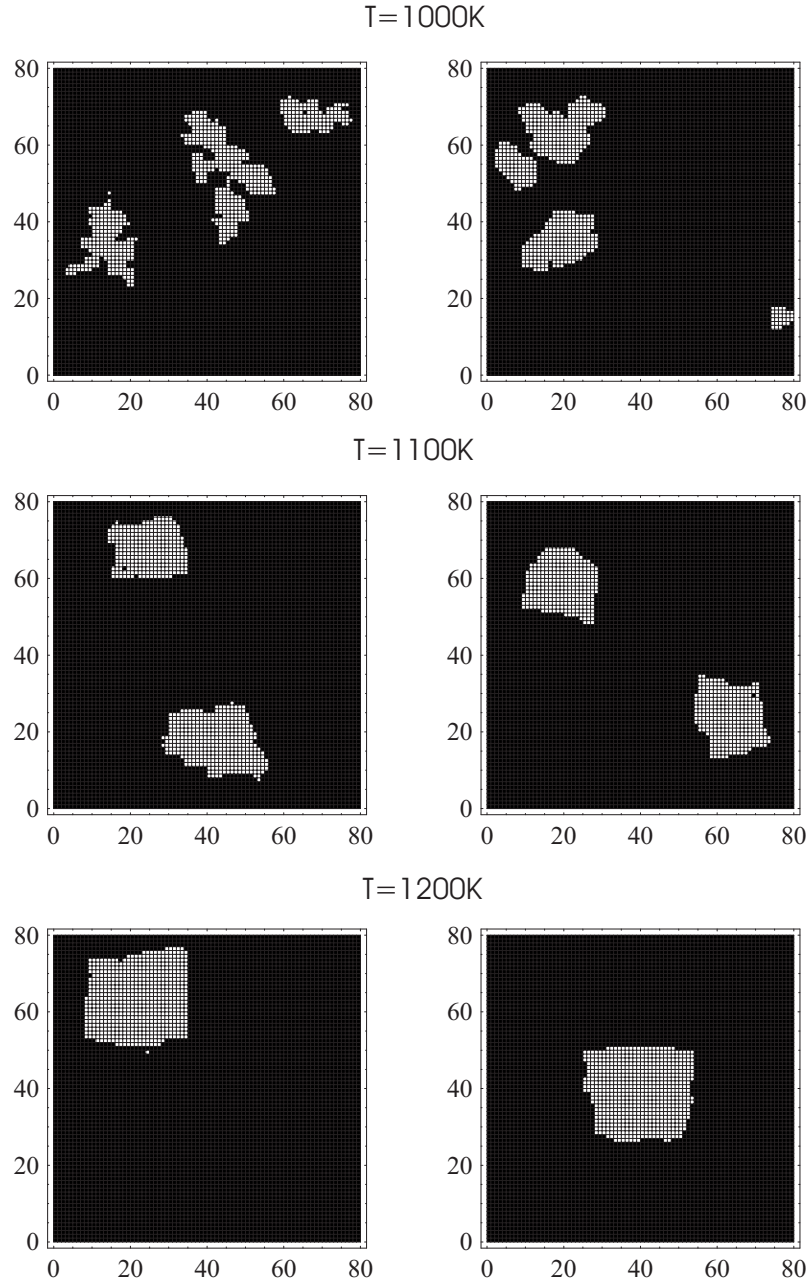


Figure 5.5: Comparison of the island shape in KMC and AD-KMC simulations for temperatures ranging from 1000 K to 1200 K. Simulations have been performed on a 80×80 matrix. Fig. from Ref. [111].

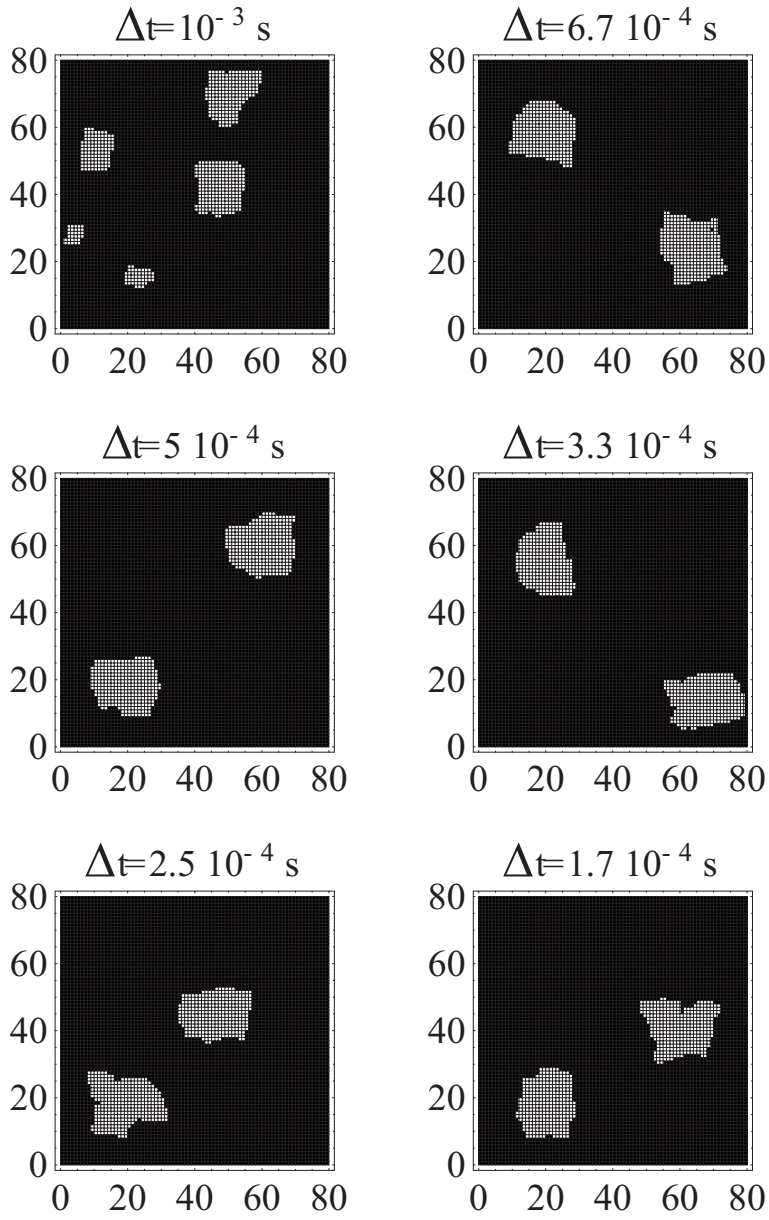


Figure 5.6: AD-KMC simulations done for $T = 1100 \text{ K}$ with $\Delta t = 10^{-3} \dots 1.7 \cdot 10^{-4}$ to test the validity of choice for the time step.

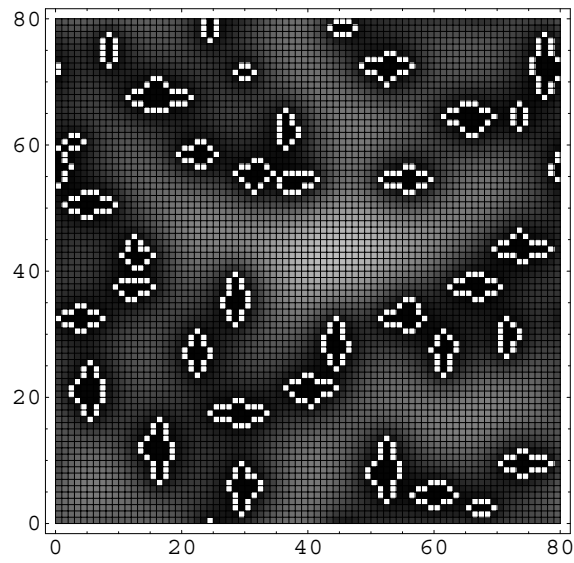


Figure 5.7: Density plot of the adatom density. Dark regions mark surface areas with low density, bright regions those with high adatom density. The island borders are easily visible by a bright rim due to the enhanced adatom density. The dark regions around the islands are adatom depleted areas (the adatoms have been captured by the islands). The density has been obtained from an AD-KMC calculation with $D/F = 10^6$. Fig. from Ref. [111].

Conclusions and Outlook

The goal of the present work was the development of new methods for the simulation of epitaxial growth at the mesoscopic scale, in particular for conditions close to the thermodynamic equilibrium. Epitaxial growth has been one of the hot topics of solid state physics during the last decades. Due to the complexity of the system involved, the understanding of epitaxial growth and its underlying mechanisms is possible only applying computational methods. Many different methods have been developed to this purpose but there is still a lot to do to reach a predictive computational theory for epitaxial growth. The present work is a contribution in this sense.

Due to the different time and length scales that are relevant for the epitaxial process, there is no single computational method available that can describe the entire process from the micro- to the macroscopic scale. Dedicated methods have been developed for the distinct scales. The mesoscopic scale is particularly interesting for practical applications because this is the typical scale of semiconductor devices. A widely used method at this scale is the Kinetic Monte Carlo (KMC) [23–26].

Starting from an accurate analysis of KMC we showed that there are large margins to improve and optimize this method in particular at high temperature for systems close to thermodynamic equilibrium. Based on this analysis we proposed a new method, which can be considered an extension of KMC. This new method is a density approach to KMC. Density approaches have proved to be very efficient in other fields like electronic structure theory, where the Density Functional Theory (DFT) is a standard tool [19, 20].

The central quantity in our approach is the adatom density (similar like the electron density in electronic structure theory). Methods based on the adatom density for epitaxial simulations like the Rate equation are available since a long time [52–56]. Recently, based on it improved methods such as the Level Set Method, which uses the adatom density, have been developed [27]. The problem of these methods is that they use empirical parameters, which are hard to be related to microscopic quantities calculated from ab-initio principles or obtained from experiments. This is not the case for the new method presented here because as for KMC it is possible to use as input the microscopic parameters calculated from ab-initio methods.

If the epitaxial growth took place at thermodynamic equilibrium, each adatom would occupy the energetically most stable position on the surface and the entire process would be deterministic. The thermodynamic equilibrium is hardly reachable because dynamic effects play an important role. To obtain a smooth surface epitaxial growth is generally performed in a layer by layer regime which is close to the thermodynamic limit. Under

these conditions adatoms diffuse over large areas of the surface before finding a stable position. The simulation of all these diffusion processes is very expensive from a computational point of view and it takes the largest part of the CPU time needed for the simulation. Physics suggests us a way to improve the treatment of these diffusion processes. The motion of the adatom is a random walk. Close to thermodynamic equilibrium it can be described by a diffusion equation for the adatom density.

The adatom density methods originate from the combination of KMC methods and the solution of diffusion like equations for the adatom density. Two different methods have been developed here, the Adatom Density Kinetic Monte Carlo (AD-KMC) and the Adatom Probability Kinetic Monte Carlo (AP-KMC). The two methods are strictly related and AD-KMC is a further approximation of AP-KMC. Both have been derived from the master equation, from which also the KMC method derives. In AP-KMC to each adatom on the growing surface corresponds a different adatom density. AP-KMC gives good results at any simulation temperature. For high temperatures the adatom densities get rapidly delocalized over the surface. Under these conditions it is possible to add all the single adatom densities in one total adatom density. This is what is done in AD-KMC, which is faster than AP-KMC but contains also more approximations.

Statistical tests have been done to check the validity of AD-KMC and AP-KMC. The advantages of these methods compared to KMC have been shown comparing the CPU times for test simulations. Developing these methods we had also to describe the nucleation process in the adatom density picture. To do this we introduced for the first time, to our knowledge, a local nucleation term. This is an open field and there needs still a lot to be done to improve the local functional for the nucleation.

In these adatom density KMC methods, most of the CPU time is used to solve the system of differential equations. To speed up this part of the algorithm we developed also the Hyper-Jump KMC (HJ-KMC), which is a KMC method in which the adatoms are allowed to perform jumps over many lattice sites. The method is still in an initial stage, but the tests performed till now are very promising, showing a further decrease of the simulation's CPU time.

For the future it will be extremely interesting to apply these adatom density KMC to real systems, in particular to semiconductors like Gallium Nitride (GaN) which are grown at high temperature and for which standard KMC simulation are hardly feasible. Another field of work is the further development of the methodology in particular for the investigation for improved nucleation terms and finally the implementation of multigrid schemes (see e.g. Ref. [114]), which would allow to further reduce the simulation time.

Appendix A

Markov Processes and derivation of the Master equation

First, a stationary stochastic process is defined which is necessary to derive the master equation from the definition of a Markov process.

A **stochastic process** is called **stationary** when the moments are not affected by a shift in time, i.e., when

$$\langle Y(t_1 + \tau)Y(t_2 + \tau) \dots Y(t_n + \tau) \rangle = \langle Y(t_1)Y(t_2) \dots Y(t_n) \rangle \quad (\text{A.1})$$

for all n , all τ , and all t_1, t_2, \dots, t_n . Here $\langle Y(t) \rangle$ is the average of the stochastic process $Y(t)$ and it is given by:

$$\langle Y(t) \rangle = \int Y_X(t) P_X(x) dx \quad . \quad (\text{A.2})$$

Here $P_X(x)$ is the probability density of X . More generally, given n values t_1, t_2, \dots, t_n for the time variable the n -th moment is:

$$\langle Y(t_1)Y(t_2) \dots Y(t_n) \rangle = \int Y_X(t_1)Y_X(t_2) \dots Y_X(t_n) P_X(x) dx \quad . \quad (\text{A.3})$$

Derivation of the Master Equation

Integrating Eq. 2.14 over y_2 one obtains for $t_1 < t_2 < t_3$

$$P_2(y_1, t_1; y_3, t_3) = P_1(y_1, t_1) \int P_{1|1}(y_2, t_2|y_1, t_1) P_{1|1}(y_3, t_3|y_2, t_2) dy_2 \quad . \quad (\text{A.4})$$

Divide both sides by $P_1(y_1, t_1)$,

$$P_{1|1}(y_3, t_3|y_1, t_1) = \int P_{1|1}(y_3, t_3|y_2, t_2) P_{1|1}(y_2, t_2|y_1, t_1) dy_2 \quad . \quad (\text{A.5})$$

This is called the **Chapman-Kolmogorov** equation (also called Smoluchowski equation). It is an identity, which must be obeyed by the transition probability of any Markov

process. For **stationary Markov processes** the transition probability $P_{1|1}$ does not depend on two times but only on the time interval; for this case a special notation is introduced:

$$P_{1|1}(y_2, t_2 | y_1, t_1) = T_\tau(y_2 | y_1) \quad (\text{A.6})$$

with $\tau = t_2 - t_1$. The Chapman-Kolmogorov equation then becomes

$$T_{\tau+\tau'}(y_3 | y_1) = \int T_{\tau'}(y_3 | y_2) T_\tau(y_2 | y_1) dy_2 \quad . \quad (\text{A.7})$$

We want now to derive the master equation. The master equation is a more convenient version of the Chapman-Kolmogorov equation. It is a differential equation obtained by going to the limit of a vanishing time difference τ' . For small τ' we can write $T_{\tau'}(y_2 | y_1)$ (see [45]):

$$T_{\tau'}(y_2 | y_1) = (1 - a_0 \tau') \delta(y_2 - y_1) + \tau' W(y_2 | y_1) + O(\tau') \quad . \quad (\text{A.8})$$

Here $w(y_2 | y_1)$ is the transition probability per unit time from y_1 to y_2 . The coefficient $1 - a_0 \tau'$ in front of the delta function is the probability that no transition takes place during τ' , hence

$$a_0 = \int W(y_2 | y_1) dy_2 \quad . \quad (\text{A.9})$$

Now inserting the expression for $T_{\tau'}$ (Eq. A.8) in the Chapman-Kolmogorov equation

$$T_{\tau+\tau'}(y_3 | y_1) = [1 - a_0(y_3) \tau'] T_\tau(y_3 | y_1) + \tau' \int W(y_3 | y_2) T_\tau(y_2 | y_1) dy_2 \quad . \quad (\text{A.10})$$

Divide by τ' , go to the limit $\tau' \rightarrow 0$:

$$\frac{\partial}{\partial \tau} T_\tau(y_3 | y_1) = \int \{W(y_3 | y_2) T_\tau(y_2 | y_1) - W(y_2 | y_3) T_\tau(y_3 | y_1)\} dy_2 \quad . \quad (\text{A.11})$$

This differential version of the Chapman-Kolmogorov equation, valid for the transition probability of any stationary Markov process obeying Eq. A.8 is called **Master Equation**. Now rewriting the previous equation and suppressing redundant indices gives:

$$\frac{\partial P(y, t)}{\partial t} = \int \{W(y | y') P(y', t) - W(y' | y) P(y, t)\} dy' \quad . \quad (\text{A.12})$$

This is the customary form of the master equation. If the range of Y is a discrete set of states with labels n , the equation reduces to

$$\frac{dp_n(t)}{dt} = \sum_{n'} \{W_{nn'} p_{n'}(t) - W_{n'n} p_n(t)\} \quad . \quad (\text{A.13})$$

In this form the meaning becomes particularly clear: the master equation is a gain-loss equation for the probability of each state n ; the first term is the gain due to transitions from other states n' , and the second term is the loss due to transitions into other states.

Appendix B

Distributions

First the binomial distribution will be defined here and it will be shown how to derive the Poisson distribution as a particular case of binomial distribution. Then the point processes will be introduced as a general class of stochastic processes to which also the Poisson processes belong. Finally the expression for the waiting time for point processes will be shown. For more details see Refs. [45, 46, 115–117]

Binomial distribution

The binomial distribution is defined on the discrete set $\{k = 0, 1, \dots, n\}$ and depends on the parameters n and p . The distribution probability is:

$$B(n, p; k) = \binom{n}{k} p^k (1-p)^{n-k} \quad . \quad (\text{B.1})$$

The distribution arises when there are only two possible values $\{x_1, x_2\}$ for the random variable X . The probability for the occurrence of the value x_1 is p , and that for the value x_2 is then $1-p$, $0 \leq p \leq 1$. Consider an n -fold realization of X . The probability that the value x_1 is obtained k times out of the n realizations is then $B(n, p; k)$. The random variable is here therefore K and is equal to the number of occurrences of x_1 .

Poisson Distribution

The Poisson distribution with the probabilities

$$p(\lambda; k) = \frac{\lambda^k}{k!} e^{-\lambda}, \quad (\text{B.2})$$

is defined on the set $\{k = 0, 1, \dots\}$ and it is dependent on the parameter λ . This distribution is an approximation to the binomial distribution when p becomes very small and n very large with fixed $\lambda = pn$:

$$\lim_{p \rightarrow 0, n \rightarrow \infty} \binom{n}{k} p^k (1-p)^{n-k} = \frac{(pn)^k}{k!} e^{-(pn)} \quad . \quad (\text{B.3})$$

In fact it results:

$$\begin{aligned}
& \lim_{p \rightarrow 0, n \rightarrow \infty} \binom{n}{k} p^k (1-p)^{n-k} \\
&= \frac{n(n-1)(n-2) \dots (n-k+1)}{k!} p^k (1-p)^n (1-p)^{-k} \\
&= \frac{n^k \left(1 - \frac{1}{n}\right) \left(1 - \frac{2}{n}\right) \dots \left(1 - \frac{k-1}{n}\right) p^k (1-p)^n}{k! (1-p)^k} .
\end{aligned} \tag{B.4}$$

The product $\left(1 - \frac{1}{n}\right) \left(1 - \frac{2}{n}\right) \dots \left(1 - \frac{k-1}{n}\right)$ is going to unity. The same is for the term $(1-p)^k$, but the term $(1-p)^n = \left(1 - \frac{pn}{n}\right)^n$ is going to e^{-np}

Poisson Processes

The Poisson processes are a particular class of Markov processes and are given by the master equation:

$$\frac{dp_n(t)}{dt} = \lambda p_{n-1}(t) - \lambda p_n(t), \quad n \geq 1, \tag{B.5}$$

$$\frac{dp_0(t)}{dt} = -\lambda p_1(t) \quad . \tag{B.6}$$

Suppose that

$$p_n(0) = \delta_{n,m}, \quad m \leq 0 \tag{B.7}$$

is the initial condition. Then the solution is

$$p_n(t) = \frac{(\lambda t)^{n-m}}{(n-m)!} e^{-(\lambda t)}, \quad n \leq m \tag{B.8}$$

$$p_n(t) = 0 \quad n < m \tag{B.9}$$

A typical example of a Poisson process is given by a radioactive source which emits α particles with an average rate of λ per second. From the Poisson distribution it is possible to calculate the probability e.g. to detect 10 α particles in 5 seconds.

Point Processes

The Poisson process is also part of a more general subclass of Markov processes, the so-called point processes. For point processes the events, such as the impact of raindrops on a surface or the impact of cosmic rays on a Geiger counter, occur at random times. Such processes are characterized by a sequence of random times (t_1, \dots, t_n, \dots) . The number

$n(t)$ of events that occur in a fixed time interval $[0, t]$ is a random variable, as are the times $t_i, i = 1, \dots, n(t)$ at which the events take place. We introduce the distribution functions

$$\{f_1(t_1), \dots, f_n(t_1, \dots, t_n)\} \quad (\text{B.10})$$

where $f_1(t_1)dt$ is the probability that an event takes place in the time interval $[t_1, t_1 + dt_1]$. In general $f_n(t_1, \dots, t_n)dt_1 \dots dt_n$ gives the probability that in each of the intervals $[t_1, t_1 + dt_1], \dots, [t_n, t_n + dt_n]$ one event occurs, independently of how many events occur outside these intervals. It is assumed that at most one event can occur in an interval $[t_i, t_i + dt_i]$ provided the interval is sufficiently small. A particular simple and frequent assumption is that

$$f_n(t_1, \dots, t_n) = f_1(t_1)f_1(t_2) \dots f_1(t_n); \quad (\text{B.11})$$

that is, each event in the interval is independent of the other events. If in addition $f_1(t) = \lambda = \text{const}$, then one speaks of a Poisson process. Then

$$f_n(t_1, \dots, t_n) = \lambda^n \quad (\text{B.12})$$

Waiting times

Frequently the following question arises in the context of the point processes: If the observation is started at time $t = t_0$, how long on the average does one has to wait for the next event? In order to answer this question one has to calculate the probability

$$g_1(\Theta, t_0)d\Theta \quad (\text{B.13})$$

that the first event after t_0 occurs in the interval $[t_0 + \Theta, t_0 + \Theta + d\Theta]$. The probability that in the interval $[t_0, t_0 + \Theta + d\Theta]$ no event occurs is $p_0(t_0, t_0 + \Theta + d\Theta)$. The corresponding probability for the interval $[t_0, t_0 + \Theta]$ is $p_0(t_0, t_0 + \Theta)$, from which follows the probability for an event precisely in the interval $[t_0 + \Theta, t_0 + \Theta + d\Theta]$:

$$g_1(\Theta, t_0)d\Theta = -p_0(t_0, t_0 + \Theta + d\Theta) + p_0(t_0, t_0 + \Theta) \quad . \quad (\text{B.14})$$

Therefore

$$g_1(\Theta, t_0) = -\frac{d}{d\Theta}p_0(t_0, t_0 + \Theta) \quad (\text{B.15})$$

For a Poisson process

$$g_1(\Theta, t_0) = -\frac{d}{d\Theta}e^{-\lambda\Theta} = \lambda e^{-\lambda\Theta} \quad (\text{B.16})$$

Appendix C

Numerical solution of the Rate Equation with Mathematica

The Rate Equations given in Eq. 2.21 and 2.22 will be solved here. Let us set $N = x$, $n_1 = y$ and $D = Diff$. The system is solved for the following input data:

$$Diff = 10^6$$
$$F = 1 \text{ Ml/s}$$
$$time = 0.01 \text{ s}$$

Here *time* is the maximum simulation time. To solve the system it is used:

```
sol=NDsolve[{x'[t]==Diff*y[t]^2, y'[t]==F-2*Diffy^2-Diff*y[t]*x[t],  
x[0]==y[0]==0}, {x,y}, {t, time}]
```

to plot the results it is used:

```
g1=Plot[Evaluate[y[t]/.sol], {t,0,time}, PlotStyle->RGBColor[1,0,0],  
AxesLabel->{"t", "adatom density"}]
```

and

```
g2=Plot[Evaluate[x[t]/.sol], {t,0,time}, PlotStyle->RGBColor[0,1,0],  
AxesLabel->{"t", "island density"}]
```

As expected the adatom density reach a maximum and than it decreases, while the island density is increasing till the end of the simulation.

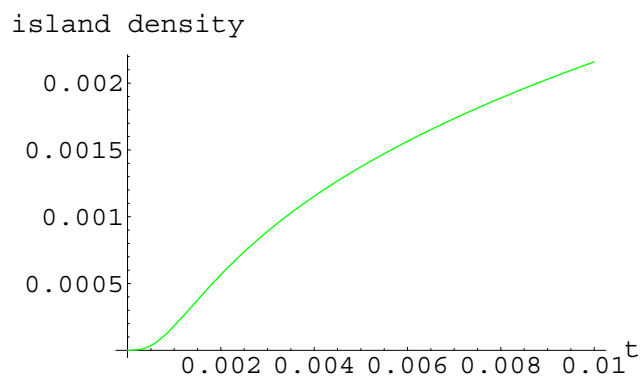


Figure C.1: adatom density with rate equation for $t = 0.01$ s, $D = 10^6$, $F = 1$ ML/s.

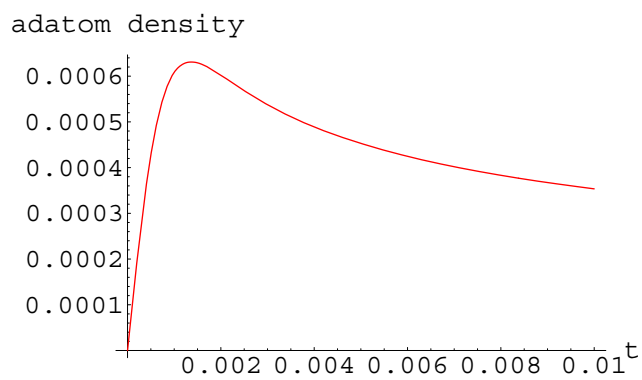


Figure C.2: island density with rate equation for $t = 0.01$ s, $D = 10^6$, $F = 1$ ML/s.

Appendix D

Analytical Solution of the Diffusion Equation

To solve the diffusion equation

$$\frac{\partial P(x, t)}{\partial t} = \Gamma \frac{\partial^2 P(x, t)}{\partial x^2} \quad , \quad (\text{D.1})$$

it is possible to use the method of separation of variables, writing $P(x, t)$ as the product of two functions, one dependent only from x and the other only from t :

$$P(x, t) = a(x)b(t) \quad . \quad (\text{D.2})$$

If Eq. D.2 is now plugged into Eq. D.1 it results

$$\frac{1}{\Gamma b(t)} \frac{\partial b(t)}{\partial t} = \frac{1}{a(x)} \frac{\partial^2 a(x)}{\partial x^2} \quad . \quad (\text{D.3})$$

In Eq. D.3 the left hand side depends only from t and the right hand side from x . Eq. D.3 is equivalent to the following system:

$$\begin{aligned} \frac{\partial b(t)}{\partial t} &= -\Gamma k^2 b(t) \\ \frac{\partial^2 a(x)}{\partial x^2} &= -k^2 a(x) \quad . \end{aligned} \quad (\text{D.4})$$

Here k is a constant. Integrating the previous equations one gets:

$$\begin{aligned} a(x) &= A(k) \cos(kx) + B(k) \sin(kx) \\ b(t) &= e^{-k^2 \Gamma t} \quad . \end{aligned} \quad (\text{D.5})$$

here $A(k)$ and $B(k)$ are integration constants depending on k . The general solution for $P(x, t)$ is:

$$P(x, t) = \int_{-\infty}^{\infty} dk e^{-k^2 \Gamma t} [A(k) \cos(kx) + B(k) \sin(kx)] \quad . \quad (\text{D.6})$$

If the initial condition is:

$$P(x, 0) = \tilde{P}(x) = \int_{-\infty}^{\infty} dk [A(k) \cos(kx) + B(k) \sin(kx)] \quad , \quad (\text{D.7})$$

than it results for $P(x, t)$:

$$\begin{aligned} P(x, t) &= \frac{1}{2\pi} \int_{-\infty}^{\infty} d\xi \tilde{P}(\xi) \int_{-\infty}^{\infty} dk e^{-k^2 \Gamma t} [\cos(k\xi) \cos(kx) + \sin(k\xi) \sin(kx)] \\ &= \frac{1}{2\pi} \int_{-\infty}^{\infty} d\xi \tilde{P}(\xi) \int_{-\infty}^{\infty} dk e^{-k^2 \Gamma t} \cos k(\xi - x) \quad , \end{aligned} \quad (\text{D.8})$$

as the previous integrand is a pair function:

$$\int_{-\infty}^{\infty} dk e^{-\alpha^2 k^2} \cos(\beta k) = 2 \int_0^{\infty} dk e^{-\alpha^2 k^2} \cos(\beta k) = \frac{\sqrt{\pi}}{\alpha} e^{-\frac{(\xi-x)^2}{4\Gamma t}} \quad , \quad (\text{D.9})$$

so using this expression $P(x, t)$ can be written as:

$$P(x, t) = \frac{1}{\sqrt{4\pi\Gamma t}} \int_{-\infty}^{\infty} d\xi \tilde{P}(\xi) e^{-\frac{(\xi-x)^2}{4\Gamma t}} \quad , \quad (\text{D.10})$$

Now for the initial condition $\tilde{P}(x) = \delta(x)$:

$$P(x, t) = \frac{1}{\sqrt{4\pi\Gamma t}} e^{-\frac{x^2}{4\Gamma t}} \quad , \quad (\text{D.11})$$

which is a Gaussian distribution.

Appendix E

Numerical Solution of the Diffusion Equation

Three different approaches to solve numerically the diffusion equation will be discussed here (for details see Ref. [114]):

$$\frac{\partial P}{\partial t} = \Gamma \frac{\partial^2 P}{\partial x^2} \quad . \quad (\text{E.1})$$

E.0.1 Explicit Method

Equation E.1 can be differenced as:

$$\frac{P_i^{n+1} - P_i^n}{\Delta t} = \Gamma \left[\frac{P_{i+1}^n - 2P_i^n + P_{i-1}^n}{(\Delta x)^2} \right] \quad . \quad (\text{E.2})$$

The solution of the difference equations can be written as:

$$P_i^n = \xi^n e^{ik_i \Delta x} \quad . \quad (\text{E.3})$$

Here k is a real spatial wave number (which can have any value) and $\xi = \xi(k)$ is a complex number that depends on k . The number ξ is called the *amplification factor*. If $|\xi(k)| > 1$ for some k the difference equations are unstable. The amplification factor for Eq. (E.2) is:

$$\xi = 1 - \frac{4\Gamma\Delta t}{(\Delta x)^2} \sin^2 \left(\frac{k\Delta x}{2} \right) \quad . \quad (\text{E.4})$$

The requirement $|\xi| \leq 1$ to have stable solutions leads to the stability criterion:

$$\frac{2\Gamma\Delta t}{(\Delta x)^2} \leq 1 \quad . \quad (\text{E.5})$$

E.0.2 Implicit Method

Eq. E.1 can also be differenced as:

$$\frac{P_i^{n+1} - P_i^n}{\Delta t} = \Gamma \left[\frac{P_{i+1}^{n+1} - 2P_i^{n+1} + P_{i-1}^{n+1}}{(\Delta x)^2} \right] . \quad (\text{E.6})$$

This is just like Eq. (E.2), except that the spatial derivatives on the right-hand side are evaluated at time step $n + 1$. Schemes with this character are called *fully implicit or backward in time*. To solve equation Eq. (E.6) one has to solve a set of simultaneous linear equations at each time step for the P_i^{n+1} . The amplification factor is:

$$\xi = \frac{1}{1 + \frac{4\Gamma\Delta t}{(\Delta x)^2} \sin^2\left(\frac{k\Delta x}{2}\right)} . \quad (\text{E.7})$$

Clearly $|\xi| < 1$ for any time step Δt . The scheme is unconditionally stable. The details of the small-scale evolution from the initial conditions are obviously inaccurate for large Δt , but the correct equilibrium solution is obtained. This is the characteristic feature of the implicit methods.

E.0.3 Crank-Nicholson

Here the explicit and implicit schemes are combined together. Eq. (E.1) is differenced as:

$$\frac{P_i^{n+1} - P_i^n}{\Delta t} = \frac{\Gamma}{2} \left[\frac{(P_{i+1}^{n+1} - 2P_i^{n+1} + P_{i-1}^{n+1}) + (P_{i+1}^n - 2P_i^n + P_{i-1}^n)}{(\Delta x)^2} \right] . \quad (\text{E.8})$$

The amplification factor is:

$$\xi = \frac{1 - \frac{2\Gamma\Delta t}{(\Delta x)^2} \sin^2\left(\frac{k\Delta x}{2}\right)}{1 + \frac{2\Gamma\Delta t}{(\Delta x)^2} \sin^2\left(\frac{k\Delta x}{2}\right)} , \quad (\text{E.9})$$

so the method is stable for any size Δt and it is second-order accurate in both time and space.

Bibliography

- [1] J. Royer. *Bull. Soc. Fr. Min.*, 51:7, 1928.
- [2] Levi A. C. and Kotrla M. *J. Phys.:Condens Matter*, 9:299, 1997.
- [3] Y. Saito. *Statistical Physics of Crystal Growth*. World Scientific Publishing, Singapore, 1996.
- [4] A.-L. Barabasi and H.E. Stanley. *Fractal Concepts in Surface Growth*. Cambridge University Press, Cambridge, 1995.
- [5] I. V. Markov. *Crystal growth for beginners*. World Scientific Publishing, Singapore, 1995.
- [6] A. Pimpinelli and J. Villain. *Physics of Crystal Growth*. Cambridge University Press, Cambridge, 1998.
- [7] T. Michely and j. Krug. *Islands, Mounds and Atoms*. Springer, Berlin, 2001.
- [8] M.A. Herman, W. Richter, and H. Sitter. *Epitaxy*. Springer, Berlin, 2003.
- [9] E. W. Müller. *Z. Physik*, 131:136, 1951.
- [10] E. W. Müller. *J. Appl. Phys.*, 27:474, 1956.
- [11] G. Binning and H. Roherr. *Rev. Mod. Phys.*, 59:615, 1987.
- [12] T. Michely, M. Hohage, M. Bott, and G. Comsa. *Phys. Rev. Lett*, 70:3943, 1993.
- [13] J. Krug, P. Politi, and T. Michely. *Phys. Rev. B*, 61:14037, 2000.
- [14] Bauer E. *Z. Kristallogr.*, 110:372, 1958.
- [15] Frank F. C. and van der Merwe J. H. *Proc. Roy. Soc. (London) A*, 198:205, 1950.
- [16] Volmer M. and Weber A. *Z. Phys. Chem.*, 119:277, 1926.
- [17] Stranski I. N. and Krastanov L. *Sitzungsber. Akad. Wiss. Wien, Math.-naturwiss. Kl. IIb*, 146:797, 1938.

- [18] K. Ohno, K. Esfarjani, and Y. Kawazoe. *Computational Materials Science. From Ab Initio to Monte Carlo Methods*. Springer, Berlin, 1998.
- [19] R. G. Parr and W. Yang. *Density-functional theory of atoms and molecules*. Oxford University Press, Oxford, 1994.
- [20] R. M. Dreizler and E. K. U. Gross. *Density Functional Theory: an approach to the quantum many-body problem*. Springer Verlag, Berlin, 1990.
- [21] J. A. Venables, G. D. T. Spiller, and M. Hanbeucken. *Rep. Prog. Phys.*, 47:399, 1984.
- [22] K. A. Fichthorn and W. H. Weinberg. *J. Chem. Phys.*, 95:1090, 1991.
- [23] S. Clarke and D. D. Vvedensky. *Phys. Rev. Lett*, 58:2235, 1987.
- [24] A. Madhukar and S. V. Ghaisas. *CRC Crit. Rev. Solid State Mater. Sci.*, 14:1, 1988.
- [25] H. Metiu, Y.-T. Lu, and Z. Y. Zhang. *Science*, 255:1088, 1992.
- [26] A. F. Voter. *Phys. Rev. B*, 34:6819, 1986.
- [27] M. F. Gyure, C. Ratsch, B. Merriman, R. E. Caflisch, S. Osher, J. J. Zinck, and D. D. Vvedensky. *Phys. Rev. E*, 58:R6927, 1998.
- [28] F. Montalenti, M.R. Sørensen, and A.F. Voter. *Phys. Rev. Lett.*, 87:126101, 2001.
- [29] G. Henkelman and H. Jónsson. *J. Chem. Phys.*, 111:7010, 1999.
- [30] G. Henkelman and H. Jónsson. *J. Chem. Phys.*, 115:9657, 2001.
- [31] M. Born and R. Oppenheimer. *Ann. Phys.*, 84:457–484, 1927.
- [32] A. Kley, P. Ruggerone, and M. Scheffler. *Phys. Rev. Lett.*, 79:5278, 1997.
- [33] J. Neugebauer, T. Zywietz, M. Scheffler, and J. Northrup. *Appl. Surf. Sci.*, 159:355, 2000.
- [34] E. Penev, S. Stojkovic, P. Kratzer, and M. Scheffler. *Phys. Rev. B*, 69:115335, 2004.
- [35] J. W. Haus and K.W. Kehr. *Phys. Rep.*, 150:263, 1987.
- [36] E. W. Montroll and G. H. Weiss. *J. Math. Phys.*, 6:167, 1965.
- [37] S. Glasstone, K. J. Laidler, and H. Eyring. *The Theory of Rate Processes*. McGraw-Hill Book Co, New York, 1941.
- [38] H. Eyring. *J. Chem. Phys.*, 3:107, 1935.
- [39] V. Bortolani, N.H. March, and M.P. Tosi. *Interaction of atoms and molecules with solid surfaces*. Plenum Press, New York, 1990.

- [40] G. H. Vineyard. *J. Phys. Chem. Solids*, 3:121, 1957.
- [41] P. Hänggi, P. Talkner, and M. Borkovec. *Rev. Mod. Phys.*, 62:251, 1990.
- [42] G. Boisvert, N. Mousseau, and L. J. Lewis. *Phys. Rev. Lett.*, 80:203, 1998.
- [43] U. Kürpick, A. Kara, and T. S. Rahman. *Phys. Rev. Lett.*, 78:1086, 1997.
- [44] C. Ratsch and M. Scheffler. *Phys. Rev. B*, 58:13163, 1998.
- [45] N.G. van Kampen. *Stochastic processes in physics and chemistry*. North Holland Physics Publishing, Amsterdam, 1981.
- [46] J. Honerkamp. *Stochastic Dynamical System*. VCH Publisher, New York, 1993.
- [47] D. D. Vvedensky, A. Zangwill, C. N. Luse, and M. R. Wilby. *Phys. Rev. E*, 48:852, 1993.
- [48] M. Predota and M. Kotrla. *Phys. Rev. E*, 54:3933, 1996.
- [49] M. Smoluchowski. *Phys. Z.*, 17:557, 1916.
- [50] M. Smoluchowski. *Phys. Z.*, 17:585, 1916.
- [51] F. Family and D. P. Landau. *Kinetics of Aggregation and Gelation*. North-Holland, Amsterdam, 1970.
- [52] G. Zinsmeister. *Thin Solid Film*, 2:497, 1968.
- [53] G. Zinsmeister. *Thin Solid Film*, 4:363, 1969.
- [54] G. Zinsmeister. *Thin Solid Film*, 7:51, 1971.
- [55] J. A. Venables. *Phil. Mag.*, 27:693, 1973.
- [56] D. Walton. *J. Chem. Phys.*, 37:2182, 1962.
- [57] M. C. Bartelt and J. W. Evans. *Phys. Rev. B*, 54:17359, 1996.
- [58] J. Krug. *Physica A*, 313:47, 2002.
- [59] J. A. Venables and D. J. Ball. *Proc. R. Soc. London, Ser A*, 322:331, 1971.
- [60] S. Stoyanov and D. Kashchiev. *Curr. Top. Mater. Sci.*, 7:69, 1981.
- [61] G. S. Bales and D. C. Chrzan. *Phys. Rev. B*, 50:6057, 1994.
- [62] M.C. Bartelt and J. W. Evans. *Phys. Rev. B*, 46:12675, 1992.
- [63] J. G. Amar, F. Family, and P. M. Lam. *Phys. Rev. B*, 50:8781, 1994.
- [64] J. G. Amar and F. Family. *Phys. Rev. Lett.*, 74:2066, 1995.

- [65] J. Villain. *J. Phys. I*, 1:19–42, 1991.
- [66] S. F. Edwards and D. R. Wilkinson. *Proc. R. Soc. London A*, 381:17–31, 1982.
- [67] Kardar M., Parisi G., and Zhang Y.-C. *Phys. Rev. Lett.*, 56:889, 1986.
- [68] J. D. Clarke and G. H. Gilmer. *Adv. Chem. Phys.*, 40:157, 1979.
- [69] D. Landau and K. Binder. *A Guide to Monte Carlo Simulation in Statistical Physics*. Cambridge University Press, Cambridge, 2000.
- [70] M. E. J. Newman and G. T. Barkema. *Monte Carlo Methods in Statistical Physics*. Oxford University Press, Oxford, 2001.
- [71] A. Bogicevic, J. Strömquist, and B. I. Lundqvist. *Phys. Rev. Lett.*, 81:637, 1998.
- [72] P. Ruggerone, C. Ratsch, M. Scheffler: Eds D.A. King, and D.P. Woodruff. *Growth and Properties of Ultrathin Epitaxial Layers, The Chemical Physics of Solid Surfaces*. Elsevier Science, Amsterdam, 1997.
- [73] T. Shitara, D. D. Vvedensky, M. R. Wilby, J. Zhang, J.H. Neave, and B. A. Joyce. *Phys. Rev. B*, 46:6815, 1992.
- [74] P. Smilauer, M. R. Wilby, and D. D. Vvedensky. *Phys. Rev. B*, 47:4119, 1993.
- [75] H. Gould and J. Tobochnik. *An Introduction to Computer Simulation Methods, Part 2*. Addison-Wesley, New York, 1998.
- [76] S. Osher and J. A. Sethian. *J. Comput. Phys.*, 79:12, 1988.
- [77] J. A. Sethian. *Level Set Methods*. Cambridge University Press, New York, 1996.
- [78] S. Chen, B. Merriman, S. Osher, and P. Smereka. *J. Comput. Phys.*, 135:8, 1997.
- [79] P. L. O’Sullivan, F. H. Baumann, and G. G. Gilmer. *J. Appl. Phys.*, 88:4061, 2000.
- [80] C. Ratsch, M. F. Gyure, S. Chen, M. Kang, and D. D. Vvedensky. *Phys. Rev. B*, 61:10598, 2000.
- [81] C. Ratsch, M. F. Gyure, R. E. Caflisch, F. Gibou, M. Petersen, M. Kang, J. Garcia, and D. D. Vvedensky. *Phys. Rev. B*, 65:195403, 2002.
- [82] F. G Gibou, C. Ratsch, M. F. Gyure, S. Chen, and R. E. Caflisch. *Phys. Rev. B*, 63:115401, 2001.
- [83] F. G Gibou, C. Ratsch, and R. E. Caflisch. *Phys. Rev. B*, 67:115403, 2003.
- [84] M. Petersen, C. Ratsch, R. E. Caflisch, and A. Zangwill. *Phys. Rev. E*, 64:61602, 2001.
- [85] M. Petersen, A. Zangwill, and C. Ratsch. *Surf. Sci.*, 536:55, 2003.

- [86] W. Ostwald. *Z. Phys. Chem.*, 34:495, 1900.
- [87] J. A. Venables, G. D. Spiller, and M. Hanbücken. *Rep. Prog. Phys.*, 47:399, 1984.
- [88] C. Castellano and P. Politi. *Phys. Rev. Lett.*, 87:56102, 2001.
- [89] J. Tersoff, A. W. Denier van der Gon, and R. M. Tromp. *Phys. Rev. Lett.*, 72:266, 1994.
- [90] K. Bromann, H. Brune, H. Röder, and K. Kern. *Phys. Rev. Lett.*, 75:677, 1994.
- [91] M. Kalff, G. Cosma, and T. Michely. *Phys. Rev. Lett.*, 81:1255, 1998.
- [92] K. R. Roos and M. C. Tringides. *Phys. Rev. Lett.*, 85:1480, 2000.
- [93] P. Politi and C. Castellano. *Phys. Rev. E*, 66:31606, 2002.
- [94] P. Politi and C. Castellano. *Phys. Rev. E*, 66:31605, 2002.
- [95] P. Politi and C. Castellano. *Phys. Rev. B*, 67:75408, 2003.
- [96] S. Heinrichs, J. Rottler, and P. Maass. *Phys. Rev. B*, 62:8338, 2000.
- [97] G. Ehrlich and F. G. Hudda. *J. Chem. Phys.*, 44:1039, 1966.
- [98] R. L. Schwoebel. *J. Appl. Phys.*, 40:614, 1969.
- [99] J. Rottler and P. Maass. *Phys. Rev. Lett.*, 83:3490, 1999.
- [100] J. Krug. *Eur. Phys. J. B*, 18:713, 2000.
- [101] F. Reif. *Statistical and Thermal Physics*. McGraw-Hill, New York, 1965.
- [102] R. Gomer. *Rep. Prog. Phys.*, 53:917, 1990.
- [103] S. Chandrasekhar. *Rev. Mod. Phys.*, 15:1, 1943.
- [104] J. D. Jackson. *Classical Electrodynamics*. Wiley, New York, 1975.
- [105] A. Zangwill, C. N. Luse, M. R. Wilby, and D.D. Vvedensky. *Surf. Sci. Lett.*, 274:L529, 1992.
- [106] C. Baggio, R. Vardavas, and D.D. Vvedensky. *Phys. Rev. E*, 64:45103(R), 2001.
- [107] D. D. Vvedensky. *Phys. Rev. E*, 67:25102, 2003.
- [108] L. Mandreoli and J. Neugebauer. *(to be published)*.
- [109] M. Meixner, E. Schöll, V. A. Shchukin, and D. Bimberg. *Phys. Rev. Lett.*, 87:236101, 2001.
- [110] E. Schöll and S. Bose. *Sol. State Electron.*, 42:1587, 1998.

- [111] L. Mandreoli, J. Neugebauer, R. Kunert, and E. Schöll. *Phys. Rev. B*, 68:155429, 2003.
- [112] J. G. Amar and F. Family. *Thin Solid Film*, 272:208, 1996.
- [113] J.A. Strosio and D.T. Pierce. *Phys. Rev. B*, 49:8522, 1994.
- [114] W. H. Press, S. Teukolsky, W. T. Vetterling, and B. P. Flannery. *Numerical Recipes*. Cambridge University Press, Cambridge, 1992.
- [115] W. Feller. *An Introduction to Probability Theory and its application, volume I and II*. John Wiley & Sons Edition, New York, 1970.
- [116] E. Belorizky and W. Gorecki. *Exercices et Problèmes corrigés de mécanique statistique*. Presses Universitaires de Grenoble, Grenoble, 1994.
- [117] E. S. Ventsel. *Teoria delle Probabilità*. Edizioni Mir, Mosca, 1983.

CURRICULUM VITAE

Name: Lorenzo Mandreoli

Born: 19.09.1975 in Bologna (Italy)

High School: Sept. 1989-July 1994, Liceo Scientifico Augusto Righi (Bologna)

Undergraduate Studies: Sept. 1994-July 1999, Physics at the University of Bologna
Sept. 1996-July 1997, exchange student at the Univeristy
Denis Diderot (Paris VII)
Sept. 1997-July 1998, exchange student at the University
of California at Santa Barbara (UCSB)
Sept. 1998-July 1999, Master Thesis with the title
"Electrical activity of extended defects in epitaxial Gallium
Nitride (GaN)" in the Semiconductor Laboratory of the
Univeristy of Bologna

Graduate Studies: Since Aug. 1999, Ph.D. at the Fritz-Haber-Institut

